ABSTRACT

Evaluating the Cellular Uptake and Translocation of Silver Nanoparticles Using *In Vitro* Models

Fan Zhang, Ph.D.

Mentor: Erica D. Bruce, Ph.D.

Nanoparticles (NPs) are used in a wide range of applications for various characteristics associated with their size and shape. This research evaluated silver nanoparticles (AgNPs) as a model NP system to evaluate uptake, translocation, and associated toxicity. This study investigated the influence of capping agents for AgNPs on the cellular uptake in two epithelial cell lines at realistic exposure levels. In addition, it also investigated the interaction between soluble proteins and modeled cell membrane using giant unilamellar vesicles (GUVs) and supported lipid bilayers, at physiologically relevant protein concentrations. Further, we developed a three-dimensional (3D) organotypic lung model resembling *in vivo* conditions, and tracked the translocation of AgNPs across the modeled lung barrier. Results show that particular capping agent on a AgNP modulates the extent of cellular uptake into different cell lines. Among the three investigated capping agents, tannic-acid coating was most efficient in delivering AgNPs into cells. Although the amount of internalized silver varied, none of the tested AgNPs resulted in cytotoxicity. Additionally, soluble proteins such as bovine serum albumin,

hemoglobin, lysozyme and fetal bovine serum could induce structural changes in GUVs due to non-specific protein adsorption onto lipid membranes. The minimum concentration of proteins required for the onset of adsorption, and the relative affinities of adsorption, were dependent on the vesicle charge and the dipolar characteristics of a protein. Furthermore, by engaging human bronchial epithelial cells, microvascular endothelial cells and macrophage-like cells into a tri-culture, 3D system the overall structure exhibited similar properties to the alveolar-capillary barrier. Tannic acid-AgNPs were tested as model NPs, and translocated through multiple cell layers at both 4°C and 37°C. Cytotoxicity of AgNPs in tri-culture was more potent than that monoculture or bi-culture. The active response from tri-culture was most physiological relevant due to secretion of pro-inflammatory markers by macrophage like cells. The overall study highlighted the important role of the physiochemical properties of AgNPs in their biological fate. The intrinsic proteins aid the cellular internalization of AgNPs by altering lipid membrane stability and permeability. Physiologically relevant *in vitro* models can be a reliable tool in the evaluation of transport and toxicity of NPs.

Evaluating the Cellular Uptake and Translocation of Silver Nanoparticles Using In Vitro Models

by

Fan Zhang, B.S.

A Dissertation

Approved by The Institute of Ecological, Earth and Environmental Sciences

_____

Joe Yelderman, Jr., Ph.D., Chairperson

Submitted to the Graduate Faculty of
Baylor University in Partial Fulfillment of the
Requirements for the Degree
of

Doctor of Philosophy

Approved by the Dissertation Committee

_____

Erica D. Bruce, Ph.D., Chairperson

_____

C. Kevin Chambliss, Ph.D.

_____

William Hockaday, Ph.D.

_____

Mary Lynn Trawick, Ph.D.

_____

Sascha Usenko, Ph.D.

Accepted by the Graduate School

August 2016

_____

J. Larry Lyon, Ph.D., Dean

Page bearing signatures is kept on file in the Graduate School.

TABLE OF CONTENTS

LIST OF FIGURES

LIST OF TABLES

ACKNOWLEDGMENTS

First I'd like to thank my advisor Dr. Erica D. Bruce. Thank her for opening Bruce Lab to me and offering me opportunities to learn and grow. Thanks for the generous support and trust in me and this project. I am forever grateful for the encouragement along the way. I can never thank her enough for caring me like a family in every aspect of my life, and teaching me things far beyond text books. My graduate life is fruitful and memorable, because of Dr. Bruce.

Thanks to all the people in Bruce Lab for teaching me skills when I just started working, and those support and help when things were not very promising. Special thanks go to Dr. Dana. D. Dean, whose passion over science influences me greatly, and I treasure every moment working with and learning from her.

Many thanks to my committee members, Dr. William Hockaday, Dr. Sascha Usenko, Dr. C Kevin Chambliss, Dr. Mary Lynn Trawick, for the valuable suggestions and comments to this project. I would also like to thank Dr. Boris Lau, who co-advised me from 2010 to 2013, for his explicit guidance getting me started with this project. Thanks for his efforts in forming me with good research habits, and connecting me with Dr. Marité Cárdenas in University of Copenhagen, Denmark to conduct research there.

To all my co-authors, it was my honor working with you. Without your help, this project would not be possible.

To my dearest parents, thanks for your full support in pursuit of my graduate degree in the United States; it was a selfless and wise decision you made. Thanks also to

my husband for always standing by my side, encouragement, and love that made these cherished memories.

最后感谢我的家人多年来的关心以及问候。尤其感谢爸爸妈妈，即便心里艰难，依然全力支持我多年的海外留学。感谢你们的无私决定，女儿已经成长得更加独立坚强。谢谢丈夫张同鑫的一路相伴，你是战友，是爱人，是生活对我的馈赠！

DEDICATION

To my dear parents and husband,
for their unconditional love and support
谨以此献给我无私伟大的父亲母亲，还有一路陪伴的丈夫！

CHAPTER ONE

Introduction

The rapid developments of nanoscience and nanotechnology have impacted diverse areas. Industry and biomedicine are two major areas significantly advanced due to applications of nanosized materials. With their exceptional physiochemical and biological properties, nanomaterials have paved a novel path for many commercial fields, including medicines, cosmetics, food processing, agriculture, energy production and etc. Globally, 1,814 products have reported use of nanomaterials as of March 2015, and 47% of those noted at least one nanomaterial component in the composition list. Metal, carbon, and silicon-containing are three major categories of nanomaterial components among them, metals and metal oxides comprise the largest composition. The expected benefits of adding these nanomaterials are mainly to confer antimicrobial protection, utilizing mostly AgNPs[1].

Recently, AgNPs have shown promising features as drug delivery systems and tumor detection probes[2]. However, the actual health risks of using AgNP-treated products remains largely unknown. Both *in vitro* and *in vivo* studies support the cellular uptake and translocation of AgNPs across epithelium linings. Adverse effects of AgNPs on cell cultures and *in* animals are found to be dependent on the dosage, specifically to certain target organs (liver, lung and kidney), and most importantly the physicochemical properties such as size, surface charge and shape[3].

Currently, the role of surface coatings on a AgNP's biological behavior is relatively less studied, and limited information is present about the translocation of AgNPs into bloodstream using appropriate models. Moreover, with the emerging applications of AgNPs in nanomedicine, i.e., nano-biotechnology, looks for affordable yet reliable *in vitro* alternative models to guide the design and evaluation of nanosilver drugs and drug delivery systems. In this regard, it is imperative to characterize the biological fate of AgNPs following potential exposure pathways, and the parameters that impact the particle-cell interactions. Investigations on cellular uptake, cytotoxicity, and translocation potentials of AgNPs through physiological barriers, are particularly urgent for an in-depth understanding of their potential harmful effects. Additionally, the results could provide directions for biomedical applications of AgNPs, and opportunities for novel therapeutics. Furthermore, AgNPs uptake and translocation data provides a means to model other NP systems for drug delivery.

Based on the limited reports in literature on these topics, it is hypothesized that 1) cellular uptake of surface functionalized AgNPs is dependent on the capping agent and cell types; 2) soluble proteins in plasma could induce changes in the properties of modeled cell membrane and facilitate NPs in the process of cellular uptake; and 3) NPs could translocate modeled alveolar-capillary barrier following inhalation, and pose damage to the lung tissue. These hypotheses were tested by investigating the following three objectives.

Objective One

To develop an understanding of the role of capping agents in the cytotoxicity of AgNPs to different cell lines at low dose levels and realistic exposure levels, as well as the extent of cellular uptake and of its relation to observed cytotoxic response

The research background and significance, experimental design, findings and discussion of this objective are presented in Chapter Three, and were published in the Journal of Applied Toxicology in 2015, entitled *Particle uptake efficiency is significantly affected by type of capping agent and cell line*. First author of the paper is Fan Zhang who conducted the research, analyzed the data and wrote the manuscript. Co-authors Phillip Durham and Christie M. Sayes at RTI International characterized the AgNPs at their facility and compiled that data. Co-authors Boris L. T. Lau and Erica D. Bruce were the principal investigators of this research

Objective Two

To determine the effect of soluble proteins, at concentrations specific to physiological levels, on the properties of model cell membranes.

The research background, methods, results, discussion and conclusion of this objective are presented in Chapter Four, and were published in Soft Matter in 2014, entitled *Non-specific interactions between soluble proteins and lipids induce irreversible changes in the properties of lipid bilayers.* Fan Zhang is the co-first author of the paper, who contributed equally with Francesca Ruggeri in conducting the experiments and writing the manuscript. Tania Lind helped with plotting figures from the results of QCM-D. Drs. Erica D. Bruce, Boris L. T. Lau and Marité Cárdenas were the principal investigators of the research

Objective Three

To develop a novel *in vitro* organotypic lung culture that resembles *in vivo* conditions, and is valuable in tracking the translocation of NPs across alveolar-capillary barriers and evaluating the resultant toxicity.

Research background, materials and methods, results, discussion and conclusion of this specific objective are presented in Chapter Five. Manuscript entitled *Assessing the translocation of AgNPs using a novel in vitro co-culture model of alveolar-capillary barrier,* regarding this objective has been submitted to Journal of Toxicology *in Vitro* and is currently in review. First author of the paper is Fan Zhang and Dr. Erica D. Bruce is the principal investigator of the research.

CHAPTER TWO

Literature Review

Nanotechnology and AgNPs

In 1959, the renowned physicist, Richard Feynman, spoke to the annual American Physical Society meeting at California Institute of Technology, giving a talk entitled "There's Plenty of Room at the Bottom", which seeded the concept of nanotechnology. In this talk, he brought up the possibilities-in-principle to manipulate and control things on a small scale. The talk was considered amusing at the time, as the method he described was not available. It undoubtedly preceded several events 20 years later, including the invention of the scanning tunneling microscope (STM) in 1981, and the book "Engines of Creation: The Coming Era of Nanotechnology" written by E. Eric Drexler in 1986[4]. The invention of STM boosted the nanotechnology and nanoscience further by allowing the visualization of individual atoms and bonds, which contributed to the discovery of Fullerenes in 1985 by Harry Kroto, Richard Smalley, and Robert Curl. Today, nanotechnology is seen as "the understanding and control of matter at the nanoscale, at dimensions between approximately 1 and 100 nanometers" defined by the National Nanotechnology Initiative launched in 2000 in the United States[5].

One nanometer is one-billionth of a meter, and many biological materials naturally occurred at this scale. For example, a DNA double-helix is only about 2 nm in diameter, and the protein hemoglobin is 5.5 nm in diameter. It is also the scale at which surfaces and interfaces dominate the properties of materials.

When in nanoscale, a material surface area to volume ratio increases significantly, providing the new entity greater amount of contact surface with the surrounding materials (Figure 2.1), thus more reactivity and unique physiochemical properties. With these new properties of nanomaterials, a wide range of applications have impacted many areas such as electronics and information technology, sustainable energy, environmental remediation, as well as medicine and health.

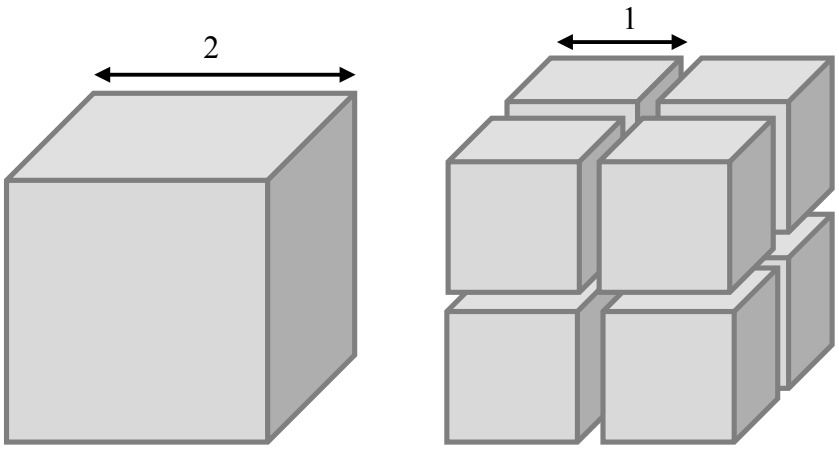

Figure 2.1. Illustration of increased surface area to volume ratio with decreased size.

In 2005, the Nanotechnology Consumer Product Inventory (CPI) was created, by the Woodrow Wilson International Center for Scholars and the Project on Emerging Nanotechnology, and for the first time it documented 54 products of nano-enabled consumer products in the marketplace. Since then, it continuously updated and improved the inventory list from worldwide sources. In 2010, over 1,012 products from 409 companies were reported. As of March 2015, a new total of 1,814 products from 622 companies in 32 countries claimed incorporation of nanomaterials. Thirty-nine types of

nanomaterials were used in the 846 products with known nanomaterial components, mainly to serve as an antimicrobial agent (31%), protective coating (15%) or dietary supplement (11%). AgNPs, with involvement in 207 products, are the leading nano-components and most popular additives in consumer products[1].

AgNPs display special optical properties that differ from their bulk parent. They absorb and scatter light with high efficiency at a particular frequency of the light due to the localized surface plasmon resonance (LSPR). According to Mie (1908), who first modeled the optical properties of NPs, AgNPs can present various colors determined by the size or shape of the particle. Therefore, AgNPs have been used as aggregate sensors and local refractive index, as their absorbance spectra shifts when particle size or surface chemistry changes[6]. Recently, material scientists have taken advantage of the optical property of AgNPs, and designed etchable plasmonic probes for tumor detection[2c]. Fluorescence labelled AgNPs were synthesized with a tumor-penetrating peptide coating. The penetration of these AgNPs into cancer cells was readily recognized by confocal microscopy, due to enhanced fluorescence-trackable signals enabled by AgNPs. Injection of these engineered AgNPs into tumor-bearing mice also showed tumor uptake, suggesting a novel nanosystem to allow the mapping of tumors *in vitro* and *in vivo*[2c].

Because of their unique thermal and electrical properties, AgNPs have been commonly added into printable electronics as a conductive layer, and in plastics and composites to improve electrical conductivity. There have also been uses of AgNPs as drug delivery vehicles. AgNPs-containing nanocapsules could be activated by remote controlled sonication, which leads to the rupturing of the nanocapsules into fragments and releases the encapsulated drug[2a].

The primary use of AgNPs is in fabrics, wound dressings, food packaging and medical devices, as AgNPs can slowly dissociate a low level of silver ions and control bacterial growth and odor. A series of studies have been performed to test the bactericidal effect of AgNPs. Evidence supported AgNPs as effective biocides against 1) bacteria such as *Escherichia coli* and *Staphylococcus aureus* 2) fungi such as *Aspergillus niger* and *Penicillium citrinum* 3) viri such as Hepatitis B and HIV-1[7]. Despite the large number of studies investigating the beneficial antimicrobial efficacy of silver nanomaterials, the mechanisms by which silver nanomaterials exert this activity is not well described. A few proposed mechanisms include generation of reactive oxygen species and membrane rupture of the bacteria, both being a result of the released silver ions from NPs; or simply the enhanced surface area to volume ratio, providing better contact with the microorganism[7]. For example, four different gram-positive bacteria, *P. Aeruginosa*, *V. Cholera*, *S. Typhus* and *E. Coli*, were treated with AgNPs of various sizes and shapes, and at the concentration of 75 μg/ml, AgNPs were effective in controlling the growth of all bacteria[8]. Scanning transmission electron microscopy demonstrated the deposition of AgNPs on the cell membrane, and distribution throughout the cell. In this study, AgNPs seemed to interact with the membrane and the interior of an *E.Coli* bacterium by disrupting its membrane permeability and damaging DNA by interacting with the sulfur and phosphorus groups. The mechanism of AgNPs antimicrobial activities was quite similar to that of silver ions, implying a significant role of released ionic silver by NPs in this property[8]. In light of the antibacterial properties, AgNPs have been used as a novel therapeutic modality to treat burn wounds. Tian et al. (2007) found that AgNPs were able to rapidly heal and improve cosmetic appearance in a wound. On top of their

antimicrobial activities, AgNPs reduced the wound inflammation and modulated fibrogenic cytokines, which all promoted the wound healing process[9]. Research was also conducted to evaluate the functionality of repaired skin. Tensile properties of healed skin were significantly improved and led to better fibril alignments after treatment with AgNPs. The regenerated skin resembled normal skin, due to remarkable alignment of collagen deposition by AgNPs[10]. These results demonstrated a new therapeutic direction for the future development of wound treatment.

Synthesis of AgNPs

AgNPs can be prepared in mainly two routes, top-down and bottom-up. Bulk source materials can be decomposed into NPs by physical forces, and stabilized by capping agents on the surface of produced particles. The size reduction from the top-down method is mainly achieved by mechanical grinding, evaporation/condensation, and more recent technology laser ablation. In bottom-up route, AgNPs can be assembled from silver salts by chemical reduction, and further stabilized by capping agents against decomposition or aggregation. The reduction of ionic Ag into a solid phase can be accomplished in both liquid and gas phases. Recently, several green synthesis strategies have emerged, including biogenic synthesis of AgNPs by bacteria and fungi, and naturally occurring reducing agents such as plant extracts and polysaccharides[6].

Physical Approach

Mechanical grinding is a simple yet cost-effective and high-yielding synthetic approach to produce a large quantity of nanomaterials. High energy ball milling has been used in the synthesis of various nanomaterials, including nanocrystalline magnesium

alloys, and Co_2Si, Ni-NiO nanocomposites [11]. Nanostructured silver was successfully obtained by milling Ag_2O and graphite using mechanochemical reduction. After 22 hr milling at a rotation speed of 450 rpm with 20 mm ball bearings, the size of Ag_2O diminished to the range of 10 nm to 50 nm, producing silver powder of 28 nm on average[12]. Mechanical grinding may be efficient in producing a large quantity of nano-sized materials; this method has one severe limitation which is the significant contamination from the grinding media. If the containers and grinding balls are stainless steel, it's very likely that samples would be contaminated with iron, in particular with the highly energetic mills[11].

Evaporation-condensation utilizes a small ceramic heater in a local heating zone to evaporate source materials (silver) into NPs in a carrier gas. Because of the steep temperature gradient on the heater surface, the evaporated vapor could cool rapidly, forming a high concentration of stable AgNPs between 6-20 nm in geometric mean. This is an advanced method over conventional tube furnace evaporation/condensation technique, for its efficient energy and space use, and rapid establishment of thermal stability[13].

Laser ablation could synthesize NPs by impinging the bulk metallic materials in a liquid medium. Stable AgNP colloidal solutions were synthesized in pure organic solvents by 1,064 nm laser ablation of bulk silver[14]. The efficiency and characteristics of the product was dependent on several parameters, including the type of aqueous media, the wavelength of the laser, frequency of the laser pulses, and ablation duration, presence of certain surfactants. The process did not need any reducing or stabilizing agents, allowing green and pure synthesis of NPs without chemical residuals[15].

Chemical Approach

The most common way to fabricate AgNPs is by chemical reduction of silver salts. Silver salt precursor such as silver nitrate can be reduced to metallic silver by organic and inorganic reducing agents. Several types of silver salt have been used to produce ionic silver. In the review of chemical approaches for nanoparticle synthesis, almost 83% of the research reported the use of silver nitrate as the salt precursor. The prevailing use of $AgNO_3$ is accredited by its low cost and stable chemical properties compared to other available salts. Thus, it is reasonable to monitor the environmental release of AgNPs and NO_3^- from a manufacturing facility, since nitrate is classified as a primary water contaminate by United State Environmental Protection Agency (US EPA)[16]. Reducing agents are chemicals that provide free electrons to silver ions to reduce its +1 valence state to zero to form silver nucleation. It is known that a strong reductant such as borohydride, leads to small monodisperse particles, whereas weaker reductants such as citrate, slowly produce a broader size range of NPs. In the NP synthesis scientific literature, over 23% of the articles reported using $NaBH_4$ as reducing agent, and around 10% with sodium citrate. Other reducing agents accounted for smaller percentages of the synthesis in special applications[16]. Sodium citrate may not be a critical environmental hazardous if released into the water bodies as a byproduct, but NaBH4 may lead to water contamination with borides. The four hydrogen atoms of BH_4^- could also participate in the reduction of other elements in nature.

Use of reducing agents, can not only convert ionic silver to solid silver but also control the growth of solid silver nuclei into desired size and shape. For example, in a study conducted by Bastus et al., citrate-coated AgNPs were synthesized from silver

nitrate by a mixture of trisodium citrate and tannic acid[17]. The sizes of synthesized particles are controllable (from 10 nm to 200 nm) by adjusting reaction parameters such as the concentrations and ratio of the reducing agents. Transmission electron microscopy images confirmed the narrower size distribution of AgNPs when decreasing the tannic acid to sodium citrate ratios. The average particle diameter increased from 13.8 nm to 58 nm following concentration change of tannic from 0.025 mM to 5 mM[17].

It's important to protect the dispersive NPs against agglomeration, for the unique properties of nanomaterials are highly dependent on their size. Selected materials were chosen as stabilizers and conjugated on the NP surface to prevent agglomeration. Popular coating materials are, citrate, polyvinylpyrrolidone, amines, amides, sugars, cetyltrimethylammonium bromide[16]. The coated NPs become more resistant to agglomeration due to electrostatic repulsion or steric exclusion[18]. Depending on the application of the NPs, certain types of stabilizing agent can be used to determine the stability, reactivity, solubility, size and shape of the particles. AgNPs coated polynisopropylacrylamide (PNIPAM) could be utilized in surface plasmon and thermal switching applications, enabled by the temperature-sensitive PNIPAM[16]. The commonly used stabilizers, such as PVP and citrate, usually leave the particles with negative surface charge; with the use of branched polyethyleneimine (BPEI), AgNPs are positively charged with enhanced detection of thiocyanate and perchlorate ions using surface-enhanced Ramon spectroscopy (SERS)[19].

Biological Approach

Due to the possible residuals of toxic reducing chemicals on synthetic AgNPs, some biosynthetic methods using biological organism and green reducing agents have

been reported[20]. AgNPs were recently synthesized using five plant extracts; *Ocimum tenuiflorum*, *Solanum tricobatum*, *Syzygium cumini, Centella asiatica* and *Citrus sinensis*. The size and species of AgNPs were confirmed and characterized by UV-vis spectrophotometer, X-ray diffractometer, atomic force microscopy and scanning electron microscopy. AgNPs reduced from these plant extracts were well dispersed and stable in the colloidal solution, bearing average sizes between 22.3 nm to 65 nm. Additionally, these NPs displayed efficient antimicrobial activity against *S. aureus* (30 mm) and *E. coli* (30 mm)[21]. Extract from green alga *Enteromorpha flexuosa* had synthesized AgNPs at room temperature, which were tested effective against both gram-negative and positive bacteria, and could be used in wastewater treatment[22].

Of the reported AgNPs synthesis methods, 6% of them were achieved with microorganisms such as bacteria and fungi[16]. These microorganisms could grow AgNPs in the presence of silver ions both intracellularly and extracellularly. A bacterial strain isolated from heavy metal-containing soil synthesized AgNPs extracellularly at room temperature. After treatment with 1 mM of $AgNO_3$, within 24 hr AgNPs in 42- 92 nm range were found around the *Bacillus* strain[23]. Exposure of silver ions to fungus *Verticillium* biomass resulted in the formation of AgNPs of (25 ± 12) nm in diameter intracellularly. The fungal cells were not harmed by the silver exposure and could continue to multiply after the treatment[24].

Toxic Effects of AgNPs

Due to the prevalence of AgNPs used as antibacterial agents in consumer and medical products, AgNPs are likely released into the environment from manufacturing facilities; in the medical field, AgNPs have been applied to wound dressings, surgical

instruments, and bone substitute biomaterials, and contact with such materials may lead to AgNPs absorption into body tissues. With the increasing application of AgNPs in industrial settings, their potential adverse effects towards environmental and human health raises significant concern both in the public and science fields. Recently, many papers evaluated the treatment of AgNPs in fish, rodents and mammalian cells and tissue using various toxicity endpoints, both *in vitro* and *in vivo*[3b, 25]. Their environmental fate, the state of form in physiological conditions and interaction with cells, are determined by a series of parameters. As a result, the behavior of AgNPs in physiological and environmental media varies depending on many physicochemical properties such as particles size, shape, surface charge and functional groups.

When AgNPs are introduced into physiological and environmental media, they undergo three main changes. First is the rearrangement or displacement of surface functional groups by the available biological macromolecules or inorganic and organic ions in the medium. This re-establishment of surface coating materials could lead to NPs aggregation, if the new coatings consist of smaller and less charged molecules affording less electrostatic or steric stability. Lastly, exposing the silver core to ambient oxygen molecules or free hydrogens may lead to surface oxidation or dissolution of silver ions. Some compounds, such as sulfide species, dissolved oxygen and chloride, have been shown to have strong affinity for silver atoms and ions, and could transform AgNPs into highly aggregated precipitates, limiting their mobility and bioavailability in biological and environmental media[26].

In the aquatic environment, AgNPs have been reported to have an effect on the fitness and population densities of many vertebrate animals. The main route of AgNPs

entering a fish body is via the gills[27]. When zebrafish were exposed to starch or bovine serum albumin coated AgNPs (TEM size 5-20 nm), they experienced a drop in heart rate, delayed hatching and higher mortality rate. AgNPs were retained in brain, heart, yolk and blood of the embryos after 48 hr treatment at 25 mg/L, determined by TEM imaging[25b]. Scown et al. (2010) treated rainbow trout with AgNPs of various sizes for ten days. They found accumulation of AgNPs in gills, liver and kidney, with significantly decreased liver weight[28]. Similar findings were reported by Farkas et al., that PVP and citrate coated AgNPs accumulated the most in the gills and caused cytotoxicity towards gill epithelium[29].

For individuals, several major exposure routes have been discussed in the literature, including inhalation through respiratory tract, ingestion through gastrointestinal tract, dermal contact and intravenous injection. AgNPs can be taken up by many types of cells following these exposure scenarios; it has become a major concern in toxicological studies of AgNPs. Recent research supports cellular uptake and toxicity of AgNPs relying on several parameters, including the physiochemical properties of the particles, such as size, shape, surface charge and coatings, as well as the exposing conditions, for example, the duration and concentration of exposure scenarios. Gliga et al. exposed BEAS-2B cells to AgNPs of various sizes and various coatings. Uncoated 50 nm AgNPs were found most efficient in cell penetration. Citrate-coated 40 nm AgNPs had more cellular uptake than 10 nm citrate-AgNPs. After 24 hr, 10 nm citrate-AgNPs had close to 25% silver ions fraction, which was the only cytotoxic AgNPs among the group[30]. Results from this study imply that cellular uptake extent may not be an appropriate index for cytotoxicity, as demonstrated by uncoated 50 nm AgNPs with the least toxicity but greatest intracellular

extent. In another work, A549 cells exposed to silver nanowires (100-160 nm in diameter), spherical AgNPs (30 nm), and silver microparticles (< 45 μm), responded differently. Due to the direct contact with the cell membrane rather than cell penetration, nanowires resulted in the strongest cytotoxicity and immunological responses in A549 cells[3d]. Negatively charged AgNPs, due to electrostatic repulsion with the negatively charged cell membrane, were thus less likely taken up and induced less toxicity compared to positively charged NPs[31]. Uptake of AgNPs by human mesenchymal stem cells was found in a concentration-dependent manner, mainly through clathrin-dependent endocytosis and macropinocytosis. AgNPs were found primarily in the endo-lysosomal structures, while larger agglomerates typically occurred in the perinuclear region[32].

Recently, an emerging entity known as the "protein corona" has been considered as a key at the nano-biointerface[33]. When AgNPs enter a biological environment, a layer of assorted biomolecules such as proteins, lipids and peptides adhered to the surface of NPs, forming a NP-protein corona. The composition of protein corona is dependent on the physicochemical properties of NPs, such as the size, surface charge, coatings and shape, and it also correlates to the physiological environment. Due to the formation of protein corona, AgNPs in the new identity with modified surface chemistry have been reported to interact with cells in different manners. For example, protein corona containing albumin or high-density lipoprotein, reduced the cellular uptake and cytotoxicity of AgNPs by activating a cell surface receptor[34]. Hence, physiologically available proteins are particularly important in the biological response towards AgNPs and providing information for related safety concerns.

Toxicity of AgNPs has been observed at both cellular and organic levels, as AgNPs could penetrate cells and translocate to other organs through bloodstream. The toxic effects of AgNPs have been proposed by many studies to be related to the dissolution of ionic silver. Historically, metallic and ionic silver are renowned antimicrobial agents and have been used since the ancient Greek and Roman Empire. Park et al. proposed a Trojan-horse type cytotoxicity mechanism, that AgNPs were phagocytized by cultured RAW264.7 cells in particulate form, and activated cellular apoptosis by ionizing inside the cells[35].

In another study, human lung epithelial cells A549 were treated with AgNP suspensions of two silver ion fractions. When higher concentrations of silver ions were present, there was significant decrease of viability in A549. AgNPs-free supernatant displayed the same toxicity with AgNPs suspensions when carrying the same fraction of silver ion in solution, which was concluded that silver ions in AgNPs played the major role in causing toxic effects on mammalian cells[25c]. AshaRani et al. proposed another mechanism of toxicity[36]. In their study, AgNPs toxicity was not differentiated by forms of silver. After internalization by either endocytosis or passive diffusion, AgNPs induced mitochondrial dysfunction, resulting in an elevated level of reactive oxygen species. Cells undergo oxidative stress, and lead to oxidation of cellular proteins and DNA, along with malfunctions of antioxidant enzymes. The interaction between silver (both particulate and ionic forms) and sulfur-containing macromolecules is particularly important in the toxicity mechanism of AgNPs, due to the strong affinity silver has over sulfur. Apart from these deleterious effects, AgNPs have also been reported to alter the membrane

permeability of mammalian cells[37], deplete glutathione level and trigger the generation of inflammatory markers[35].

There have been a few studies that evaluated the chronic effects of AgNPs following inhalation and ingestion using *in vivo* models. In 2007, Ji et al. published a work testing inhalation toxicity of AgNPs in Sprague-Dawley rats following 28 days exposure. With 1.32×10^6 particles/cm^3 (equivalent to 61 μg/m^3) per day, there were no distinct histopathological changes, nor hematology and blood biochemical values difference resulted from AgNPs[38]. However, when similar experiments were extended to 90 days, the health of Sprague-Dawley rats was significantly affected by 18 nm AgNPs. Both the male and female rats had a dose-dependent increase in bile-duct hyperplasia in the liver. Mixed inflammatory cell infiltration, chronic alveolar inflammation, and small granulomatous lesions were also noted in the histopathological examinations. More AgNPs accumulated in the lungs and liver than other organs following inhalation exposure, and a no observable adverse effect level (NOAEL) of 100 μg/m^3 was recommended based on their evaluation[39]. In another 90-day sub-chronic inhalation study, the genotoxicity of 18 nm AgNPs was evaluated in male and female Sprague-Dawley rats. After the last exposure routine, rats were sacrificed to collect bone marrow cells for micronucleus examination. No significant changes were found in the micronucleated polychromatic erythrocytes compared to the control group, indicating no genetic toxicity of AgNPs to rat bone marrow *in vivo*[3b]. Subchronic oral toxicity of 56 nm AgNPs was tested in F344 rats over 90 days. Rats were given AgNPs at 30 mg/kg, 125 mg/kg or 500 mg/kg daily. At the end of the oral exposure, rats experienced significant drops in body weight, and changes in alkaline phosphatase and cholesterol levels. Again,

bile-duct hyperplasia increased dose dependently, with occasional necrosis, fibrosis, and pigmentation in treated rats. AgNP accumulation was found in all tissues examined, but two-fold higher accumulation were observed in the female rats' kidney compared to the male kidney[40]. In the most recent oral subchronic exposure study completed by Garcia et al. (2016), 20-30 nm PVP coated AgNPs were given orally to male Sprague-Dawley rats at 0, 50, 100 or 200 mg/kg/day over 90 days. It was found that silver was mostly excreted in animal feces, but accumulation still occurred in the ileum, liver, kidneys, brain, thymus and spleen, suggesting translocation of AgNPs through GI tract barrier into other tissues. Also, administration with AgNPs could alter the concentration and distribution of zinc and copper in the brain, kidney, and thymus. Although there was no change in organ weights or mortality, the increased binucleated hepatocytes, proliferating cells and the altered metal homeostasis in various tissues, pointed out the necessity of further chronic studies on the toxicity of AgNPs after oral exposure[41].

Current in Vitro Methods to Study the Translocation of AgNPs

While cellular uptake and acute local toxicity have been routinely evaluated by classical *in vitro* models, a monoculture system lacks the insight and understanding of particle-cell interactions involving the interplay of several cell types. Little information about the efflux or translocation of AgNPs through biological barriers could be gained by monoculture systems[42]. Animal systems, on the other hand, are more valuable in the prediction of the effects to be affected. Several *in vivo* models have noted the distribution and accumulation of NPs following exposure via inhalation, ingestion, dermal contact and intravenous injection. Depending on exposure conditions and the physiochemical properties, NPs could cross the pulmonary, gastrointestinal tract, skin, placenta and brain

barriers, and circulate through the body in the bloodstream. While these animal studies provide information on systemic effects of NPs, the use of animal models has to be reduced. Due to the ethical issues, it is impossible to test all nanomaterials of interest through *in vivo* models. In this regard, several novel *in vitro* co-culture models have been established recently to track the translocation of NPs through biological barriers. With their unique three-dimensional architectures, these models have the advantages of being physiologically relevant as *in vivo* conditions, time and cost efficient for fast screening of toxicities, as well as offering insight on both local and systemic effects at cellular and intracellular levels. Since co-culture models typically only engage cells originated from the human source, they are expected to be more predictive than animal models that typically use rodents.

These *in vitro* co-culture models are commonly constructed with the support of a porous membrane insert. Cells can be grown on both sides of the membrane inserts, to encourage cell-cell communication and simulate important physiological barrier properties. So far, the literature supports the development and usage of such models in the study of NP translocation across the lung barrier, intestinal barrier, skin barrier, and placental barrier. Only limited types of nanomaterials have been studied the translocation potency due to the short development of co-culture models. Therefore, the following review will focus on the relative more established lung and gut models, but not be restricted to AgNPs studies alone.

Lung Barrier Models

The lungs have been one of the major target organs for NPs exposure. They have an overall 100 to 150 m^2 surface area, contributed by the hundreds of millions of end

structures alveoli. Alveolar-capillary region is the major site of gas exchange. With effective thickness only 400 nm to 2 μm, the alveolar-capillary barrier is likely to play a vital role in the absorption of inhaled NPs into systemic blood circulation[43]. Therefore, several *in vitro* models mimicking lung-blood barrier (alveolar-capillary barrier) have emerged. The most commonly used pulmonary epithelial cell lines are A549, Calu-3, H441 and 16HBE14o-. Among these cell lines, A549 and H441 are not able to form tight junctions[44]. Besides differences in cell types, *in vitro* lung barrier models also differ in the culture conditions, submerged or at the air-liquid interface (ALI). Submerged models are less realistic than ALI models mimicking the inhalation exposure. However, they could produce more reproducible data due to relatively more stable and controlled experimental conditions than at the ALI[45].

Co-culture models containing more than one cell type are usually started with lung epithelial cells, and developed into co-culture by adding different cell types. These additional cell types are typically endothelial cells that mimic the microvascular endothelium lining; activated macrophages and mast cells that provide an immunological response to foreign particles in the lung; fibroblasts and dendritic cells that are present at the base of the alveolar epithelium. Only limited types of NPs have been tested on these models, and they are titanium dioxide NPs, quantum dots, polystyrene NPs, cerium dioxide NPs, gold NPs, silica NPs and single-walled carbon nanotubes[45].

Rothen-Rutishauser and coworkers (2005) have been actively using A549, macrophage and dendritic cells for their pulmonary tri-culture models. Human alveolar type II epithelial cells A549 are seeded on the apical side of membrane inserts with macrophage cells, and dendritic cells are seeded on the bottom of the inserts. Both

macrophage and dendritic cells are vital elements of the airway epithelial barrier. After the tri-culture has been constructed, the formation of a polarized epithelium is confirmed by the expression of a tissue-specific protein, E-cadherin. However, the tri-culture system failed to develop high transepithelial resistance (TEER), an indication of a poor intracellular tight junction complex. Polystyrene particles with 1 μm in diameter were administered to the system. After 24 hr, particles were found in all types of cells, although dendritic cells on the bottom of the inserts were not directly exposed to these particles. TEER of the tri-cultures was not decreased upon the exposure to polystyrene particles, suggesting no changes in the properties of tight junctions[46].

A more physiologically relevant tri-culture model was recently published by Dekali et al. In their research, human bronchial epithelial cells Calu-3 were used as the basis of the model, for their high TEER values developed on the membrane inserts. Differentiated Thp-1 macrophage-like cells are cultured together in the apical region of the inserts, and microvascular endothelial cells were grown on the basolateral side. After 9 days in co-culture, the model produces >1000 $\Omega \cdot cm^2$ TEER readings, demonstrating a robust and tight alveolar-capillary barrier. Fluorescent polystyrene nanobeads (primary sizes of 51 and 110 nm, non-functionalized and aminated) were then introduced to the system for the assessment of translocation. All tested nanobeads were detected at the basolateral side of the system, and this translocation has been found to be affected by both the size and surface chemistry. However, no cytotoxicity was observed by any nanobeads in the tri-culture system[44].

Gut Barrier Models

In vitro gut models have been focusing either on the transit of ingested NPs through the dynamically changing gastrointestinal (GI) tract conditions, or on the uptake and translocation of NPs by cellular models. The translocation of NPs through the gastrointestinal wall involves multiple steps. First is the diffusion through the mucus lining, and having contact with epithelium, before finally taken up by cellular or paracellular transport. Human epithelial colorectal cells, Caco-2, are the most commonly used cell type in gut barrier models. To overcome the potential drawback of lacking a mucus layer in Caco-2 monolayers, they are often co-cultured with HT29-MTX cells. The mucus layer in the small intestinal poses a physical barrier to NP deposition. It contains mucin glycoproteins that form viscoelastic gels, and could hinder the selective passage of materials, entrapping NPs at the small intestine and protect Caco-2 from direct exposure to lumen content stimulants[45]. Brun et al. (2014) revealed 5-fold higher TiO2 NPs in the Caco-2/HT29-MTX model than Caco-2 monoculture. These NPs were found mostly by the microvilli lacking HT29-MTX cells, in the cytoplasmic vesicles located close to the apical membrane[47]. NPs that are orally ingested experience various gastric fluids in the GI tract, which could alter their surface chemistry and interaction with cells. It is reasonable to include *in vitro* gastrointestinal digestion of the NPs in the study of intestinal translocation. When polystyrene NPs (PS-NPs) were pre-digested in an *in vitro* gastrointestinal digestion model, translocation for positively and negatively charged NPs were 4-fold higher and 80-fold higher respectively, compared to the pristine (un-digested) particles. The change in translocation efficacy was possibly due to shifts in the

composition of protein corona of PS-NPs. The digestion decreased the presence of high molecular weight proteins and replaced with low molecular weight proteins[48].

Human intestine microfold (M) cells have been co-cultured with epithelial monolayers for their important role in the uptake and translocation of particulate matters. Co-culture of Caco-2 cells and human Raji B lymphocytes trigger the partial conversion of Caco-2 cell into M-cells. AgNPs ranging from 20 nm to 113 nm induced a series of stress responses in intestinal epithelium, including oxidative stress, endoplasmatic stress response and apoptosis[49]. The observed gene expression changes were comparable between AgNPs and silver ions, and it was suggested that the toxic effects of AgNPs were contributed by the dissociated silver ions. Translocation of 20 nm and 30 nm AgNPs did not differ significantly to $AgNO_3$, and the epithelium integrity was not compromised by this process either[49].

CHAPTER THREE

Particle Uptake Efficiency is Significantly Affected by Type of Capping Agent and Cell Line

This chapter published as: Zhang, Fan, Phillip Durham, Christie M. Sayes, Boris L. T. Lau, and Erica D. Bruce. "Particle Uptake Efficiency Is Significantly Affected by Type of Capping Agent and Cell Line." Journal of Applied Toxicology 35, no. 10 (2015): 1114-21. http://dx.doi.org/10.1002/jat.3138.

Abstract

Surface-functionalized AgNPs (AgNPs) are the most deployed engineered nanomaterials in consumer products because of their optical, antibacterial and electrical properties. Almost all engineered NPs are coated with application-specific capping agents (i.e., organic/inorganic ligands on particle surface) to enhance their stability in suspension or increase their biocompatibility for biomedicine. The aim of this study was to investigate the contribution of the selected capping agents to their observed health impacts using realistic dose ranges. AgNPs capped with citrate, polyvinylpyrrolidone (PVP), and tannic acid were studied with human bronchoalveolar carcinoma (A549) and human colon adenocarcinoma (Caco-2) cell lines and compared against exposures to Ag ions. Cellular uptake and cytotoxicity were evaluated up to 24 hr. Tannic acid capped AgNPs induced higher cellular uptake and rate in both cell lines. Citrate-capped and PVP-capped AgNPs behaved similarly over 24 hr. All three of the capped AgNPs penetrated more into the A549 cells than Caco-2 cells. In contrast, the uptake rate of Ag

ions in Caco-2 cells (0.11 ± 0.0001 μg/hr) was higher than A549 cells (0.025 ± 0.00004 μg/hr). The exposure concentration of 3 mg/L is below the EC50 value for all of the AgNPs; therefore, little cytotoxicity was observed in any experiment conducted herein. Exposure of Ag ions, however, interrupted cell membrane integrity and cell proliferation (up to 70% lysed after 24 hr). These findings indicate cellular uptake is dependent on capping agent, and when controlled to realistic exposure concentrations, cellular function is not significantly affected by AgNP exposure.

Short Abstract

AgNPs (AgNPs) capped with citrate, PVP and tannic acid were studied with human bronchoalveolar carcinoma and human colon adenocarcinoma cell lines to investigate the contribution of capping agents to their observed health impacts at realistic dose ranges. Results showed higher cellular uptake and rate from tannic acid capped AgNPs in both cell lines, and no observed toxicity from any type of the AgNPs treatment. Similar doses of silver ions, however, significantly altered cellular functionality.

Key Words

Dosimetry, low dose, A549, Caco-2, kinetics, cytotoxicity

Introduction

Silver is the dominating nanomaterial used in consumer products due to its growing popularity as an antibacterial agent[50]. According to Project on Emerging Nanotechnologies (2014), more than 20% of nano-enabled consumer products are incorporated with silver, including personal care, household and medical products (http://www.nanotechproject.org/cpi). Current production of AgNPs (AgNPs) in US is

estimated to be as high as 20 tons per year[51] and is expected to grow significantly in the coming years. Consequently, exposures to AgNPs are likely to increase in proportion to their production and applications. The novel properties which enable AgNPs to be beneficial may also underlie potent toxic effects, which have created a public debate about the health effects and environmental impact of exposures to AgNPs.

It is estimated that approximately 14% of nanotechnology products could release particles into the air during use[52]. Studies also revealed that these airborne NPs (NPs) can be easily inhaled and deposited in lungs or other organs, posing potential risk on health[53]. In additional to respiratory exposures, NPs may enter the gastrointestinal (GI) tract via contaminated water or food. Inhaled NPs trapped in the mucus of the respiratory tract can also translocate to GI tract[54].

One of the major health concerns is the possible uptake of AgNPs into cells. Studies have shown that NPs can be imported into cells via endocytosis for smaller particles that are less than 120 nm[55]. Previous studies have suggested that biological activities such as cellular uptake and health effects of NPs, are greatly affected by their size, shape[56], and surface charge[57]. Researchers explore novel synthesis methods to control these surface properties by using different capping agents (i.e., selected organic or inorganic materials to serve as stabilizers during the synthesis of engineered AgNPs, also known as stabilizers, coatings, surface functionalization) to gain desired characteristics. Recently, studies on the influence of capping agents on aquatic organisms and mammalian cells have been published[50, 58]. For instance, 300 nm vitamin E polyethylene glycol succinate (TPGS)-coated polymeric NPs were internalized by Caco-2 cells, 1.4 times more than 260 nm polyvinyl alcohol (PVA) NPs[58d]. Toxicity induced by AgNPs is

also dependent on the coating material. Citrate, gum arabic (GA), and PVP-AgNPs (7 nm, 6 nm, and 10 nm respectively) induced significantly different toxicities to Japanese medaka (*Oryzias latipes*)[58b]. Both citrate coated (6 nm) and PVP coated AgNPs (10 and 50 nm) impaired neural cells (PC-12, rat adrenal medulla), but the different potencies and outcomes were combined functions of particle size, coating and release of Ag ions[58a]. Different capping agents enable distinguishing behaviors of AgNPs, and therefore, studies of AgNPs with modified surfaces are relevant and imperative. Moreover, many studies have evaluated acute toxic effects of AgNPs at a relatively high concentration. These concentrations may be less relevant when extrapolating to *in vivo* results in risk assessments, etc. It is thus encouraged to evaluate cellular response to AgNPs at realistic doses for meaningful results, as AgNPs may be trapped in target organs and develop prolonged internal exposure[59].

The overall objective of this work was to develop an understanding about the role of capping agent on the cytotoxicity of AgNPs to different cell lines at low and realistic exposure levels as well as the extent of cellular uptake and of its relation to observed cytotoxic response. We conclude that cellular response after exposure to surface functionalized silver NPs is dependent on the capping agent and vary between cell lines. To examine the effects of uptake by capping agents, AgNPs of same size, shape and concentration, with diverse capping agents, were tested on *in vitro* models with human colon adenocarcinoma (Caco-2) cell line and human bronchoalveolar carcinoma (A549) cell line. Potential toxic effects due to AgNPs exposure were evaluated by checking on several toxicity endpoints including cellular viability, lactate dehydrogenase (LDH) release, and proliferative activity.

Materials and Methods

Description of NPs

Spherical AgNPs (with a core diameter of 50 nm ± 4 nm, based on TEM measurements by the manufacturer) capped with citrate, PVP, and tannic acid in a stock concentration of 1.0 mg/ml (NanoComposix Inc., San Diego, CA, US) were used in this study. Capping agents were chosen based on their commercial availability and their different levels of stability (critical coagulation concentrations are 2.1 mM, 4.9 mM, and 3.7 mM $CaCl_2$ respectively)[60].

Characterization of NPs

Transmission Electron microscopy (TEM). Imaging of the particles were performed as described by Berg et al[61]. Briefly, samples were prepared at 3 ppm in ultrapure (18.2 mΩ/cm^2) water. Five (5) µL of the suspension was deposited onto a copper grid and evaporated before imaging at 100 keV (Hitachi 7000 Analytical Electron Microscope). Average particle diameter was determined using image analysis and ImageJ software by analyzing 250 particles within 20 images.

Dynamic Light Scattering and Zeta-Potential. Measurement of the particle size and electrophoretic mobility were performed as described by[57a]. Briefly, samples were prepared at 3 ppm in DMEM/F12 (media) or ultrapure (18.2 mΩ/cm2) water and incubated at 37°C on an orbital shaker. Samples were analyzed at 0 and 24 hr on Zetasizer Nano ZS (Malvern Instruments, UK). Media samples were analyzed utilizing the diffusion barrier method (i.e., a method in which electrophoretic mobility is minimized in order to produce a more reliable reading) with phosphate buffered saline

(PBS) in clear disposable zeta cells at 37°C[62]. Zeta potential determinations of AgNPs samples suspended in media were obtained at 15V, while AgNPs samples suspended in ultrapure water were measured using 150V. All measurements were conducted in triplet. While performing size and charge measurements in culture medium simulates the physiological conditions where AgNPs interacts with the cell, it is important to note that the techniques do not offer differentiation between "background" particles in the medium and AgNPs. The hydrodynamic diameter and zeta potential values listed in Table 1 were interpreted under the assumption that they represent only the size and charge of AgNPs.

Cell Culture

Human bronchoalveolar carcinoma (A549) and human colon adenocarcinoma (Caco-2) (HTB-37TM) cell lines were obtained from American Type Culture Collection, Manassas, VA (ATCC) and cultured in Dulbecco's modified eagle media nutrient mixture F-12 (DMEM/F12) supplemented with 10% fetal bovine serum (FBS) and 1% penicillin-streptomycin. They were both reported to retain similar properties to type II pulmonary epithelial cells and intestinal epithelial cells[63], respectively, and have been used in numerous toxicological studies as standard *in vitro* models.

Cell Culture Conditions and Doses

Cells were grown in a humid atmosphere with 5% CO_2 at 37°C until 95% confluency was reached, during which medium was changed and cell health and morphology were examined each day. Cells were then inoculated with AgNPs stock solution to achieve a final concentration of 3 mg/L. Incubation was followed until sampling or assay. The concentration used in this study was derived from a model,

estimating proper particle dose for *in vitro* toxicology studies, where surface deposition of particles ranges from 0.185 to 10.69 μg/cm^{-2} in a scenario close to interest [64], and 1.0 μg/cm^{-2} (equivalent to 3 mg/L at 95% confluency) is applied in this work for easy visualization and representation.

Sampling

Samples were collected every 8 hr, for a 24 hr time period. Four flasks of cells were processed in each sampling period, including three replicates and one control for each test condition. First, the media was removed from the flask and kept in a centrifuge tube, which contained the portion of AgNPs that was not taken up by cells. Then, PBS was used to wash the cell surface. Three washes were performed and kept in a fresh centrifuge tube to evaluate the portion of AgNPs adsorbed onto the surface of the cells. Finally, 350 μl cell lysis buffer (Sigma-Aldrich Co., St. Louis, MO, USA) was added, and cells were incubated for 15 minutes, after which culture was scraped from the flask, and transferred to a separate centrifuge tube. The flask was then rinsed three times with PBS and the eluent was added to the same tube, to evaluate the AgNPs internalized by cells. Flasks were evaluated under a microscope following this treatment to ensure cells were completely removed from the flask. Approximately 2 to 2.5 million cells were collected from each sampled flask. Samples were stored in dark at room temperature. Additionally, 100 μL of nitric acid (67%-70%) was added to sample solution to reserve the silver.

ICP-MS Analysis

Digestion. Samples were subject to digestion with 5 ml of concentrated nitric acid (67-70%) and heated at 105°C for 12 hr to completely dissolve the particulate silver. After digestion, samples were diluted by a factor of 12 with Milli-Q water (18.2 mΩ/cm^2) at 25°C, (Millipore Corporation, Billerica, MA, USA) to minimize the matrix interference when analyzed by ICP-MS (PerkinElmer SCIEX, ICP Mass Spectrometer ELAN 9000).

Centrifugation. To differentiate ionic and particulate Ag in test conditions, samples were directly centrifuged without digestion, using an ultra-performance centrifuge Beckman-JA25.50 (Beckman Coulter, Inc., Brea, CA, USA) at 20,000 rpm for 30 min, and supernatant were collected carefully without disturbing the pellet. The supernatant was then diluted and analyzed for ionic silver by ICP-MS.

Toxicity Tests

Viability. 5-Carboxyfluorescein Diacetate, Acetoxymethyl Ester (5-CFDA, AM, Molecular Probes®, Invitrogen) was dissolved in DMSO to a stock solution of 4 mM, which was further diluted 1000 times in ACAS medium (phenol red free, serum free) as a working solution (4 µM). Following 24 hr of incubation at 37°C with the test AgNPs, the medium was removed and cultures were washed twice with PBS (with $CaCl_2$). 5-CFDA, AM working solution (100 µL/well) was added to cells. After 30 min of incubation at 37°C, medium was replaced, followed by two washes with ACAS medium to remove the excess dye. Finally, fluorescence was measured at 485 nm excitation/535 nm emission using a fluorescence plate reader (Fluoroskan Ascent FL Microplate Fluorometer,

Thermo Scientific). Assay was verified with 5% DMSO dosing as positive control and Milli-Q water as negative control.

Lactate Dehydrogenase (LDH). Cell membrane integrity was evaluated by measuring extracellular LDH activity (OPS Diagnostics, Lebanon, NJ). Cells were exposed to AgNPs the same way as for the viability assay mentioned previously. After incubation with the indicated AgNPs for 24 hr, cell culture medium was collected for the quantification of LDH in the supernatant using LDH reagents. Briefly, 150 µl of LDH reagent and 50 µl of culture medium were mixed in each well followed by subsequent incubation for 5 min at room temperature. Fifty (50) µl of LDH stop solution was then added to each well. Optical intensity was then read at 490 nm on a microplate reader (ELx800, Biotek). Assay was validated using 2% Triton-X solution as positive control and Milli-Q water as negative control.

Proliferation. Proliferative activity of AgNPs-treated cells was evaluated using Janus Green B dye (Sigma-Aldrich, St. Louis, MO). This is an exclusion dye, which only stains mitochondria and nuclei of damaged cells. Cells were prepared and treated the same way as viability assay. For the assay, culture was washed twice with PBS, followed by one minute fixation with absolute ethanol. Culture was then subjected to one minute staining by Janus Green B dye solution and twice PBS wash to remove the excess dye. Then the encapsulated dye from these cells was extracted with absolute ethanol, and an additional part of water was added to each well to maintain samples. Optical intensity was then read at 630 nm on a microplate reader (ELx800, Biotek). Janus Green gives intensive staining of the nuclei with light staining of the cytoplasm, thus outlining cells

clearly. Therefore, morphologic changes of cells were screened after the assay using an inverted microscope (Axio Observer A1, Zeiss).

Results

Characterization of AgNPs

When examined under TEM, all AgNPs were homogeneous and roughly spherical within the anticipated size range (Figure A.1). Only PVP-AgNPs showed a bimodal distribution with small particles attached on the surface of the large particles (Figure A.2). Citrate-AgNPs were found to have diameters of 49.1 ± 5.5 nm, very similar to the reported size from manufacturer. Both PVP- and tannic-AgNPs were smaller in size from in-house measurements, compared to manufacturer reported measurements (Table 3.1). AgNPs in original suspension range in pH from 7.3 to 8.5, but when mixed in culture medium, they were immediately neutralized by the vast medium body of pH 7.25 to pH ranging from 7.3-7.5 (Table 3.1). Aggregation behavior of AgNPs in test medium was also affected by capping agents. PVP-AgNPs were close to the initial hydrodynamic diameters (HDD) both in ultrapure water and medium after 24 hr incubation. Citrate- and tannic-AgNPs formed aggregates (HDD 190 nm) in medium, significantly larger than the primary NPs, while their HDDs remained almost unchanged in ultrapure water. Unlike the highly negative zeta potential (-55.6 ± 1.04 mV) reported by the manufacturer, citrate-AgNPs were found to be the least negative (-37.2 ± 0.8 mV) in zeta potential among three tested AgNPs. Zeta potential of AgNPs became significantly more negative in water compared to medium (-40 mV vs -10 mV). Over time, surface charge tended to become weaker in both water and medium.

Table 3.1. Characterization of AgNPs by manufacturer and measured in-house.

Characterization reported by manufacturer						
Capping agent	Citrate		PVP		Tannic Acid	
Primary particle diameter (nm)	49.1 ± 4.5		53.4 ± 5.0		53.5 ± 4.1	
Zeta potential (mV)	-55.6 ± 1.04		-30.6 ± 0.57		-54.7 ± 1.5	
pH in aqueous solvent	7.8		8.5		7.3	
Characterization measured in-house						
Capping agent	Citrate		PVP		Tannic Acid	
Primary particle diameter measured by TEM (nm)	49.1 ± 5.5		45.4 ± 6.3		49.8 ± 5.7	
pH in media	7.3		7.5		7.3	
Diameter measured by DLS (HDD, nm)	Water	Media	Water	Media	Water	Media
0 hr	54.1 ± 0.8	120.1 ± 1.8	72.0 ± 2.0	67.1 ± 2.3	58.8 ± 1.1	133.9 ± 10.3
24 hr	54.6 ± 1.9	194.5 ± 7.7	64.3 ± 3.6	69.2 ± 1.3	56.2 ± 1.9	189.6 ± 9.0
Zeta potential (mV)	Water	Media	Water	Media	Water	Media
0 hr	-37.2 ± 0.8	-10.5 ± 0.6	-43.5 ± 0.9	-9.5 ± 0.5	-48.3 ± 2.1	-11.2 ± 0.7
24 hr	-26.6 ± 3.7	-9.9 ± 0.4	-42.9 ± 2.4	-9.6 ± 1.2	-32.3 ± 1.4	-10.4 ± 0.6

Data are presented as mean ± standard deviation of three replicates.

Cellular Uptake of AgNPs

The internalization of three types of AgNPs within A549 and Caco-2 cells was measured up to 24 hours of exposure and the results are shown in Figure 3.1. The uptake rate was only determined at 24 hr using linear regression model.

When A549 cells were exposed to these AgNPs, up to 2.6 µg (11%) of total silver was found intracellularly in the first 8 hr of exposure (Figure 3.1 A). In the next 16 hr, two distinct scenarios were observed. While intracellular citrate- and PVP-capped AgNPs levels remained constant, tannic-AgNPs were constantly internalized by cells, and resulted in an overall 25 ± 0.51 % of AgNPs internalized by A549. The uptake rate for tannic-AgNPs was 0.2495 µg/hr, two times faster than citrate- and PVP-AgNPs at 0.0871

and 0.0986 μg/hr respectively. Ag ions were able to cross cell membrane steadily at 0.0238 μg/hr, with a final uptake of 2.4 ± 0.06 % at 24 hr.

When Caco-2 cells were exposed to AgNPs, differences in uptake extent and rate were observed (Figure 3.1 B). Tannic-AgNPs were internalized faster than other AgNPs in the first 16 hours. They were constantly internalized by Caco-2 cells, until the last 8 hr of exposure, when the net Ag concentration remained unchanged with an uptake rate of 0.935 μg/hr. Citrate- and PVP-AgNPs behaved similarly in this condition. They were slowly but continuously internalized by Caco-2 cells for the first 16 hr, and the net uptake was similar to tannic-AgNPs at 24 hr at rates 0.078 and 0.0622 μg/hr (citrate- and PVP-AgNPs respectively). Interestingly, all type of AgNPs showed a slower and lower uptake (as much as 15%) in Caco-2 cells than A549 cells, with the exception of Ag^+ where silver content kept climbing over the experimental period, and close to 11% of ionic silver was found intracellularly at an uptake rate of 0.1045 μg/hr, faster and higher than both citrate- and PVP-AgNPs.

To further explain the uptake results, spatial distribution of AgNPs in the culture system at 24 hours is shown in Figure 3.2. Across the three types of AgNPs, as much as 70% to 85% of the particles remained in the media, and the amount of AgNPs in media corresponded well with the uptake data. For instance, tannic-AgNPs had the highest cellular contents of all tested AgNPs, and they were the least abundant in the cell media. On average, 4% of AgNPs were found to be adsorbed on the cell membrane, and the extent did not change significantly over time regardless of capping agent (Figure A.3). It seems that they had reached an equilibrium right after the contact of AgNPs with cell

membrane, and the amount of adsorbed AgNPs did not differ. The remainder 8 to 25% of AgNPs was identified to be internalized by cells.

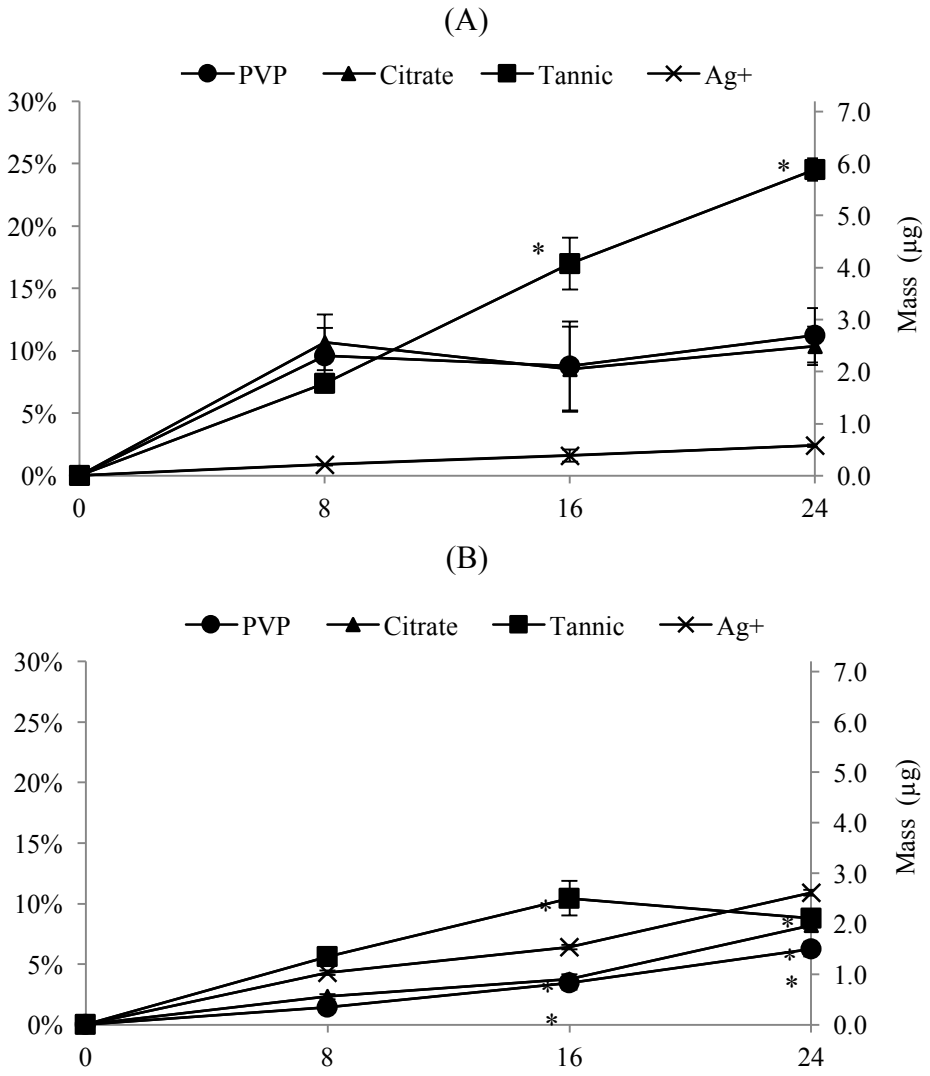

Figure 3.1. The cellular uptake kinetics of AgNPs with three capping agents by (A) A549 and (B) Caco-2 cell lines during 24 hr exposure. Data were presented as mean values ± SD. *p* values indicate statistical significance, where * $p < 0.05$ when compared to 8 h same type of capping agent. See Figures 2 and A.3 for significance between different capping agents at the same testing time. Significance between particulate and ionic silver is not shown.

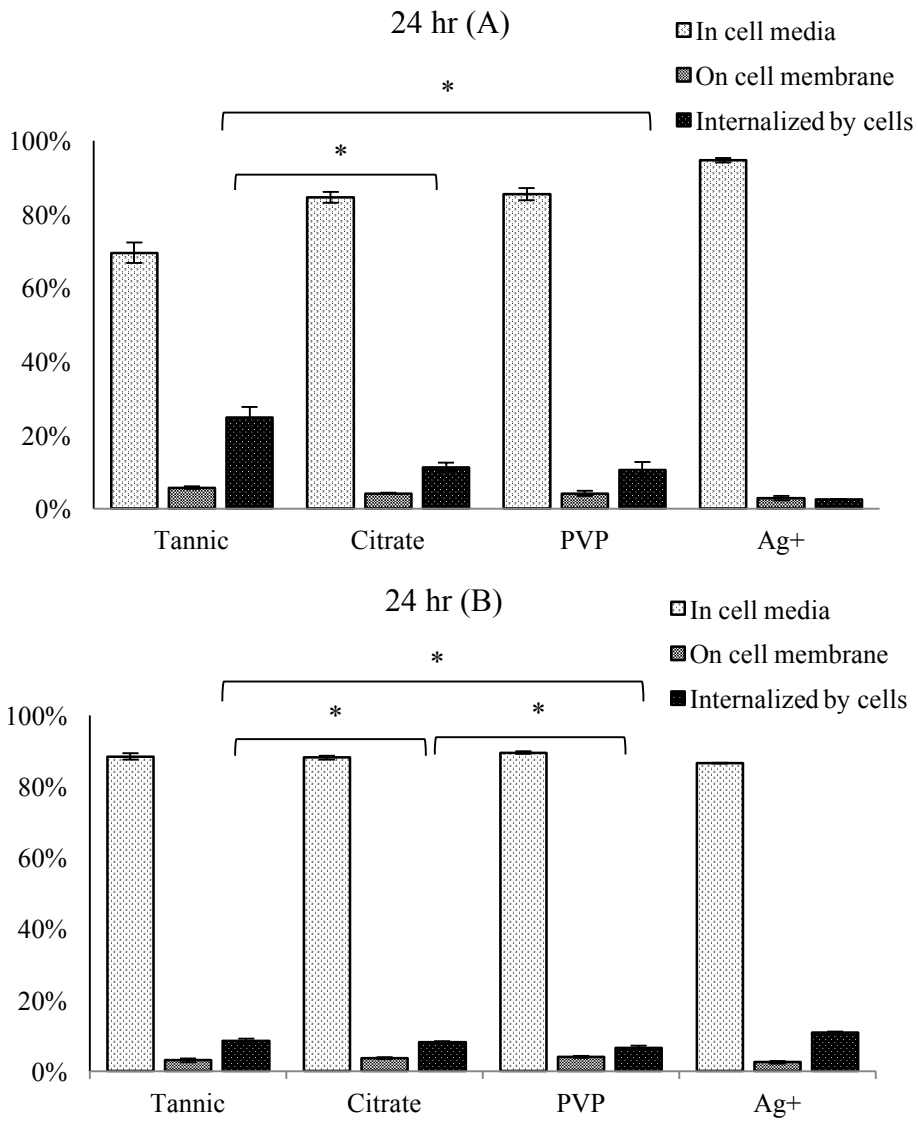

Figure 3.2. Spatial distribution of AgNPs in (A) A549 and (B) Caco-2 at 24 h. Data were presented as mean values ± SD. *p* values indicate statistical significance, which was accepted when $p < 0.05$. Significance between particulate and ionic silver is not shown.

Determination of Ionic Silver

Although AgNPs are stabilized by capping agents, when in cell culture media and contact with cells, many factors may disrupt their stability and lead to aggregation/dissolution. To differentiate the form of silver and understand the role of ionic silver in cellular toxic effects, A549 samples collected at 24 hr were subjected to

centrifugation prior to analysis. Both intracellular and extracellular ionic silver were presented in Table 3.2. Overall, greater proportion of AgNPs dissolved into ions in the media than those presented inside the cells. Among the tested AgNPs, PVP-AgNPs was more susceptible to dissolution in media.

Table 3.2. Ionic silver in A549 cells at 24 h.

	Intracellular	Extracellular
	Ag^+/Total Ag (%)	
Tannic	7.07 ± 0.868	16.9 ± 2.12
Citrate	10.8 ± 0.333	14.6 ± 0.812
PVP	9.99 ± 0.955	21.1 ± 0.353

Data are presented as mean ± standard deviation of three replicates.

Toxicity Assays

Several toxicity assays were performed to evaluate the potential hazardous effects elicited by the internalized AgNPs. One of the routinely used approaches to probe cellular viability is the CFDA-AM assay, which is a quantitative fluormetric assay. Living cells have the essential cytoplasmic milieu that is needed to support the conversion of the non-polar, nonfluorescent CFDA-AM to the polar, fluorescent dye, carboxyfluorescein (CF)[65]. The cell viabilities after 24 h exposure to tested materials were shown in Figure 3.3. In both cell types, cell viability slightly decreased by 2% when treated with citrate-AgNPs, and increased by 5% with PVP-AgNPs, though none of the changes were statistically significant. Overall, no significant deduction of viability was observed post 24 hr exposure with AgNPs (Figure 3.3). Treated cells were similarly viable as control cells. Though the uptake rate and extent differed among AgNPs, they did not alter cellular viability to a significant level. However, cells treated with Ag^+ were significantly

damaged. Ag ions were more potent in reducing cellular viability of A549 cells than Caco-2 cells, despite of the fact that Caco-2 cells had greater uptake.

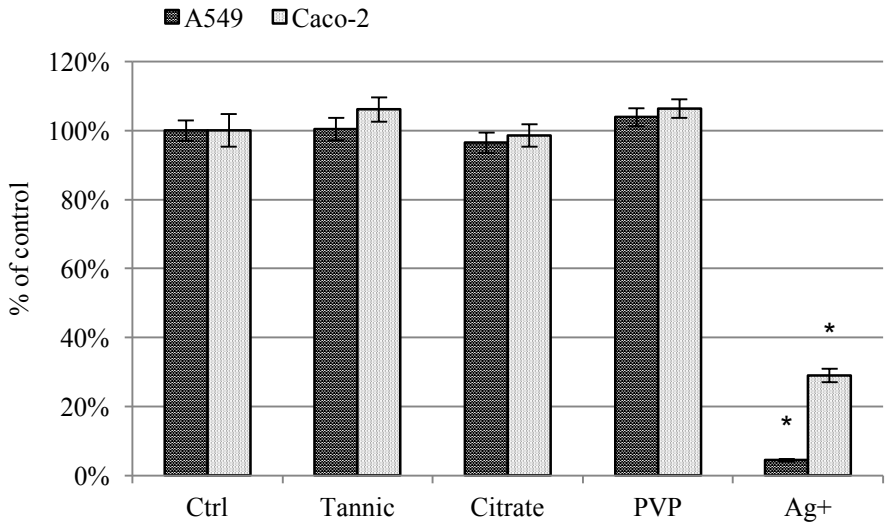

Figure 3.3. Viability for A549 and Caco-2 using CFDA, AM fluorescence dye. Student t-test was applied for statistical analysis. Data were presented as mean values ± SEM (standard error of mean). *p* values indicate statistical significance, where * $p < 0.05$.

LDH is an enzyme in the cytosol. It is released when a cell dies and membrane integrity fails. The amount of released LDH can be used as a parameter to monitor cell death and disruption. When cells were treated with AgNPs, LDH activity was not detected in the culture medium. Regardless of cell types and treatment, cell membranes were capable of maintaining LDH intracellularly, indicating negligible cell death and membrane disruption (Figure 3.4). Cell membrane integrity in both A549 and Caco-2 was compromised by Ag ions, and A549 to a larger extent.

Cellular growth activity after AgNPs treatment was assessed by Janus Green proliferation assay. Cells were exposed to all tested AgNPs as well as Ag ions for comparison. After 24 hr exposure, cell population of AgNPs-treated groups did not decline compared to control groups irrespective of cell type, indicating negligible impacts

of AgNPs on cell proliferation. In contrast, Ag ions inhibited cell growth pronouncedly. Cell population was significantly reduced by nearly 40 and 70 % in A549 and Caco-2, respectively (Figure 3.5).

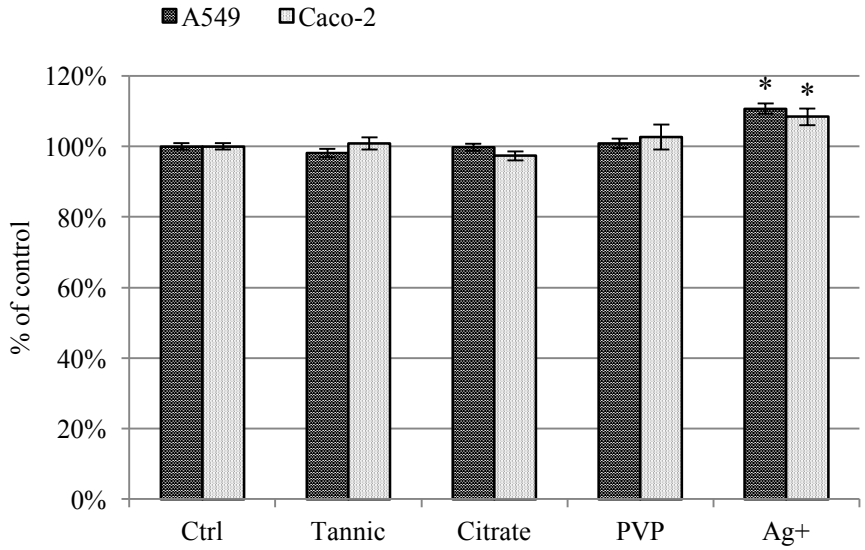

Figure 3.4. Extracellular LDH activity in A549 and Caco-2. Student t-test was applied for statistical analysis. Data were presented as mean values ± SEM. *p* values indicate statistical significance, where * $p < 0.05$.

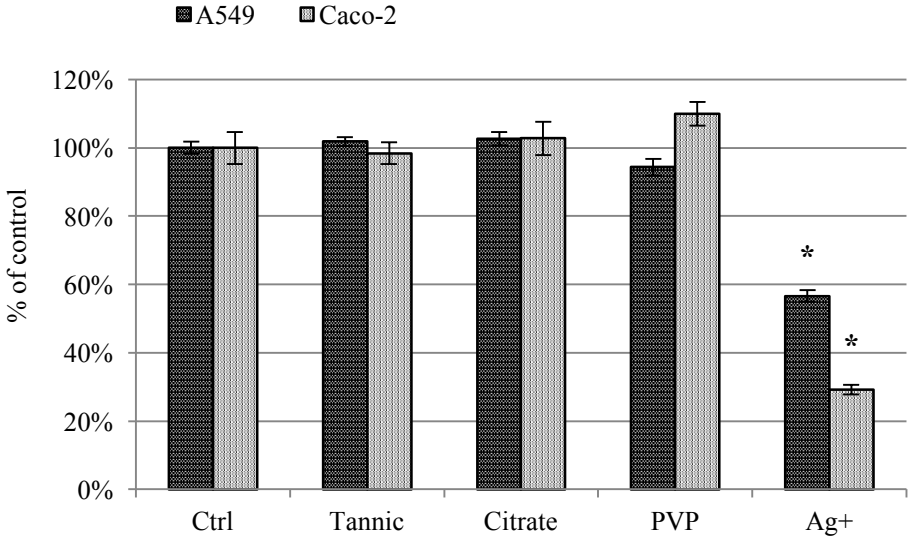

Figure 3.5. Proliferation for A549 and Caco-2 using Janus Green B dye. Student t-test was applied for statistical analysis. Data were presented as mean values ± SEM. *p* values indicate statistical significance, where * $p < 0.05$.

Cell morphological changes usually lead to changes in function; in turn functional changes affect cell structure and morphologies[66]. Hence, cell morphology was examined at the end of proliferation assay, when cells were stained by Janus Green B dye and individual cells were clearly seen (Figure 3.6). In accordance with the findings from previous toxicity tests, AgNPs-treated cells looked similarly to control group, irrespectively of cell or capping agent type. Cell body was stretchy but full, with well-defined membrane and sharp boundaries between each other for A549 cells. In contrast, cells treated with Ag ions had dark round nuclei in the center, with blurry boundaries between cells. Cells were shrunk and light in the cytosol, while some of the membranes were not intact. Caco-2 cells were most lysed after treated by Ag ions, cell debris attached on the well, and no sight of intact cells.

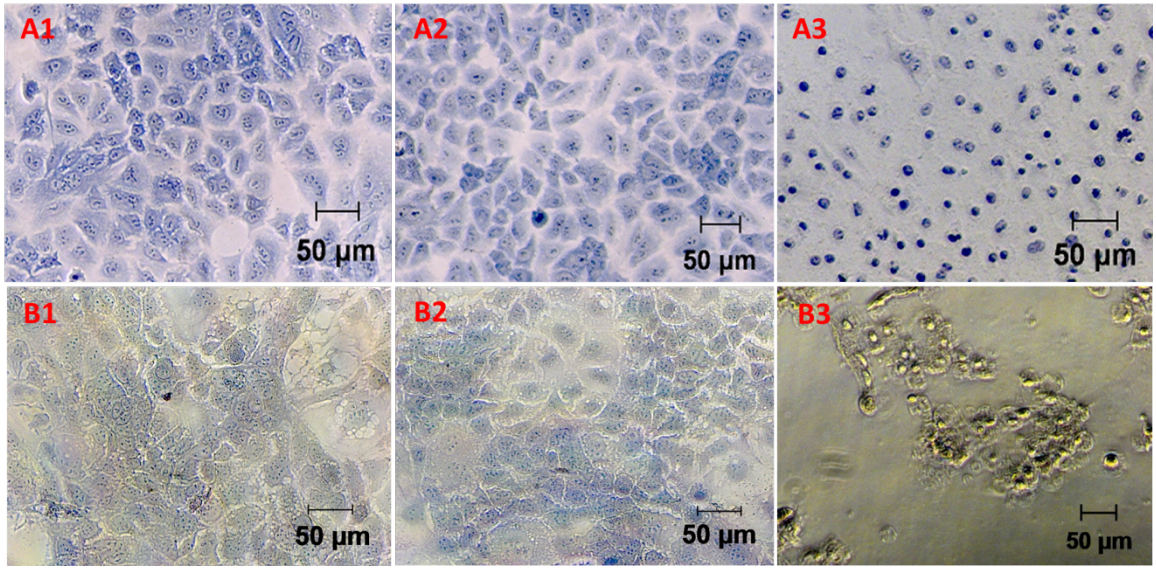

Figure 3.6. Images of A549 (A1 to A3) and Caco-2 (B1 to B3) after Janus Green B stain of the proliferation assay. A1 and B1 are images of control cells. A2 and B2 exemplify images of AgNPs treated cells. A3 and B3 are images of cells treated with Ag ions.

Discussion

Silver Nanoparticle Characterization

Once introduced into the biological environment, NPs encounter bio-macromolecules and changes in pH and salinity, which may alter their surface characteristics and affect the stability[67]. For NPs like PVP-AgNPs, they are more likely to stay in suspension and interact with cells due to their small size. Those tending to aggregate like citrate- and tannic- AgNPs, they have less mobility. Therefore, the rate and extent of aggregation of AgNPs greatly affect their distribution in the system and availability for cellular uptake. HDD results in Table 3.1 are generally in agreement with literature findings that citrate is a relatively weak capping agent in maintaining AgNPs size[50], and PVP is a stronger capping agent.

Both citrate and tannic acid provide AgNPs stability by electrostatic forces. PVP provides stability for the NPs by electrosteric forces [68]. The stronger stability of PVP-AgNPs could be explained by the steric repulsion from the large (average molecular weight 10 kDa), non-charged PVP polymers[60b]. When in medium, AgNPs have weaker negative charge than in water (with the exception of citrate-AgNPs), possibly because of the effects of charge screening/neutralization by the ionic strength of the medium (199 mM) and the concentration of serum proteins in the medium (10% FBS)[60b].

Interestingly, PVP-AgNPs showed a bimodal distribution, with small particles (approximately 10 nm in diameter) attaching on the surface of large particles (Figure A.2). Ruling out the possibility of contamination during synthesis by manufacturer, other research have shown evidence of a mechanism that over time, Ag ions dissociate from

the particle core and re-deposit over time in an equilibrium manner onto the surface of the parent particle as a polar body[69].

Cellular Uptake

As the incorporation of capping agents can change the surface chemistry (e.g., surface charge, hydrophobicity and chemical functionality) of AgNPs which can exert variable biological impacts, we compared the effects of three types of AgNPs (citrate, PVP, and tannic), on cellular uptake kinetic, extent and potential toxicity using human lung and colon epithelial cell lines.

A549 are type II pulmonary epithelial cells that can secrete pulmonary surfactant, a complex mixture consisted of 90% lipids and a small portion of proteins (10%), pulmonary surfactant associated proteins (SPs): SP-A, -B, -C and –D [70]. It seems to indicate that the higher uptake level observed from A549 (Figures 1 and 2) was perhaps due to the presence of pulmonary surfactant, since it would be the first biological surface AgNPs encountered on the alveolar epithelium. Ruge et al., found that SP-A treated magnetite NPs (110 - 180 nm) had increased cellular binding and uptake, indicating SP-A forms a more effective protein coating on NPs and associates NPs to cell membrane for subsequent translocation[71]. This finding could also help explain the differential uptake extents exhibited by AgNPs with different capping materials. The surface chemistry greatly affected the extent and composition of protein adsorption, which in turn affected the SP-A efficacy in bringing AgNPs to cell membrane. For instance, although highly negative in surface charge, the three types of AgNPs possess different stability in media. Regardless of its smaller molecular weight (189 g/mol) and easier displacement by other molecules in the media[50], citrate-AgNPs internalized similarly to PVP-AgNPs possibly

due to the similar composition and/or quantity of protein coating that camouflaged AgNPs, to be recognized equally by cells. The layer of proteins on AgNPs surface could have also influenced on other particles characteristics, such as aggregate size and surface charge which minimized the distinction between the two AgNPs.

Unlike the impotent uptake of AgNPs in Caco-2, Ag^+ vigorously crossed cell membrane, and was lastly more abundant than most of the AgNPs, and three times of that in A549 (Figures 3.1 and 3.2). The greater Ag^+ extent in Caco-2 cells could possibly due to the presence of finger-like microvilli structures on the apical side of Caco-2 cells, which prominently enlarged the surface area and enhanced ion absorption across the membrane[63b].

Toxicity Tests

To date, many studies have evaluated acute toxicity effects of AgNPs and provided evidence that AgNPs, in a range of sizes, are highly toxic to mammalian cells, causing cellular damage including reactive oxygen species generation, inflammatory response, cell membrane rupture and DNA/RNA damage. Previous study of PVP-coated AgNPs on A549 cells (human bronchoalveolar carcinoma) showed dose-dependent cellular cytotoxicity, including early apoptosis, mitochondrial damage and DNA damage[3c]. Similar results were obtained when researchers examined the cytotoxicity and genotoxicity of starch-coated AgNPs on human lung fibroblast cells and human glioblastoma cells[72]. The uptake of citrate-coated AgNPs by rainbow trout gill cells was observed, and significant reduction in viability in terms of membrane integrity and oxidative stress were detected[29]. Additionally, in-vitro studies have documented toxicological effects, with AgNPs being reported to be toxic to rat liver (BRL 3A) cells

by increasing the formation of reactive oxygen species[73] and to be genotoxic to human lung fibroblast cells (IMR-90) and human hepatoma cells (HepG2)[74]. Though many of these toxic effects were striking, they were evaluated in acute toxicity tests at relatively high doses. The safety of AgNPs remains to be tested at a more realistic dose. In this study, internalized AgNPs were identified and carefully quantified in both cell lines, demonstrating that even at low dose exposure scenario; AgNPs can enter the cells regardless of cell type and surface. Interestingly, although the uptake amount varied, cellular viability, extracellular LDH activity, proliferation and morphology were all normal compared to control groups (Figures 3.3 to 3.6), indicating no observable adverse effects resulting from AgNPs treatment over 24 hours. The negligible cell damage may be due to the low dosage (3 mg/L) used in the study, since the toxic effects of AgNPs have been observed in a dose-dependent manner (0-20 μg/ml) [3c] and EC50 values of tested AgNPs range from 40 to 240 μg/ml (Figure A.4). Other than the minor effects of AgNPs reported here, Foldbjerg et al. observed cytotoxicity and genotoxicity of citrate- and PVP-AgNPs starting at 2.5 μg/ml in A549. One possible reason that could account for the opposite effects is the size and shape of AgNPs in the two studies. Foldbjerg et al. used AgNPs of TEM size 69 ± 3 nm, described as less spherical with slightly elongated shape, and our particles, as previously mentioned, were 50 ± 4 nm and spherical in shape. This highlighted the significant role of size and shape of AgNPs in biological activities.

The toxic effects of AgNPs were proposed to be related to the release of ionic silver. Limbach et al., suggested AgNPs acted in a “Trojan-horse” like mode where cells internalize particulate silver, and the subsequent intracellular liberation of Ag ions contributed to the dysfunction of cells [75]. Beer et al. also revealed ionic silver contributed

most of AgNPs toxicity when the Ag^+ fractions were more than 5.5 % of AgNPs suspension, indicating important toxicity role of ionic silver [25c]. Accordingly, dissolution activity of each type of AgNPs in A549 was examined to facilitate the explanation of minor damage expressed by cells. The detected Ag^+ fractions were over 5.5% of total silver in all three AgNPs (Table 3.2), but it did not affect cell function to a significant level at the concentration used in this study. Since the uptake of Ag ions was as little as 2.4 ± 0.06 %, and all AgNPs had higher concentration of ionic silver (15-20%, Table 3.2), it seems that majority of the free Ag ions found intracellularly were likely to be liberated from the internalized AgNPs, as described by Limbach et al. While a small amount of Ag ions were able to pass through membrane, uptake of silver was mainly in the form of particulates.

Overall, we concluded that at the tested doses, AgNPs can enter the two cell lines (A549 and Caco-2), and the efficiency is greatly affected by type of capping agent of the particles. Although they differ in surface chemistry when manufactured, AgNPs can behave similarly, interacting with cells possibly through proteins formed on the surface of AgNPs. AgNPs do not elicit cytotoxic effects. Cellular viability, LDH release and proliferative activity were not compromised after treatment of any of the tested AgNPs. In contrast, same dose of Ag ions greatly violated cellular functionality, and was lethal to both A549 and Caco-2 cell lines. These data suggested that AgNPs may not induce adverse effects on living cells despite the minor internalization at occupational and incidental exposure levels. In light of our findings, we also suggest that researchers discreetly choose the experimental doses for future *in vitro* toxicological studies that represent the exposure levels of humans to NPs for appropriate risk evaluation. Future

investigation on surface protein characterization will enable a better understanding of cell-NP interactions.

Supplementary Data

Additional figures including TEM images of AgNPs, spatial distribution of AgNPs at 8 hr and 16 hr, as well as dose response toxicity tests are presented. Supplementary data are available online at http://toxsci.oxfordjournals.org/.

Funding Information

This work was supported by C. Gus Glasscock, Jr., endowed fund for excellence in environmental sciences in the College of Arts and Sciences by Baylor University, USA.

Acknowledgements

The authors would like to thank the Molecular Biosciences Center and Mass Spectrometry Center at Baylor University for access to their instrumentations.

CHAPTER FOUR

Non-Specific Interactions between Soluble Proteins and Lipids Induce Irreversible Changes in the Properties of Lipid Bilayers

This chapter published as: Ruggeri, F.; Zhang, F.; Lind, T.; Bruce, E. D.; Lau, B. L. T.; Cardenas, M., Non-specific interactions between soluble proteins and lipids induce irreversible changes in the properties of lipid bilayers. *Soft Matter* **2013,** *9* (16), 4219-4226.

Abstract

Soluble proteins in the extracellular matrix experience a crowded environment. However, most of biophysical studies performed to date focus on proteins concentrations within the dilute regime (well below mM range). Here, we systematically studied the interaction of model cell membrane systems (Giant Unilamellar Vesicles and Supported Lipid Bilayer) with soluble globular proteins, Bovine Serum Albumin, Hemoglobin and Lysozyme at physiological relevant concentrations. To mimic the extracellular environment more closely, we also used Fetal Bovine Serum as a good representative of biomimetic protein mixture. We found that regardless of the protein used (and thus of their biological function), the interactions between a model cell membrane and these proteins are determined by their physico-chemical characteristics, mainly their dipolar character. In this paper we discuss the specificity and reversibility of these interactions and their potential implications on the living cells.

Key Words

Protein-lipid interactions, Quartz Crystal Microbalance with Dissipation, fluorescence microscopy, model cell system, macromolecular crowding, labeling

Introduction

The extracellular matrix is a crowded environment where a wide variety of biomacromolecules coexist, including collagen, fibronectin and proteoglycans[76]. Earlier it was shown that increasing the protein concentration by using crowding agents can dramatically affect the mobility[77] and folding[78] of proteins. Despite of this, dilute conditions are often used in biophysical and biochemical studies precisely in the aim of avoiding intermolecular interactions for simpler data interpretation. For instance, monolayer saturation of globular proteins (e.g., Bovine Serum Albumin, BSA) on solid surfaces typically occurs at ~ 50 nM[79] and thus little attention has been paid to interfacial processes occurring at higher protein concentrations (> mM) where non-specific[80] protein-protein and protein-lipid interactions may take place. This is quite surprising given that both Fetal Bovine Serum (FBS) and BSA are commonly used in cell culture medium or as blocking agent for molecular diagnostics[81] at a concentration of 1-10 volume%[82]. Therefore, there is a need for deeper understanding of protein-lipid behavior in experimental systems that mimic physiological conditions more closely[83]. The mM concentration regime for soluble proteins is of high biological relevance given that in plasma, a good example of biological medium, the concentration of albumin and Hemoglobin are ~ 0.75 mM[84] and 0.15[85] - 2.0 mM[86] respectively.

In this work, we focused on determining the effect of soluble proteins at concentrations closer to their physiological levels on the properties of model cell

membranes. These chosen protein concentrations were close to the dilute to semi-dilute regime limit for small globular proteins in solution, which occurs at ~ 19 mM to 81 mM (3.4-5.5 nm in diameter), and thus we expect stronger effects due to inter-protein interactions. The semi-dilute regime for a polymer starts at a critical concentration defined as the monomer concentration that is smaller than the solvent concentration but higher than the overlapping concentration[87]. As model proteins, we used the most abundant protein in plasma (BSA) and two other globular proteins[88] that either carry similar net charge (Hemoglobin)[89] or opposite charge (Lysozyme)[90] to BSA (for physical chemical properties of the proteins used see Table 4.1). We also used FBS since it represents a good model of native extracellular protein mixture.

As model cell membranes system, we used either giant uni-lamellar vesicles (GUV) or supported lipid bilayers (SLB). Using Fluorescence Microscopy and GUV, we assessed major changes in the vesicle structure and/or permeability against a soluble dye[91] while Quartz Crystal Microbalance with Dissipation monitoring (QCM-D) and SLB allowed us to follow protein adsorption and the degree of binding reversibility. We used two different types of lipid membranes that were either negatively charged (containing both 1-palmitoyl-2-oleoyl-sn-glycero-3-phosphocholine, POPC, and 1-palmitoyl-2-oleoyl-sn-glycero-3-phosphoglycerol, POPG) or neutral (containing POPC only) at pseudo-physiological conditions (pH and salt concentration). Our results indicate that soluble proteins can induce major rearrangement on model cell membrane at relatively high protein concentrations mainly due to partially reversible binding of proteins to the lipid bilayers at high bulk protein concentrations. In this paper we discussed the specificity and reversibility of these interactions and their potential implications on the

living cells. We show initial data suggesting that glycosylation in lipids have the additional role of restricting unspecific protein binding or at least limits the protein non-specific binding effect on the permeability of lipid bilayers.

Table 4.1. Characteristics of proteins in terms of molecular weight, zeta potential and average hydrodynamic diameter.

Protein used in this work	Molecular Weight [kDa]	Zeta-potential [mV]	Hydrodynamic Diameter [nm]
BSA	66.5	-11.37 ± 0.96	6.8[92]
Hemoglobin	64.5	-2.14 ± 0.90	5.5[93]
Lysozyme	14.3	2.59 ± 0.30	4.2[92]
FBS	NA	-9.05 ± 0.99	NA

*BSA, Hemoglobin and Lysozyme were measured at 1 mM, and FBS 1% in PBS solvent. Zeta potential data were reported as average ± standard deviation of six replicates.

Results

Effect of Proteins Co-addition on the Permeability of Giant Unilamellar Vesicles

Wide-field fluorescence microscopy experiments were performed to characterize the effect of various proteins on the permeability of lipid membrane against eventual leakage of the soluble dye (Alexa 488) encapsulated in the GUV's lumen. The vesicles carried either a neutral (POPC only) or a net negative charge (POPC/POPG). Furthermore, any major change in the conformation of the lipid bilayers was visualized using $DiIC_{18}(5)$ as a lipid dye. Table 4.2 presents the minimum protein concentrations required to induce contained dye leakage in at least 5% of the vesicles within one hour upon exposure to the proteins. Figure 4.1 A exemplifies the leakage events occurred for negatively charged vesicles in the presence of Hemoglobin. It is clear that all the proteins were capable of inducing leakage from vesicles regardless of their net charge, except for BSA at neutrally charged vesicles. However, the minimum concentration required for dye

leakage in 5% of the vesicles significantly differed among both the proteins studied and the net charge of vesicles.

Table 4.2. Minimum concentrations needed to induce vesicle leakage in 5% of the imaged vesicles.

GUV composition/protein	POPC	POPC/POPG
BSA	NA*	10 μM
Hemoglobin	10 μM	1 μM
Lysozyme	100 μM	10 μM
FBS	1%	0.1%

*NA refers to no observable leakage up to a total protein concentration of 1 mM. Experiments were repeated at least three times.

All proteins showed higher affinity against negatively charged than neutral GUV. For BSA, leakage events were observed for negative vesicles starting from 10 μM, while no leakage events were recorded for neutral vesicles up to 100 μM. Similarly, Hemoglobin was more efficient in affecting the permeability of lipid bilayers than BSA regardless of the vesicle charge: one-fold higher concentration was needed to observe dye leakage for 5% of the charged vesicles while dye leakage occurred at 10 μM for the neutral ones. These results are in agreement with previous studies for Hemoglobin[94], where small unilamellar vesicles aggregated and presented peroxidative decomposition in the presence of Hemoglobin.

As expected from its overall positive charge Lysozyme was more efficient in increasing the permeability against the soluble Alexa dye for the negative vesicles than their neutrally charged counterpart (one-fold increase in concentration was necessary to affect the permeability of the neutral bilayers). However, the net Lysozyme concentrations required to induce leakage was one order of magnitude higher than for Hemoglobin, even though the latter carried a net negative charge (Table 4.1). This

suggests that there are other mechanisms besides the electrostatic interaction of proteins and lipids that contributed to the enhanced capability of Hemoglobin to change the permeability of lipid bilayers.

FBS was very reactive against the GUV: Leakage events were observable already from 0.1% dilution for negative vesicles and from 1% dilution for neutral ones. Finally, at the protein concentrations used, no further modification on the vesicle structure (in terms of bridging, fusion, or vesicle collapse) was observed besides simple content leakage of Alexa dye except for the case of Lysozyme for which vesicle bridging and fusion occurred (Figure B.1), in accordance with the recent findings by Al Kayal et al.[95].

The kinetics of leakage events was recorded for single vesicles and representative data are shown in Figure 4.1 B. When neutral vesicles were exposed to Hemoglobin and Lysozyme, the fluorescence intensity of Alexa dye was fairly stable for ~ 6 and ~ 8 min respectively until it dropped sharply (1-2 min) to gradually level out at minimal levels. Thus, there seems to be a time threshold for significant dye leakage to occur in the presence of these proteins. However, vesicles dye leakage occurred immediately after the injection of FBS -although the overall process occurred rather slowly- until reaching 80% of the initial dye intensity (after ~ 10 min of mixing). At this point, an abrupt decrease in intensity occurred and, within 1 min, the signal reached minimal levels where it remained stable. In contrast, the dye intensity of vesicles incubated with BSA (at least up to 1 mM) remained constant throughout the experiment.

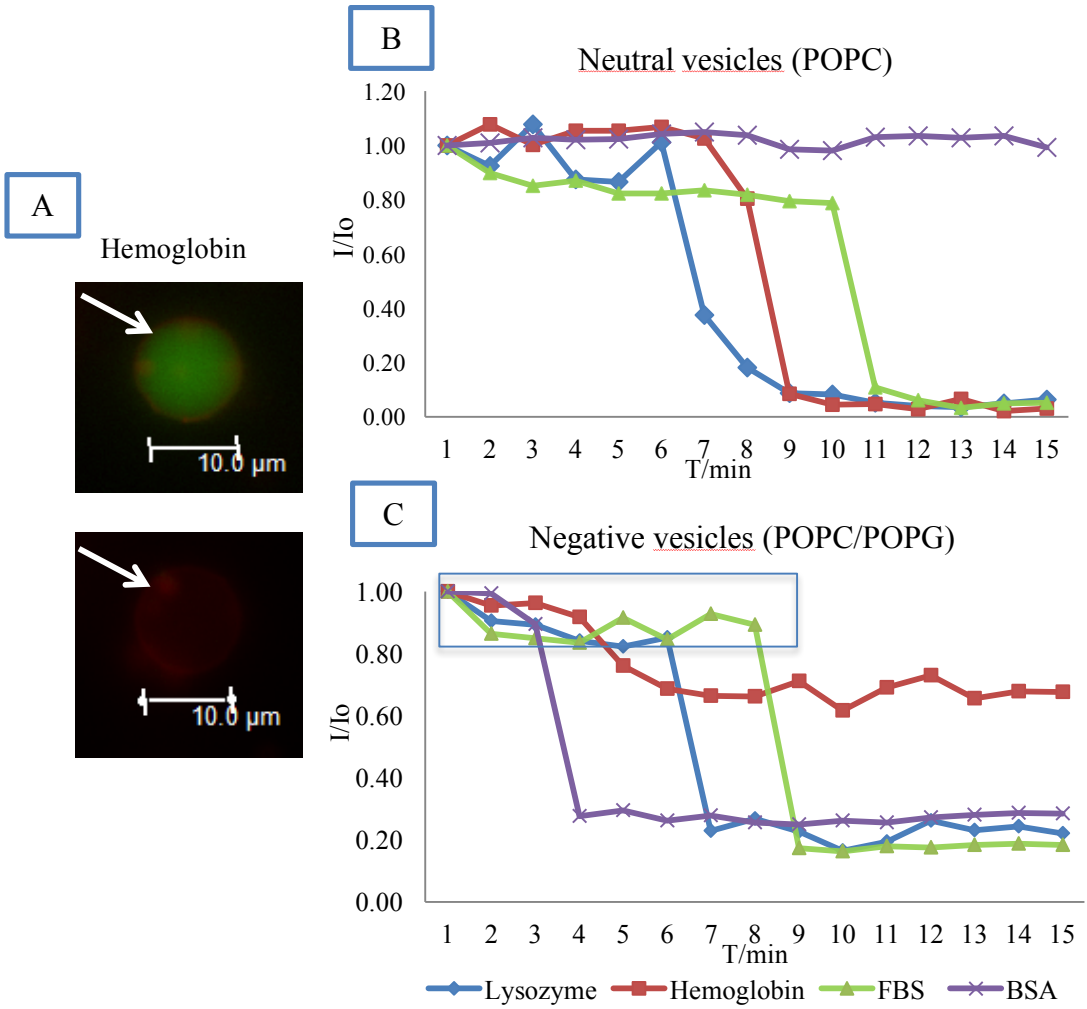

Figure 4.1. Fluorescence microscopy results for the effect of soluble proteins on GUV permeability against a soluble dye. A representative image for a single vesicle leakage event is given in A. Representative leakage rate of individual vesicle expressed as the ratio of real time intensity and initial intensity, I/I_0, versus elapsed time on GUV carrying either a neutral charge (B) or a net negative charge (C) upon exposure to Lysozyme, Hemoglobin, FBS or BSA. The protein concentrations used in B and C are those reported in Table 4.2.

Interestingly, the negative vesicles were more susceptible to the disruption by these proteins despite the electrostatic repulsion expected for the negatively charged BSA and Hemoglobin (Table 4.1): not only were the minimum protein (BSA, Lysozyme, Hemoglobin and FBS) concentrations required for leakage in general one order of magnitude lower (Table 4.2), but the intensity drop due to leakage at the individual

vesicle level occurred sooner (Figure 4.1 B, C) in this case. Moreover, all proteins presented two kinetic regimes (slow and fast) during dye leakage. In the slow regime, the initial dye intensity dropped by 20% (expanding over 3-8 min depending on the type of protein). In the fast regime, an additional 60% intensity drop occurred within 1 min for all proteins used except Hemoglobin for which only a total of 40% of intensity drop occurred.

Adsorption of Proteins to Lipid Bilayers

We used QCM-D to measure the interfacial properties of proteins at negatively and neutrally charged SLB. For comparative studies, protein adsorption on bare silica substrate was also performed. Silica carried a negative charge at the ionic conditions used (~ 0.25 e^-/nm^2 for SiO_2 [96] as compared to ~ 0.54 e^-/nm^2 for the negative GUV as estimated from the nominal composition and average mean molecular area for a lipid on a SLB[97]). Figure 4.2 summarizes the measured change in frequency (ΔF) and dissipation (ΔD) for neutral and negative SLB exposed to various protein concentrations. We started by exposing the SLB to the concentrations reported in Table 4.2 for which dye leakage reported was observed by fluorescence microscopy. For negative bilayers, no adsorption was observed for Lysozyme and Hemoglobin, while only a small ΔF (-5 Hz) and ΔD ($+1.25 \times 10^{-6}$) was observed for BSA and FBS. These ΔF and ΔD values correspond to ~ 50 weight% of a full protein monolayer (of the size of BSA[98]) on top of the SLB or ~ 77 ng/cm^2 based on the Sauerbrey equation ($\Delta m = - C \bullet \Delta f_n/n$)[79b].

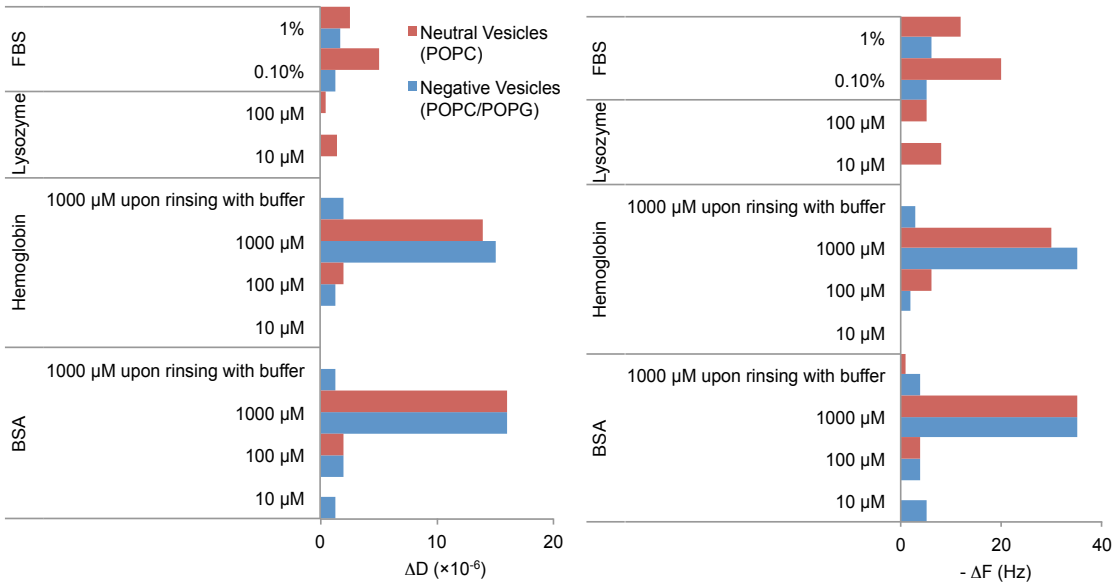

Figure 4.2. Net absolute changes in Frequency (ΔF) and Dissipation (ΔD) upon addition of proteins to POPC (neutrally charged) or POPC/POPG (negatively charged) SLB. The Figure includes the steady state values upon dilution or extensive rinsing with buffer after exposure to 1 mM BSA and Hemoglobin. Red and Blue correspond to neutral or negative SLB respectively. The QCM-D ΔF and ΔD signals typically varied by 2 Hz or 2×10^{-6} dissipation units respectively upon replicating the experiments. Examples of the individual experiments are given in Figures B.3-16.

For neutral membranes, on the other hand, a more pronounced effect was measured for 1% FBS where a steep increase in ΔF (-11 to -14 Hz) was observed. Exposure to 100 µM Lysozyme induced a more complex behavior (see Figure 4.3) than just simple adsorption (decrease in ΔF and increase in ΔD), where substantial adsorption (ΔF decrease and ΔD increase) was followed by mass removal (ΔF increase and ΔD decrease). Upon reaching steady state conditions, the net ΔF and ΔD values were larger than those for the lipid bilayers prior to Lysozyme addition thus indicating that more wet mass than a full lipid bilayer remained bound to the surface. Recently, similar QCM-D responses were obtained for the unfolded equine Lysozyme (> 3 µM) at negatively charged fluid SLB (80% PC, 20% PG) while no such effect was observed for native equine Lysozyme up to 10 µM[99], in agreement with our results. Indeed at protein

concentration < 3 µM, titration of unfolded equine Lysozyme lead only to adsorption and no film rearrangement. Thus, there is here in this case also evidence for a threshold surface protein concentration required for major rearrangement of the lipid bilayer.

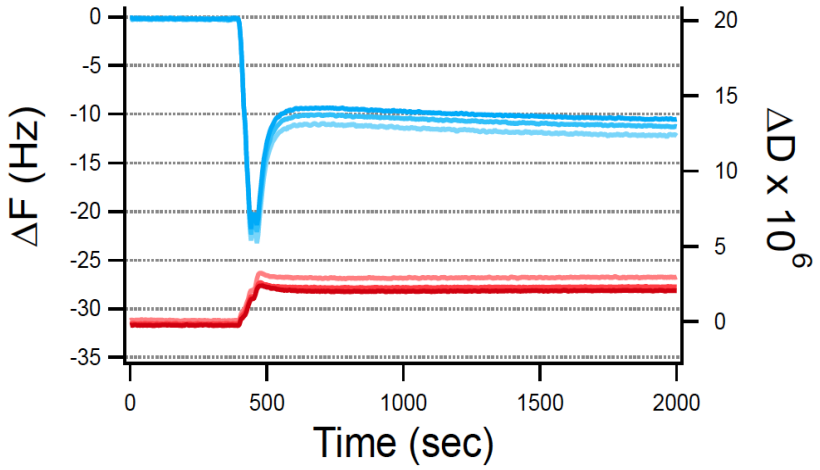

Figure 4.3. QCM-D signals (ΔF and ΔD in blue and red respectively) for the adsorption of 100 µM Lysozyme against time (sec) on neutral SLB. Upon adsorption, a sudden change in the direction of frequency shift indicates the onset of mass removal at t = 500 s after which steady state conditions were reached under continuous flow at 0.1 mL/min. Overtones shown: 5-7-11. The small overtone spreading indicates the formation of relatively compact and homogeneous layers.

Interestingly, upon increasing protein bulk concentration a certain critical point is reached where proteins adsorbed on the SLB regardless of the membrane composition or the type of protein as typically expected for non-specific protein binding. The higher the protein concentration, the larger the ΔF and ΔD measured (Figure 4.2). Indeed, upon reaching the mM regime (and at comparable concentrations than in blood plasma) the ΔD was quite dramatic and there was a considerable spreading of the overtones (Figure B.4). The observed ΔD and ΔF are not related to changes in viscosity of the bulk solution since the exposure of the same solutions to a bare-SiO_2 interface gave considerably different results (see Figure 4.4) with Hemoglobin having a larger capability to self-associate and

form multilayers at the SiO_2 surface since almost twice larger change in frequency was observed in this case.

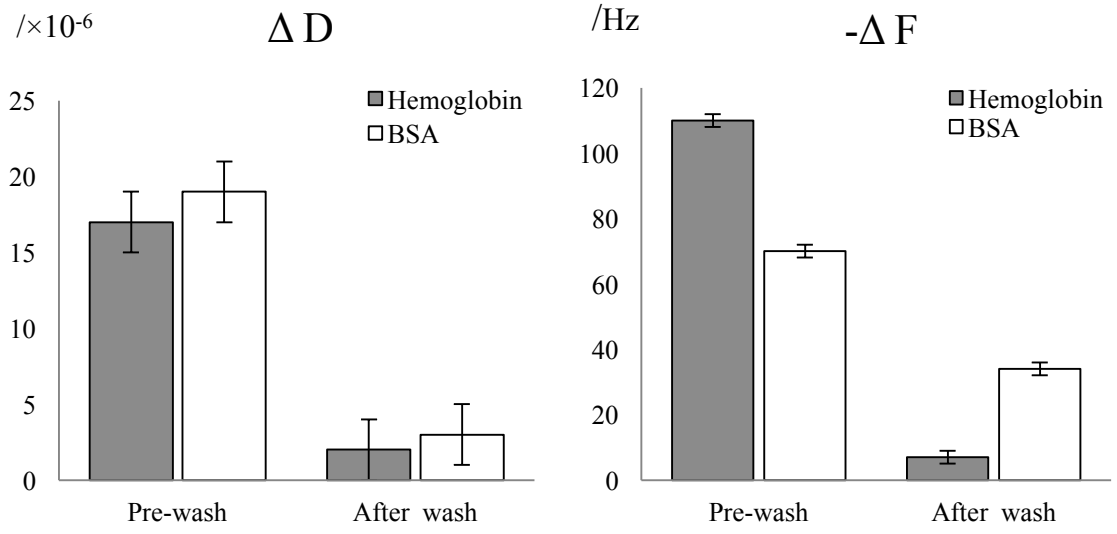

Figure 4.4. Net changes in Frequency (ΔF) and Dissipation (ΔD) upon addition of 1 mM BSA or Hemoglobin to a bare-SiO_2 surface. The Figure includes the steady state values upon dilution with excess buffer.

Extensive rinsing with buffer after exposing the lipid bilayers to 1 mM BSA (Figures B.4,7) or Hemoglobin (Figures B.11,12) was performed to assess the strength of such non-specific protein-lipid binding, see Figure 4.2. There was complete protein removal from neutral SLB since both ΔF and ΔD signals returned to their values prior to protein addition, while only partial removal was achieved for the negative bilayers (the net frequency change after protein removal was -3 Hz) and SiO_2 (Figure 4.4). The remaining ΔF (-34 and -7 Hz for BSA and Hemoglobin respectively on SiO_2) and the relative low D values corresponded well with the reported values for monolayer formation on SiO_2, at least for BSA (typically for a small globular protein as BSA a full monolayer is 160 ng/cm^2 or a F change of -45 Hz)[98]. However, less than a full monolayer remained on the negative bilayers (Figure 4.2). Thus, even though relatively similar

extent of protein adsorption seems to occur upon reaching the mM range on lipid bilayers, the reversibility of the adsorption is hampered on the negative charged bilayers but correspond to lower values than a full monolayer (assuming that lipids are not removed during the washing step).

Since only small ΔF and ΔD were found for BSA on SLB at the conditions for which dye leakage occurs from the vesicles (compare Table 4.2 and Figure 4.1), we used commercially available fluorescently labeled (Alexa Fluor® 647) BSA to corroborate the occurrence of BSA adsorption on negatively charged vesicles (Figure 4.5). One hour after GUVs exposure to 1 μM labeled-BSA, it was possible to observe an Alexa 647 fluorescent signal around the vesicle membrane, thus suggesting that the Albumin indeed adsorbed around the lipid membrane. Note that this very same BSA concentration was below the threshold to induce leakage and thus non-specific protein adsorption to lipid bilayers occurs readily before any lipid bilayers restructuring occur. This seems to be in agreement with the two-step mechanism observed for leakage events.

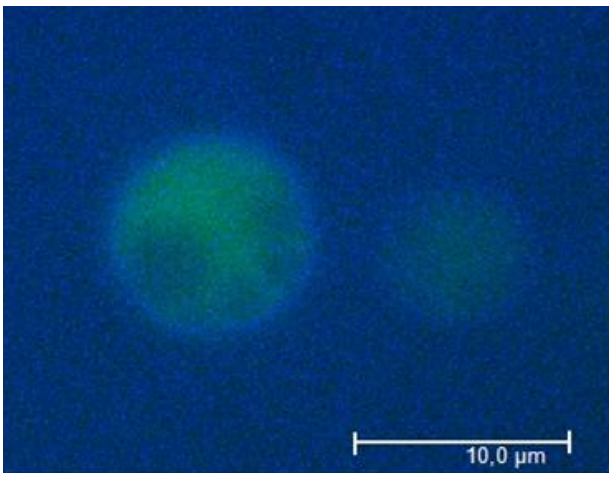

Figure 4.5. Determination of the effect of labeled BSA on negative GUVs by wide field fluorescence microscopy one hour after protein addition. Alexa 488 (green) was used to visualize the membrane vesicle aqueous lumen. Vesicles were exposed to 1 μM Alexa 647-labeled BSA. These results are representative of three different replicates.

Discussion

All proteins studied affected the permeability of giant unilamellar vesicles regardless of the charge of the lipid membrane, except for BSA at neutral vesicles (Figure 4.1, Table 4.2). The change in permeability is related to protein adsorption onto lipid membranes, as measured by QCM-D (Figures 4.2 - 4.4) and Fluorescence Microscopy (Figure 4.5 for BSA only). However, the concentration required for onset of adsorption (Figure 4.1, Table 4.2) as well as the extent of adsorption (Figure 4.2) was not only dependent on the type of protein but also on the vesicle charge. The relative affinities in terms of extent of adsorption (net ΔF, Figure 4.2) and concentration required to induce content leakage from 5% of the total vesicles imaged (Figure 4.1, Table 4.2) was not correlated with the zeta potential or apparent surface charge densities of the proteins at the conditions used (Table 4.1). More intriguingly, higher affinity in terms of the concentration needed to induce vesicle content leakage was found for similarly charged proteins (Hemoglobin) and vesicles (POPG-containing) than for the oppositely charged Lysozyme (Table 4.1) and vesicles (POPG-containing). This seems counterintuitive and surprising due to the overall negative charge of Hemoglobin. However, both BSA and Hemoglobin possess a highly heterogeneous surface charge distribution[88-89], that gives them a dipolar character with positive patches across the domains (for an extensive recent review on effects of charge patches in protein interactions see ref[100]). These positive patches are likely to be attracted by the negative charged head group of the lipids. Indeed, BSA was recently shown to possess affinity towards negatively charged objects[101] and to form a full monolayer on SiO_2 at around 1 μM[27]. Finally, BSA forms a full monolayer at the air-water interface at bulk concentrations around 10 μM[102] thus suggesting that

hydrophobic interactions also contribute to protein-surface interactions although short range interactions are known to be more important for the dissociation than for association constant[103]. BSA, on the other hand, presented similar affinities than Lysozyme regardless having a more negative zeta potential than Lysozyme (Table 4.1). At the same time, BSA presented lower affinity than Hemoglobin that could be explained based on the differences in zeta potential between these two proteins (Table 4.1) related to the difference in the protein isoelectric point, 6.8 and 4.7 for Hemoglobin and BSA respectively[104].

A closer look at the kinetics of dye leakage indicates that leakage occurs in a two-step mechanism: 1) slow kinetics where no or small change in permeability occurs and 2) fast kinetics where most of the dye intensity leaks within one or two minutes (Figure 4.1 B, C). This suggests that protein adsorption occurs readily upon contact with the vesicles leading to some degree of lipid rearrangement, but a critical surface density threshold for the proteins is needed prior to major leakage occurs. Indeed, the use of labelled BSA corroborated that protein adsorption occurs prior to any onset of vesicle leakage (Figure 4.5). Thus leakage may be related to pore formation via protein penetration into the lipid bilayers[105] or local changes in membrane curvature due to protein adsorption as suggested earlier for NP-lipid interactions[97b], while the kinetics could be dependent on the effects of both vesicle composition and protein properties, as the rate of leaking was only observed in POPC/POPG vesicles.

We measured vast changes in ΔD and ΔF values upon protein exposure to the lipid bilayers that could be related to the formation of soft protein multilayers due to non-specific protein-protein and protein-lipid forces. Interestingly, the lipid membranes were

less prone for protein adsorption than the pristine SiO_2 surface since the net ΔF and ΔD was larger in the later case. In this respect, non-specific inter-protein interactions were detected for a transferrin coated NP incubated in blood plasma, for which a soft corona of proteins was identified by fluorescent correlation spectroscopy[106]. Within this soft corona protein exchange occurred in the time scale of two minutes and faster, showing the highly dynamic nature of such inter-protein non-specific interaction. [106] Indeed, the existence of such soft protein corona arises from typical non-specific protein-protein interactions in the crowded protein environment induced by the up concentration of proteins at the interface between the solution and any surface. Our results suggest that such reversible, dynamic and "soft" protein-protein interactions occur also in the close vicinity of lipid bilayers and together with non-specific protein-lipid interactions may indeed have an irreversible effect on the lipid bilayer structure, in terms of their permeability against soluble dyes and the colloidal stability of the vesicles.

Lysozyme presents quite a distinct behavior: not only it induces dye leakage from the vesicles' lumen (Figure 4.1), but also vesicle aggregation (Figure B.1). Moreover, initial Lysozyme adsorption on SLB was followed by a regime of desorption (Figure 4.3) and thus a more complex phenomenon than just protein adsorption in this case. Previously, Lysozyme was thought to unfold in contact with lipid membranes upon induction of vesicle fusion[95] while it was also reported that lipid bilayers could induce refolding of denatured Lysozyme[99]. The QCM-D responses presented in Figure 4.3 are indeed typical responses for lipid bilayer restructuring for instance due to molecular insertion and mixed micelle formation[107]. Interestingly, unfolded Lysozyme due to complexation with oleic acid was found to induce a similar restructuring effect on

negative SLB but such effect was not observed for native Lysozyme below 10 μM[99]. Thus, it is clear that the protein concentration is critical since the same mechanism for unfolded Lysozyme is reported here for native Lysozyme at 100 μM.

Even though all three proteins tested have very different biological functions, they all presented similar behavior around lipid bilayers in terms of dye leakage and extent of adsorption once a certain protein concentration was reached which was close to the mM range or the semi-dilute regime for small globular proteins. In particular, BSA binds to lysolipids and diacyglycerol[108], Hemoglobin can induce peroxidation of unsaturated lipids at physiological conditions[109] and Lysozyme is a proteolytic enzyme. The latter was also shown recently to induce fusion in negatively charged liposomes at pseudo physiological condition[95]. In particular, Lysozyme is aggressive against Gram-Positive Bacteria cell membrane and this is mainly associated to its anti-bacterial function. [110] The antibacterial function of Lysozyme could, in the light of present results, be indeed related to actual destabilization of the lipid membrane. Overall, the effect of Hemoglobin, BSA and Lysozyme on the structure of the lipid bilayers does not seems to be related to their structure but rather to their colloidal properties, mainly in terms of their surface charge density distribution. All proteins are charged and carry a permanent dipole, thus explaining their higher affinity for negative lipid membranes than for neutral ones. Although relatively similar extent of adsorption occurred upon reaching the mM concentration range at least for similarly charged membranes (Figure 4.2), the reversibility of the non-specific protein adsorption was hampered on the negatively charged bilayers only, at least for BSA and Hemoglobin (Figures 4.2 and 4.4). Thus, the stronger electrostatic interactions between the proteins and the lipids also induced non-

reversibility effects. Thus, it is clear that besides favorable electrostatic interactions between the charged patches of the proteins and the lipid bilayer that drive the protein-lipid binding there are other short range interactions (van der Waals, hydrogen bonds, hydrophobic interactions and salt bridges) that decrease the protein dissociation from the lipid bilayers. This is a typical behaviour observed for proteins and polyelectrolytes in general as profoundly revised recently by Kayitmazer et al[100].

For FBS, on the other hand, leakage events were observable starting from 0.1% dilution for negative GUVs and from 1% dilution for neutral GUVs (Table 4.2, Figure 4.1). The concentration commonly used[111] in cell culture study is 10% dilution in volume of this media, and thus FBS addition should induce protein adsorption on cell membranes given that conditions are kept similar to the ones hereby used (cell versus vesicle densities). However, FBS or BSA addition does not induce cell lysis in cell cultures. Indeed, we used protein concentrations close or within their physiological values. Thus, none of these proteins should be able to affect the cell membrane structure *in vitro* or *in vivo*. Therefore, the cell must possess other mechanisms to protect itself from the action of soluble proteins in the mM concentration regime. The head groups of glycosylated lipids are highly hydrated and are known to actively protect lipid membrane from desiccation[112] and peroxidation[113]. We hypothesize that glycolipids have yet another biological function[114] related to the hindrance of soluble protein binding. This hypothesis is supported by the fact that sugars are used in surface coating for preventing non-specific protein binding[115]. Indeed, preliminary experiments show that the use of phosphatidyl inositol (PI) instead of phosphatidylglycerol (PG) at the same molar ratio (and thus same surface charge density) decreases the effect of protein binding on the permeability of

lipid membranes since no leakage event was recorded for titration with up to 50 μM BSA, see Figure 4.6. However, further experimentation with various conditions is needed to corroborate this hypothesis as a general effect for other proteins.

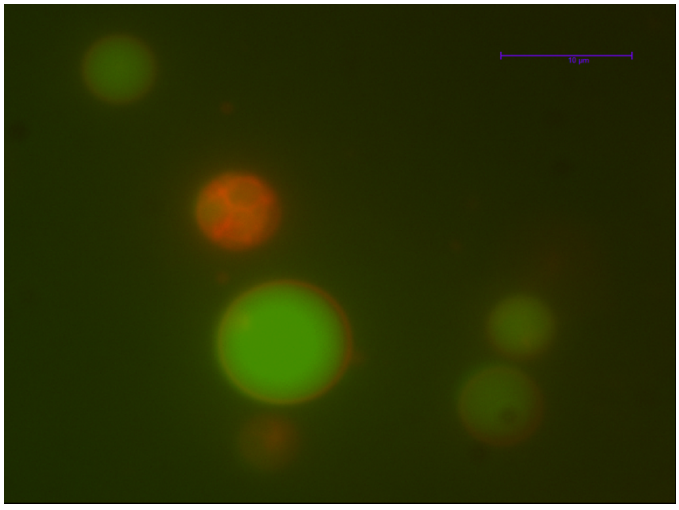

Figure 4.6. No significant leakage was observed by wide field fluorescence microscopy upon exposing negative GUVs made of phosphatidylinositol (25 mol%) one hour after 50 μM BSA addition. Alexa 488 (green) was used to visualize the membrane vesicle aqueous lumen. Vesicles were exposed to 1 μM Alexa 647-labeled BSA. These results are representative of three different replicates.

Experimental

Materials

POPG, POPC and 1, 2-dioleoyl-sn-glycero-3-phosphoethanolamine-n-cap biotinyl (DOPE-Biotin) were purchased from Avanti Polar Lipids, Inc. (Alabaster, AL) while 1,2-dipalmitoyl-phosphatidylinositol (DPPI) was purchased from Larodan Fine Chemicals AB. All lipids were used without further purification. The dyes $DiIC_{18}(5)$ (1,1'-dioctadecyl-3,3,3',3'-tetramethy-lindodicarbocyanine perchlorate) and Alexa Fluor® 488 hydrazide (Alexa) were used as received from Invitrogen (Paisley, UK). Alexa

Fluor® 647 conjugate was purchased from Invitrogen (Paisley, UK), dispersed in PBS to a concentration of 100 μM, and stored at -20 °C until use.

Preparation and Characterization of Vesicles

Two types of GUV were prepared by mixing the two lipids, POPG and POPC, at the molar ratios of 1:3 and 0:1, respectively. Based on the pKa of the head groups at physiological pH, POPC/POPG vesicles carried a negative charge, while POPC carried a net charge of zero. [116] Additionally, DPPI was mixed with POPC at a molar ratio of 1:3 to give vesicles with the same charge as those made using POPG but carrying an inositol instead of a glycerol.

For the leakage studies, both types of vesicles contain 1% molar ratio of the lipids dye $DiIC_{18}(5)$ and 0.5% molar ratio of DOPE-biotin, to tether the vesicles to the surface of sample chamber. The lipids were dissolved in chloroform at appropriate ratios and the solvent was evaporated under vacuum for at least one hour. The films were then rehydrated with 10 μM Alexa 488 hydrazide in sorbitol solution, followed by overnight water bath incubation at 37°C. This procedure enabled the vesicles to carry $DiIC_{18}(5)$ in the lipid bilayers while the soluble Alexa 488 is confined in the vesicle lumen. The final vesicle solutions were stored at 4°C and used within a week.

For QCM-D experiments, small unilamellar vesicles (SUV) were prepared at the same molar ratios of two lipids as stated above. However, the vesicles did not contain $DiIC_{18}(5)$ or Dope-biotin in this case. The POPC/POPG vesicles were rehydrated in 2 mM $CaCl_2$ to facilitate the formation of the supported lipid bilayer by bridging the negatively charged vesicles with the SiO_2 surface, while POPC were simply rehydrated in

Milli-Q water. Vesicles were subjected to two to five minutes of sonication until the solution was clear and transparent before use.

Preparation and Characterization of Proteins

Bovine serum albumin (BSA) with a purity of above 98%, human blood hemoglobin (Hemoglobin), fetal bovine serum (FBS) and chicken egg white lysozyme (Lysozyme) were purchased from Sigma-Aldrich (Denmark) and used without further purification. The proteins were first dispersed in phosphate buffer saline (pH 7.4, ionic strength 127 mM) and diluted further in the same buffer to the experimental concentrations. In this study, protein concentrations for BSA, Hemoglobin and Lysozyme ranged from 1 μM to 1 mM, while FBS was studied at 0.1%, 1% and 2% volume ratios. The zeta potential of each type of protein was determined by electrophoretic mobility measurements using a Malvern Zetasizer NS (Worcestershire, U.K.), see Table 4.1. In this case, the samples were prepared by dispersing the proteins in PBS for a final concentration of 1 mM, FBS was diluted in PBS to 1% by volume; and six measurements were performed on each sample at 25°C.

Description of Microscopy Experiments

The sample chambers were incubated with 1.0 g/l BSA-biotin/BSA solution (1:10, volume ratio), 0.025 g/l streptavidin and PBS, respectively, at ambient temperature for 10 minutes, plus rinsing with PBS five times. Fluorescent vesicles were added to the chamber to achieve a final concentration of 0.01 mg/ml. The vesicles were allowed to settle and stabilize at the bottom of the chamber for 30 minutes before injection of proteins into the solution. After exposure to proteins, the behaviors of GUVs were

monitored for up to 60 minutes on a Leica AF6000LX wide-field microscope (Wetzlar, Germany). For each dye leakage experiment, 10 to 15 locations were imaged with approximately 20 vesicles in each location, which made up to 200 to 300 vesicles in every study. The fluorescence of Alexa was excited at λ=488 nm with an argon laser and emission was captured at λ=491-563 nm. The lipid dye, $DiIC_{18}(5)$, was excited at λ=633 nm and recorded at λ=640-700 nm. A mercury lamp with filter cubes EGF cube 49002 ET, EC5 cube 49006 ET (Chroma Technology Corp, Bellows Falls, USA) were used to excite Alexa and $DiIC_{18}(5)$ respectively. For each experimental setup, illumination, intensity and exposure time were optimized for signal collection. The integrity of vesicles was checked in buffer solution during control experiments, without exposure to proteins, to ensure their stability against mechanical stress, and no sign of dye leakage was observed. Each set of experiments was repeated at least three times.

Description of QCM-D Experiments

QCM-D (quartz crystal microbalance with dissipation monitoring) is an acoustic technique for measuring 1) the change of wet mass per unit area by sensing ΔF of a quartz crystal resonator and 2) the viscoelastic properties of the adsorbed film by sensing the energy dissipation (D). A decrease in resonance frequency is an indicator of an increase in adsorbed mass on the sensor surface while an increase in dissipation is related to a decrease in rigidity of the adsorbed film. In this study, we used a Q-Sense E4 system (Gothenburg, Sweden). All SiO_2 sensors were soaked in 2% hellmanex for 10 minutes and washed by 15 rinsing cycles of water and 96% ethanol, followed by an UV-ozone cleaning process for another 10 minutes to remove any possible contamination layer on the sensor surface. Each measurement was performed at 25 °C when the frequency

changes were within 0.5 Hz. 5% of sodium dodecyl sulfate (SDS) was applied for cleaning, and 96% ethanol was used to remove bubbles in the tubing when necessary. Upon obtaining a stable signal, a vesicle solution (200 μg/ml) was injected at a rate of 100 μl/min. After the formation of SLB, PBS was pumped into the system to wash off excess lipids before the injection of proteins. A series of protein titrations were then performed, starting from 1 μM to 1 mM for all proteins except FBS for which 0.1% to 2% of FBS was used.

Conclusions

Non-specific protein adsorption has now been studied in view of its effect on the structure of lipid bilayers in terms of vesicle colloidal stability and lipid bilayers permeability. We found that all proteins studied (bovine serum albumin, chicken egg lysozyme, bovine hemoglobin and bovine fetal serum) were able to induce leakage from lipid vesicles regardless of their surface charge (negative or neutral) expect for albumin on neutral vesicles at least up to 1 mM. The protein concentrations required for leakage to occur were well above the μM range where strong inter-protein interactions occur. At the same time, this is the concentration regime that is physiologically relevant. Evidently, vast soluble protein adsorption on the cell membranes does not occur *in vivo*. We propose that the cell possesses other mechanisms to defend itself from this type of non-specific protein adsorption among which the glycosylated coatings introduced by lipids and membrane proteins could be a major parameter in play.

Acknowledgments

We thank Karen Martinez for access to the wide field microscope and Thomas Günter Pomorski for fruitful discussions. Moreover, the authors gratefully acknowledge financial support from "Center for Synthetic Biology" at Copenhagen University funded by the UNIK research initiative of the Danish Ministry of Science, Technology and Innovation, and C. Gus Glasscock, Jr., endowed fund for excellence in environmental sciences in the College of Arts and Sciences by Baylor University, USA.

Supporting Information

Electronic supplementary information (ESI) available: QCM-D graphs with raw data and Fluorescence Microscope leakage images. See DOI: 10.1039/c3sm27769k

CHAPTER FIVE

Assessing the Translocation of AgNPs Using an *in Vitro* Co-Culture Model of Alveolar-Capillary Barrier

(In review, Toxicology in Vitro)

Abstract

As the lung is a major targeted organ for NP exposure, the authors have developed a novel *in vitro* co-culture model of the alveolar-capillary barrier to track the translocation of NPs for potential drug delivery. Human bronchial epithelial cells Calu-3, differentiated Thp-1 and microvascular endothelial cells EA.hy926 were grown on apical and basolateral sides of microporous membrane supports in a two-chamber system. Calu-3 cells, with high TEER development, enabled a robust and tight barrier similar to *in vivo* conditions. AgNPs were used as a model nanoparticle (NP) system. AgNPs of 50 nm in diameter with tannic acid coating were monitored after being introduced to the co-culture models. Movement of AgNPs across the modeled barrier and any resultant cytotoxicity were quantitatively evaluated. Results revealed the ability of AgNPs to translocate through multiple layered barriers at both 4ºC and 37ºC, indicating cellular uptake via both passive diffusion and active transport. Cytotoxicity of AgNPs was observed in cells from both compartments in tri-culture models regardless of concentration or temperature. This differs from the response of these same cells in monoculture or bi-culture. The sensitive response from tri-culture models was most representative of *in vivo* conditions, due in part to secretion of pro-inflammatory mediators by macrophage-like differentiated Thp-1 cells upon AgNPs exposure. To evaluate the permeability of microporous membranes,

the particle retention was evaluated for AgNPs into the basolateral region of the system. Altogether, the chosen cell lines interacted and presented a functional alveolar-capillary barrier that is more physiologically relevant for nanoparticle translocation studies. This novel tissue model provides researchers with a system for evaluating translocation, cellular trafficking, uptake, and novel drug delivery systems.

Key Words

Co-culture, organotypic, thp-1, calu-3, translocation, alveolar-capillary barrier

Introduction

Nanomaterials, with significantly increased surface to volume ratio in the nanoscale, display many unique physiochemical properties compared to their bulk parent. These new properties have led to the novel applications of engineered nanomaterials in energy production, medical therapeutics and diagnostics, food packaging and cosmetics[117]. A primary metal material used in nanotechnology is silver. Nanoscale silver comprises roughly one-quarter of the presently available commercial nano-enabled products, mainly as an antimicrobial agent[1]. In light of their antimicrobial, optical and thermal properties, AgNPs have also been used in several platforms in nanomedicine. Tian et al. revealed that AgNPs were a novel therapeutic modality to treat burn wounds with rapid healing ability and improved cosmetic appearance in a wound[9]. Fluorescence labelled AgNPs appeared about one magnitude brighter when taken up by cells, showing great potentials in tumor detection[2c]. AgNPs containing nanocapsules could also be externally activated by sonication for controlled drug targeting and delivery[2a]. As the increasing influx of silver-based nanomaterial into the commercial market and medical

fields, it is imperative to evaluate whether contact with AgNPs will result in adverse effects in workers, consumers and patients.

One major exposure route for AgNPs (AgNPs) is inhalation. Animal studies demonstrated pulmonary toxicity of inhaled AgNPs and their accumulation in other organs. Treated rats experienced asthma-like symptoms including pulmonary eosinophilic and neutrophilic inflammation, as well as bronchial hyper-responsiveness after 7 days' exposure to citrate-capped and PVP-capped AgNPs[118]. Aggregated forms of AgNPs were found in the spleen and kidney in adult mice following intranasal exposure for 7 days[119]. Multiple *in vitro* studies have reported cellular uptake of AgNPs into both normal and cancer lung cell lines[30, 120]. The internalized AgNPs can trigger generation of reactive oxygen species, and further cause membrane rupture and DNA damage[30, 120]. Cell inflammation was also observed as part of the body's immunological response to this foreign material[25d].

When NPs are inhaled, they can deposit deep in the lung, specifically, in the alveolar region[121]. Pulmonary alveoli are located at the terminal ends of the respiratory system and represent 70 to 90 m^2 of the pulmonary surface area. Around each alveolus, there is a net of capillaries; together it is the region for gas exchange. To allow sufficient oxygen diffusion, the alveolar-capillary barrier is a thin-wall structure (0.1 μm to 0.2 μm thick), and consists of pneumocytes that line the alveolar wall, endothelial cells of the capillaries, basement membrane between the two linings and macrophages that defend the lung from foreign materials[121-122]. This barrier is difficult to access in *in vivo* studies due to the complexity of multilayered tissues which limits the insight into process of particle-cell interaction[46].

Recently, several *in vitro* models have been developed to evaluate the translocation of NPs through the alveolar-capillary barrier. However, these models either fail to show acceptable barrier properties due to choice of cell types or lack controllability and reproducibility of the experimental conditions due to complexity of the system. This hampers the ability to provide the most physiologically relevant cellular response to the translocation process. For example, Rothen-Rutishauser et al. designed a triple co-culture using alveolar epithelial cells A549, dendritic cells and macrophages that mimic the human respiratory tract. The constructed barrier only developed less than 200 $\Omega \cdot cm^2$ of transepithelial electrical resistance (TEER), indicating higher epithelium permeability than physiological condition[46], and potentially over-estimated translocation of NPs due to possible concurrent paracellular transport. Lung barrier simulation was[123] also attempted at the air-liquid interface. With advantages of this method being more realistic to inhalation exposure and limited interference from culture medium, researchers experience problems maintaining constant temperature and humidification of the system, resulting in less reproducible results[45].

In the present study, the authors introduce a three-dimensional, organotypic co-culture model that mimics the alveolar-capillary barrier, by assembling bronchial epithelial cells, microvascular endothelial cells, and macrophage-like cells in a two-chamber system. Cellular uptake of AgNPs, their translocation through the barrier and resultant acute toxicity were examined using this model. Tannic-coated AgNPs were used as a "model" particle and tested on established bi-culture and tri-culture systems. These AgNPs were previously determined highly penetrative through human epithelial models compared to other commercially available silver nanomaterials[37].

Methods

Silver Nanoparticles

Spherical AgNPs (with a core diameter of 50 nm ± 4 nm, based on TEM measurements by the manufacturer) capped with tannic acid in a stock concentration of 1.0 mg/ml (NanoComposix Inc., San Diego, CA, US) were used in this study. Choice of this type of AgNPs was based on our previous study where tannic acid-AgNPs of same production line exhibited the most efficient penetration efficacy through cell membranes compared to two other coated AgNPs used in that study[37]. Characterization of particle size and surface charge were performed using TEM and DLS, described in the previous study[37].

Cell Lines and Culture Media

Human micro-vascular endothelial cells EA.hy926 (CRL-2922), human bronchial epithelial cells Calu-3 (HTB-55) and human acute monocytic leukemia Thp-1 (TIB-202) were obtained from American Type Culture Collection (ATCC, Manassas, VA). EA.hy926 cells were cultured in Dulbecco's Modified Eagle Medium (DMEM) with 4.5 g/L glucose (4.5 g/L) and 0.584 g/L L-glutamine. Calu-3 cells were cultured in Dulbecco's Modified Eagle Medium (DMEM) with 1.0 g/L and 0.292 g/L L-glutamine. Thp-1 cells were cultured in Roswell Park Memorial Institute (RPMI)1640 medium with 4.5 g/L glucose and 2.383 g/L HEPES. Sodium bicarbonate, sodium pyruvate, 1% penicillin-streptomycin and 10% of heat-inactivated fetal bovine serum were added to all media. Cell culture was routinely incubated at 37°C in humid air with 5% CO_2 until the desired confluence.

Co-culture Model

In this study, two or three types of cells were grown and developed on the opposite sides of a porous membrane in a two-chamber system. To assemble a bi-culture unit, porous membrane inserts (1.0 μm pore size, 12 mm diameter, polyester, Corning Incorporate, NY) were inverted in a petri dish, bottom side facing up. Endothelial EA.hy926 cells were then seeded onto the basolateral membrane in the volume of 200 μl, at a density of 2.5×10^4 cells/cm^2. These membrane inserts were then covered in the petri dish and carefully transferred to the incubator, allowing cell attachment for 2 hr in standard culture conditions. The excess medium on the bottom side was then removed by gentle aspiration, and rinsed with fresh medium twice to remove any loose cells. Inserts are then righted and placed into receiving wells (medium volume: 1.5 ml). Cell attachment on the basolateral side of the membrane can be confirmed under a light microscope. Epithelial Calu-3 cells were subsequently added to the apical side of the membrane in a volume of 0.5 ml to achieve cells density at 5.0×10^4 cells/cm^2. The tri-culture model can be further developed by introducing Thp-1 monocytic cells into apical side of the inserts when bi-culture TEERs have exceeded 1000 Ω·cm^2. To do so, medium in the apical region needed to be removed and replaced with DMEM high glucose/RPMI1640 mixture (mixed media) in the ratio of 9:1, containing 1.0×10^4 Thp-1 cells. After seeding, PMA was added into the apical medium (PMA concentration in the medium = 100 ng/ml) and incubated for 48 hr to induce differentiation of the Thp-1 cells. At the end of incubation, PMA-containing medium was discarded and replaced with fresh mixed media. Cells rested here for another 48 hr to reach the optimal differentiation

status. Differentiated Thp-1 cells will attach to the apical region of Calu-3 cells (Figure 5.1).

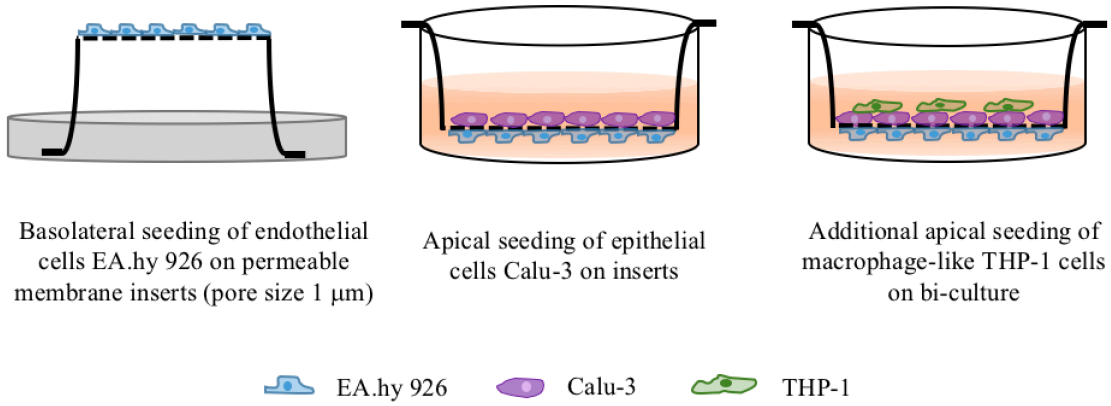

Figure 5.1. Schematic drawing of the steps to assemble bi-culture and tri-culture using endothelial, epithelial and macrophage-like cells.

TEER Measurements

Transepithelial electrical resistance measurements were conducted on both bi- and tri-culture systems using an EVOM Voltohmmeter (World Precision Instrument, Inc. FL). Blank control, $TEER_0$, was measured on cell-free inserts. The TEER value of cell layers is calculated by the following formula:

$$TEER = (TEER_e - TEER_0) \times A$$

where $TEER_e$ is the preliminary reading directly from the Voltohmmeter, $TEER_0$ is the value of blank control, and A is the surface area of the membrane insert (1.12 cm^2). TEER measurements were collected daily after co-culture units were assembled, to monitor formation of epithelial tight junction and barrier integrity.

Cellular Uptake and Translocation of AgNPs

The uptake and translocation of tannic-AgNPs were evaluated at 3 mg/L and 30 mg/L during a 24 hr exposure period. When desired TEER was achieved in co-cultures, AgNPs were added into the system from the apical side of the inserts. The lower concentration 3 mg/L was chosen as this dose was determined to be non-lethal to pulmonary cells and more environmentally relevant from the previous work [37]. The culture was incubated for 24 hr at either 4°C or 37˚C. Next, cells grown on apical and basal sides were separated from the inserts. To do so, medium from the upper chamber (the inserts) and lower chamber (the receiving wells) was extracted first, PBS buffer was added to wash both sides of the membrane to remove any unattached AgNPs. Trypsin was then added and incubated to dislodge the cells, followed by another PBS rinse to ensure cells detachment. In bi-cultures, the upper chamber samples contain only Calu-3, for tri-culture, it is a mixture of both Calu-3 and Thp-1 cells, as they were harvested simultaneously and analyzed collectively. Samples were then combined with 5 ml of concentrated nitric acid (67-70)% and subjected to heat digestion at 105°C for 6 hr, before quantitative analysis by inductively coupled plasma mass spectrometry (ICP-MS, PerkinElmer SCIEX, ELAN 9000). Rhodium (atomic weight 103) was used as an internal standard throughout the measurements of silver in all samples.

Acellular Translocation Test

Tannic Acid-AgNPs were dispersed in the same medium that was used to culture cells, at a concentration of 30 mg/L. In an empty membrane insert (polyester, pore size 1 μm), 0.5 ml of the AgNPs dispersion was added to the upper chamber, and 1.5 ml of the same medium in the lower chamber. The authors then incubated the AgNPs in these

inserts at 37°C regular culture conditions for 24 hr, after which, samples from both upper and lower chambers were collected and subjected to acid digestion and ICP-MS analysis as described in the previous text. After removal of AgNPs-containing medium, the membrane from each insert was cut off and visually checked for particle accumulation. The same test was also performed with 0.4 μm and 3 μm sized porous polyester membrane inserts for comparison.

Cytotoxicity Measurements

Lactate dehydrogenase is an intracellular enzyme found in healthy cells, its leakage into the extracellular environment can be used as a viability probe. In this study, LDH in co-culture medium was measured to gain information about cytotoxicity induced by AgNPs. Assay was performed as previously described in Zhang et al.[37]. Breifly, 50 μl cell medium was mixed with 150 μl LDH reagents, and samples were analyzed on a microplate reader (ELx800, Biotek) for optical intensity. Cytotoxicity evaluated in terms of LDH leakage was evaluated in monocultures, bi-cultures and tri-cultures. When measuring LDH in co-cultures, the media in the inserts and in the receiving wells were separately determined for independent cytotoxicity from each type of the cell line.

Results

TEER Measurements

In order to compare properties of co-culture barrier to those of monocultures, membrane inserts seeded with EA.hy926 only, Calu-3 only and both cell lines were prepared on the same day. Post-seeding, beginning at 24 hrs, the TEER of each culture was followed until it reached over 1000 $\Omega \times cm^2$. The development of TEER in these

individual cultures is presented in Figure 5.2. On day 1, EA.hy926 and Calu-3 cells each possessed a resistance value of (14 ± 5.57) $\Omega \cdot cm^2$ and (49.33 ± 5.51) $\Omega \cdot cm^2$ respectively, both significantly lower than that in bi-culture (98.67 ± 7.23) $\Omega \cdot cm^2$. Endothelial cells EA.hy926 did not gain significant resistance after day 7, showing rather stable values between 14 $\Omega \cdot cm^2$ to 23.67 $\Omega \cdot cm^2$. TEER of epithelial Calu-3 cells, on the other hand, continuously increased from day 1 to day 7, similar to those observed in bi-culture. At the end of day 7, Calu-3 and bi-culture each possessed TEER of (876.67 ± 75.64) $\Omega \cdot cm^2$ and (1352.00 ± 110.27) $\Omega \cdot cm^2$, which is 13-16 times more electrical resistant than day 1.

Addition of Macrophage-like Cells on Bi-culture

Thp-1 monocytes were added into bi-cultures at day 7 post-seeding. The monocytes were then differentiated by 100 ng/L PMA *in situ* on the apical side of Calu-3 cells. Interestingly, instead of increasing the resistance further, TEER readings of the highly developed bi-culture drastically decreased upon the attachment of differentiated Thp-1 on Calu-3. A decrease of 78.3% in the TEER readings was noted on day 8. As the Thp-1 continued to differentiate on Calu-3 cells, the resultant tri-culture increasingly regained electrical resistance after the initial drop, until day 12 post-seeding, when it rebounded to (1267 ± 142.08) $\Omega \cdot cm^2$(Figure 5.3). Prior to the experiments, the toxicity of PMA on Calu-3 cells at the concentration used was confirmed (Data not shown).

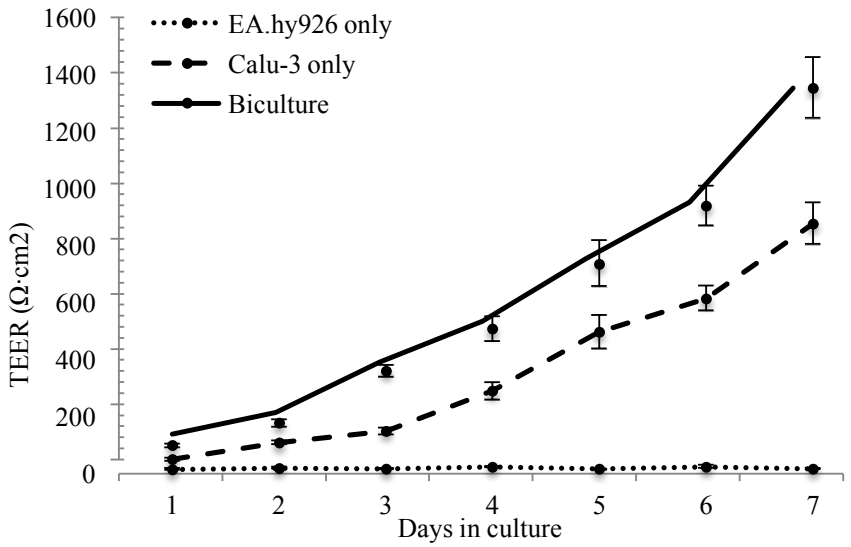

Figure 5.2. TEER development in monocultures and bi-culture of Calu-3 epithelial cells and EA.hy926 endothelial cells. Monocultures of EA.hy926 and Calu-3 cells were represented by dotted and dashed curves, respectively, and bi-culture by the solid curve. Data represent the mean ± SD of three independent samples.

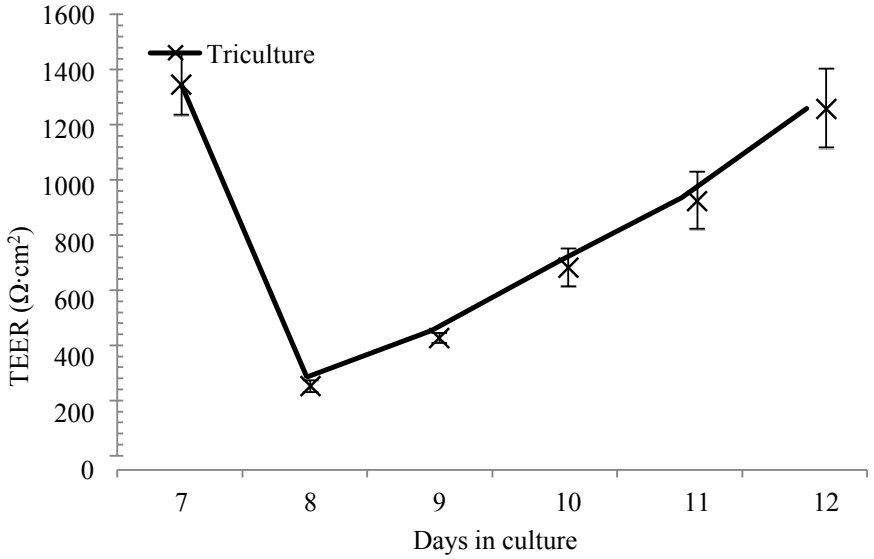

Figure 5.3. Changes of TEER in tri-culture when Thp-1 were differentiated and added into bi-culture system. TEER was measured daily to follow the development of tri-culture over five days. Data represent the mean ± SD for three independent samples.

Cellular Uptake and Translocation of AgNPs in Co-culture

Bi-culture. The amount of silver in the tissue culture was analyzed by ICP-MS, a sensitive yet reliable quantitative analytical instrument for detection of metals that allows for low detection (part per trillion). After cellular exposure to 3 mg/L for 24 hr, the majority of AgNPs were found in the upper chamber medium where the NPs were added, however, a significant amount of silver had interacted with cells. Approximately 6% of silver was internalized by Calu-3 cells at 37°C, similar to (5.8 ± 0.1%) of that found in Calu-3 at 4°C. Although the initial cellular uptake by epithelial cells was equivalent for both temperatures tested, 3 times more silver (0.148 μg) was detected in the endothelial cells at 37°C compared to 4°C. Only 1% and 4% of that was found in the lower chamber medium for 37°C and 4°C respectively (Figure 5.4 A). The total mass recovery of silver from this method was 82% and 106%, among which more than 17% (37°C) and 13% (4°C) of the AgNPs translocated from upper chamber medium into the tissues or lower chamber medium.

For both temperatures, there was a ten-fold increase in silver that was transported by cells in the bi-culture system when exposed to 30 mg/L of AgNPs. Again, over 50% of the silver was found in the upper chamber medium.

Interestingly, the distribution pattern and amount of silver within the bi-culture system were similar at 37°C and 4°C. More than 1 μg of silver was found intracellularly in Calu-3 at 37°C, and 0.934 ± 0.118 μg at 4°C, both over one magnitude higher than the intracellular concentrations observed at 3 mg/L. More than 17% of total silver, penetrated the Calu-3 cells and was transported by EA.hy926 into the lower chamber medium at 37°C, accounting for 61% of the silver that interacted with cells. Although the

translocated silver at 4°C and 30 mg/L, in lower chamber medium, was less, (11.9 ± 1.2)%, it was still three times higher than that in 3 mg/L. The total recovery of silver at 30 mg/L, however, was not as good as 3 mg/L. At 37°C and 4°C, only 61% and 47% of silver, respectively, was collected from the entire system, leaving a question regarding the membrane retention.

Tri-culture. The cellular uptake and translocation of tannic-AgNPs was evaluated in tri-culture systems. Shown in Figure 5.5 A, nearly 73% and 90% of silver was recovered from tri-culture upper medium incubated at 37°C and 4°C (Figure 5.5 A). Differentiated Thp-1 and Calu-3 cells had a combined uptake of 9.2% of silver at 37°C, slightly higher than the 7% found at 4°C. Overall, 17% of total administered silver (equivalent to 0.256 μg in mass), was translocated through the tri-culture tissue at 37°C, compared to 14% (0.21μg) at 4°C. The cellular uptake by EA.hy926 was three times higher at 37°C, but the silver in basolateral medium was 83% lower than 4°C. The overall recovery of silver in tri-culture was above 90% for both temperatures.

When a concentration equal to one magnitude more silver was introduced to the system at 37°C, 20 times more of it actively interacted with cells and was found either intracellularly or present in the lower chamber medium (Figure 5.5 B). Approximately 15% of silver (2.2 μg), was found concurrently in the apical side mixed cells and lower chamber medium. At 4°C, less silver was detected throughout the system, however, uptake and translocation did occur. Collectively, 63% (37°C) and 43% (4°C) of silver were recovered from the tri-cultures, similar to the extent in bi-cultures exposed to 30 mg/L silver.

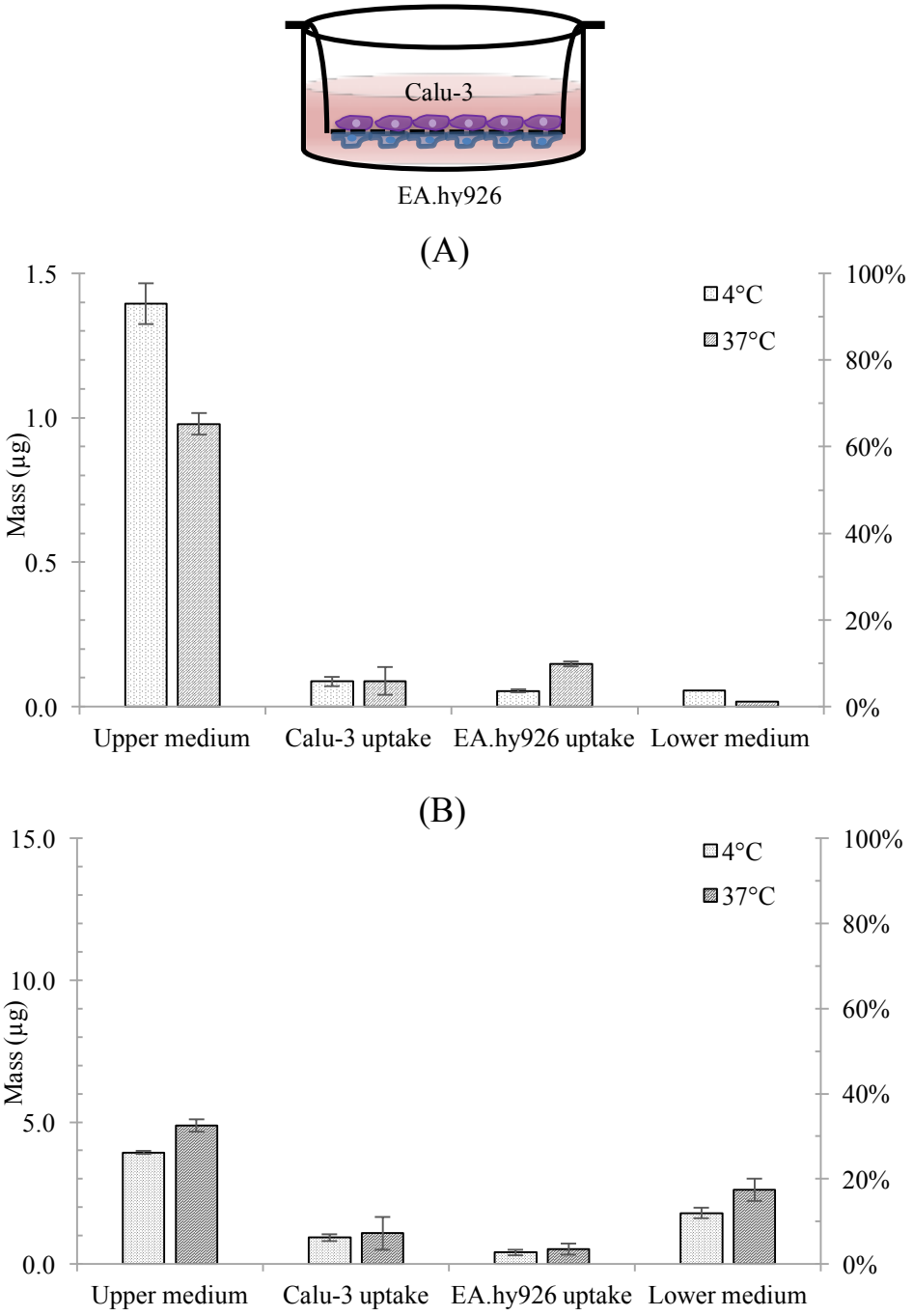

Figure 5.4. Cellular uptake and translocation of AgNPs in bi-culture. (A) depicts the mass of silver distributed in each component of the bi-culture system at 3 mg/L of AgNPs, and (B) at 30 mg/L. Data are presented as mean ± SD of three samples.

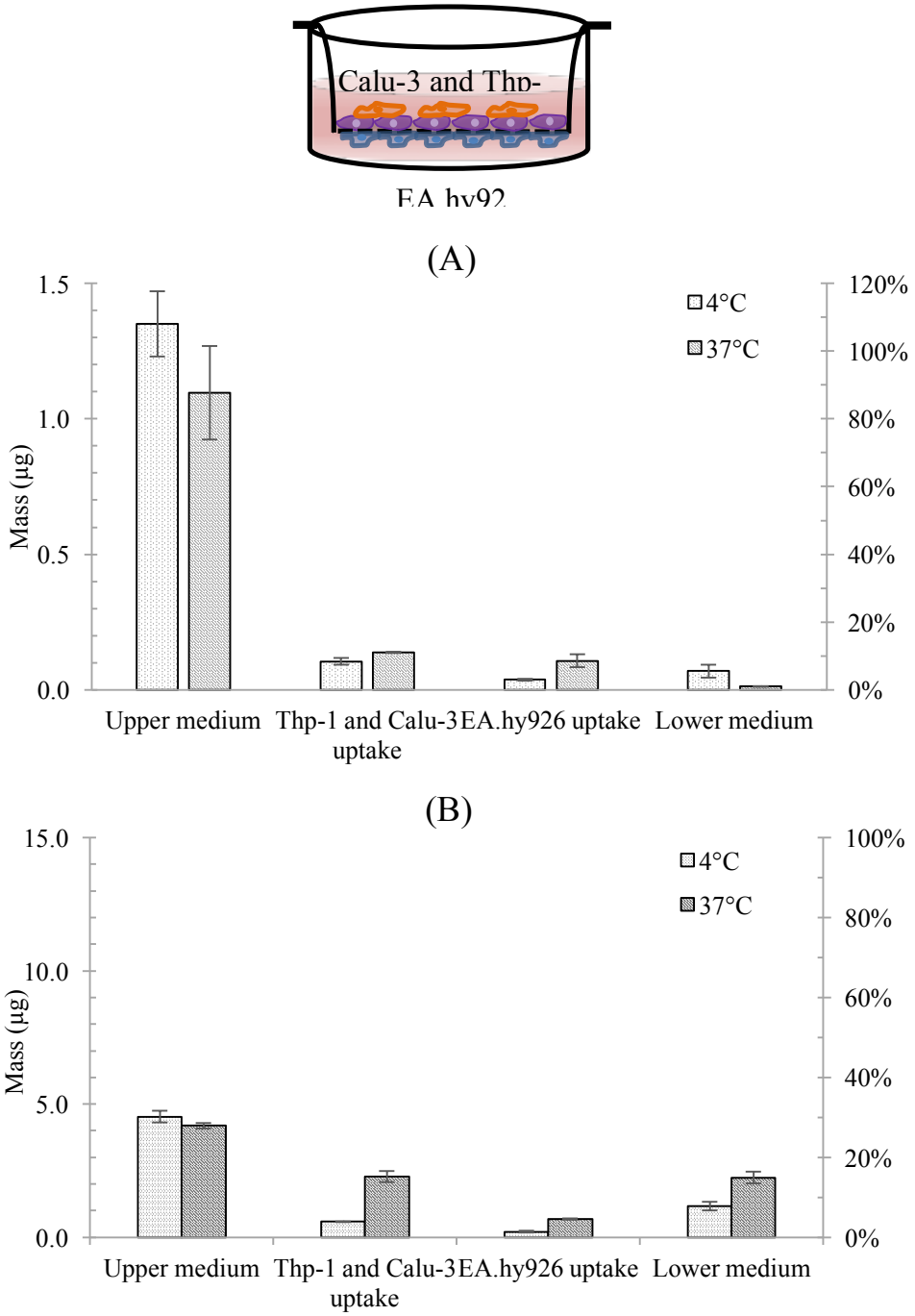

Figure 5.5. Cellular uptake and translocation of AgNPs in tri-culture. (A) depicts the mass of silver distributed in each component of the tri-culture system at 3 mg/L of AgNPs, and (B) at 30 mg/L. Data are presented as mean ± SD of three samples.

Acellular Translocation of AgNPs

AgNPs were added into acellular dual chambers systems, exactly the same as the chambers used in these experiments, to evaluate the retention of particles by permeable membranes of various pore sizes. After 24 hr, significant amounts of NPs were found in the lower chambers for all membranes tested. The medium pore size membrane (1 μm), surprisingly, had the most Ag detected in the lower chambers, averaging (44 ± 8)% from the three replicates. Approximately 41% of AgNPs successfully translocated through 3 μm membranes, and less than 20% through the 0.4 μm membranes (Figure 5.6 A). Although significantly different in pore size, the 3 μm and 1 μm sized porous membranes exhibited similar NP permeability, only 1.6% of the silver was in the upper chamber medium. In addition to the loss of AgNPs during sample preparation and analysis, over 50% of silver was unaccounted from each experiment condition. The dissected membranes shown in Figure 5.6 B, displayed varied degrees of discoloration compared to the blank control. This is considerable evidence of accumulation of silver particulate over time. Those trapped and retained by the membranes account for most of the unaccounted for AgNPs.

Cytotoxicity of AgNPs

Monoculture. The evaluation of potential adverse effects due to AgNPs exposure in monocultures of epithelial cells, endothelial cells, and macrophage-like cells was performed in a 96-well plate using the LDH assay. Triton X dilution, a cell lysis buffer, was used in the experiment as a positive control and all data were normalized to a blank control. Among all types of cells, epithelial, Calu-3 cells are the most tolerant to AgNP exposures. Regardless of culture temperature or concentration administrated, the cell

membrane was not disrupted or damaged compared to blank control at 4ºC and 37ºC, indicating negligible cellular stress (Figure 5.7). Differentiated Thp-1 cells were the next tolerant cells among those tested. A concentration-dependent toxic response to the AgNPs was observed. Cells remained intact at the lower dosage but failed to contain LDH intracellularly upon a higher dosage. When incubated at 37ºC, Thp-1 membrane exacerbation was about 28% higher than that of 4ºC. The same pattern was noted with the Triton-X positive control in all three monocultures, where the cellular response was more intense in the warm (37°C) medium compared to cold (4°C) conditions. EA.hy926, endothelial cells, were significantly injured after AgNPs treatment. LDH activity in both 3 mg/L and 30 mg/L wells at 4ºC was almost equivalent to that seen in positive control, indicating potent membrane disruption from AgNP exposures at the lower temperature. Warmer medium, because of its physiological relevance, appears to be more protective of cells, as observed with endothelial cells exposed to 3 mg/L of AgNPs at 37ºC. There was no statistically significant reduction in viability observed 24 hr post exposure.

Bi-culture. When bi-cultures (Calu-3 and EA.hy926) were established (TEER > 1000 $\Omega \cdot cm^2$), the toxicity of AgNPs in each cell line was evaluated separately for LDH release after 24 hr exposure. This experiment aimed to understand if the toxicity observed from monocultures was altered due to the addition of another type of cell. When in bi-culture, EA.hy926 cells exhibited different response patterns upon AgNP treatment. At 4°C, regardless of concentration administered, LDH leakage was not significantly increased, cellular response was similar to those in the control group. However, cells incubated at 37°C were more responsive towards AgNPs treatment. At both 3 mg/L and 30 mg/L, the cell membrane was significantly damaged, producing elevated amounts of

LDH (67% and 104% more, respectively), in a dose-dependent manner. A similar toxic response was also observed in Calu-3 cells in the upper chambers. For both temperatures and concentrations tested, increasing amounts of LDH were detected in medium; except for 3 mg/L at 4°C, where LDH leakage was minor and negligible.

Tri-culture. When in tri-culture, the lower incubation temperature was no longer as protective as was observed in bi-culture for EA.hy926. In fact, all treated cells showed some injury, and those at 4ºC displayed significant cellular stress. Approximately 15% and 65% more LDH, was found in the endothelial cell medium at 3 mg/L and 30 mg/L, respectively, compared to 10% and 25% at 37 ºC. A similar toxic response was also observed in the tissue co-culture of Thp-1 and Calu-3 cells in the upper chambers. The toxicity observed was less severe when the exposure was conducted at 37ºC than 4ºC, although the damage was still significant.

Discussion

Barrier Properties

To mimic the human alveolar-capillary barrier *in vivo*, the lung model has to display acceptable pulmonary barrier characteristics, such as epithelial tight junctions, the presence of alveolar macrophages, pulmonary surfactant, and endothelium of blood micro-vessels[44]. Many researchers have tried to establish these models by engaging A549, a type of alveolar type II cell line extracted from human lung carcinoma, for their relevant origin and ultrastructural characteristics[46, 124]. However, it has been discussed in recent manuscripts that A549 are not suitable for NP translocation studies, due to their suboptimal formation of tight junctions and poor control of macromolecules passing

through the epithelium[44, 125]. Calu-3 cells, on the other hand, are able to develop high TEER values on porous membranes in this study, both alone (876.67 ± 75.64 $\Omega \cdot cm^2$) and with other cells (1267 ± 142.08 $\Omega \cdot cm^2$). The models express a similar formation of tight junctions as required for an alveolar epithelium. Therefore, Calu-3 were chosen to replace A549 and co-cultured with PMA-differentiated Thp-1 macrophages, EA.hy926 microvascular endothelium to simulate the alveolar-capillary barrier *in vivo*. When stable bi-cultures were further extended by adding differentiated macrophages to the apical side of Calu-3, TEER drastically dropped within 24 hr. This decrease is similar to that observed by Klein et al. (2013) who also reported higher permeable pulmonary tri-culture after adding activated Thp-1 to the system[126]. Luyts et al. (2015) found that PMA-activated macrophages impaired the bi-culture barrier functionality by 1) secreting TNF-α, a cell signaling protein primarily secreted by activated macrophages when in systemic inflammation; and 2) simply the macrophages having direct contact with the epithelium[127]. Dekali et al.(2014) also further demonstrated morphological changes of Calu-3, including length reduction and disappearance of microvilli structures when Thp-1 macrophages deposited onto their apical side[44]. Interestingly, despite the 78.3% decrease in TEER in the first 24 hr, it continuously regained the electrical resistance, continuing for another 4 days. When TEER readings were over 1000 $\Omega \cdot cm^2$, this indicated the impairment of the barrier was temporary and reversible, and the resultant tri-culture again exhibits the same appropriate barrier properties. To the best of our knowledge, this is the first time the rebound of TEER, in a tri-culture for 5 days after an initial drop, has been reported in literature. Other investigators have only documented the decreased TEER occurring for up to 24 hrs.

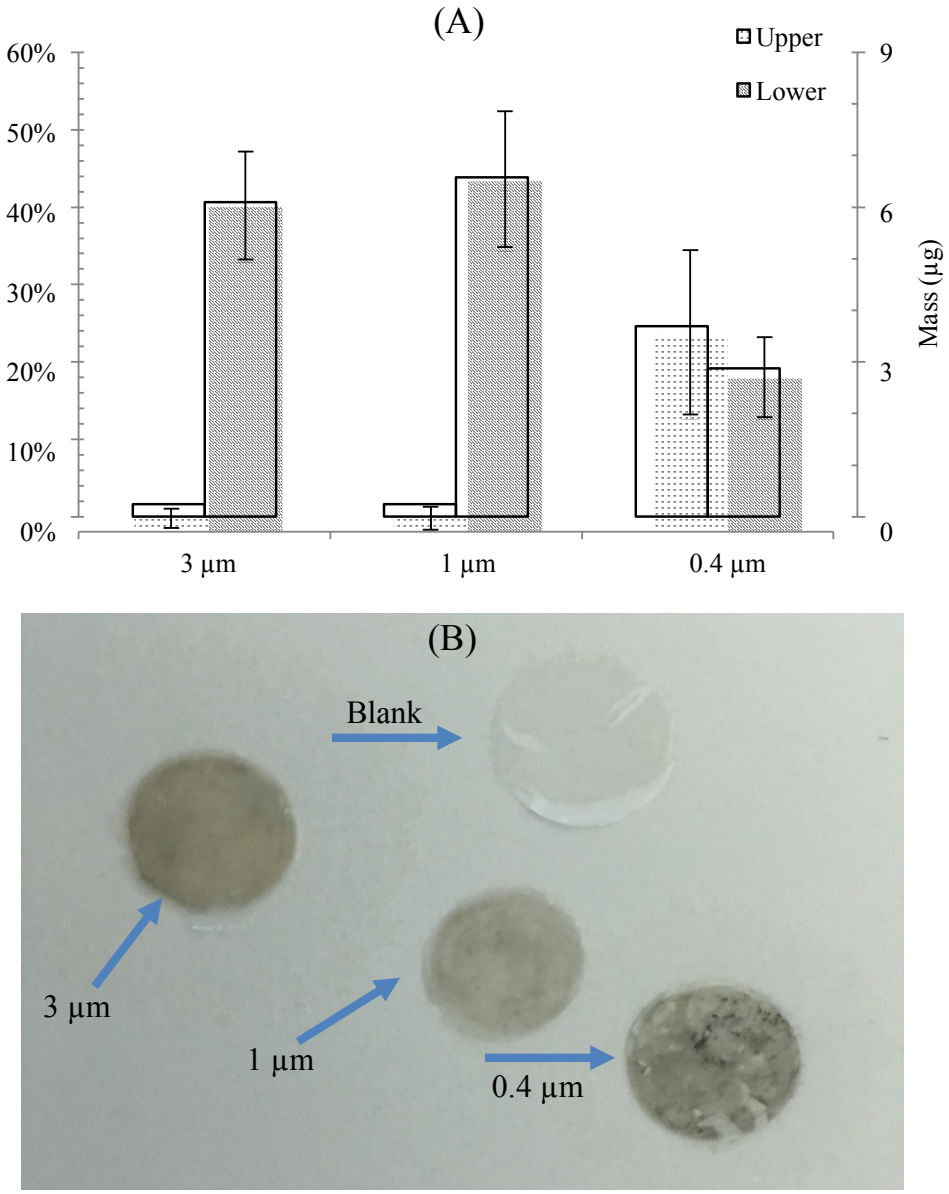

Figure 5.6. (A) AgNPs found in the upper and lower chambers after 24 hours of incubation. Membranes bearing pore sizes 3 µm, 1 µm and 0.4 µm were exposed to 30 mg/L of AgNPs, acellularly. Data are presented as mean ± SD of three samples. (B) Images of permeable membranes with various pore sizes treated with 30 mg/L AgNPs for 24 hr. Blank refers to membranes that were not exposed to AgNPs which represents the natural coloring of the material. Samples shown in (B) each was a stack of three membranes from replicate experiments to improve the visual effects. All membranes are made with polyester.

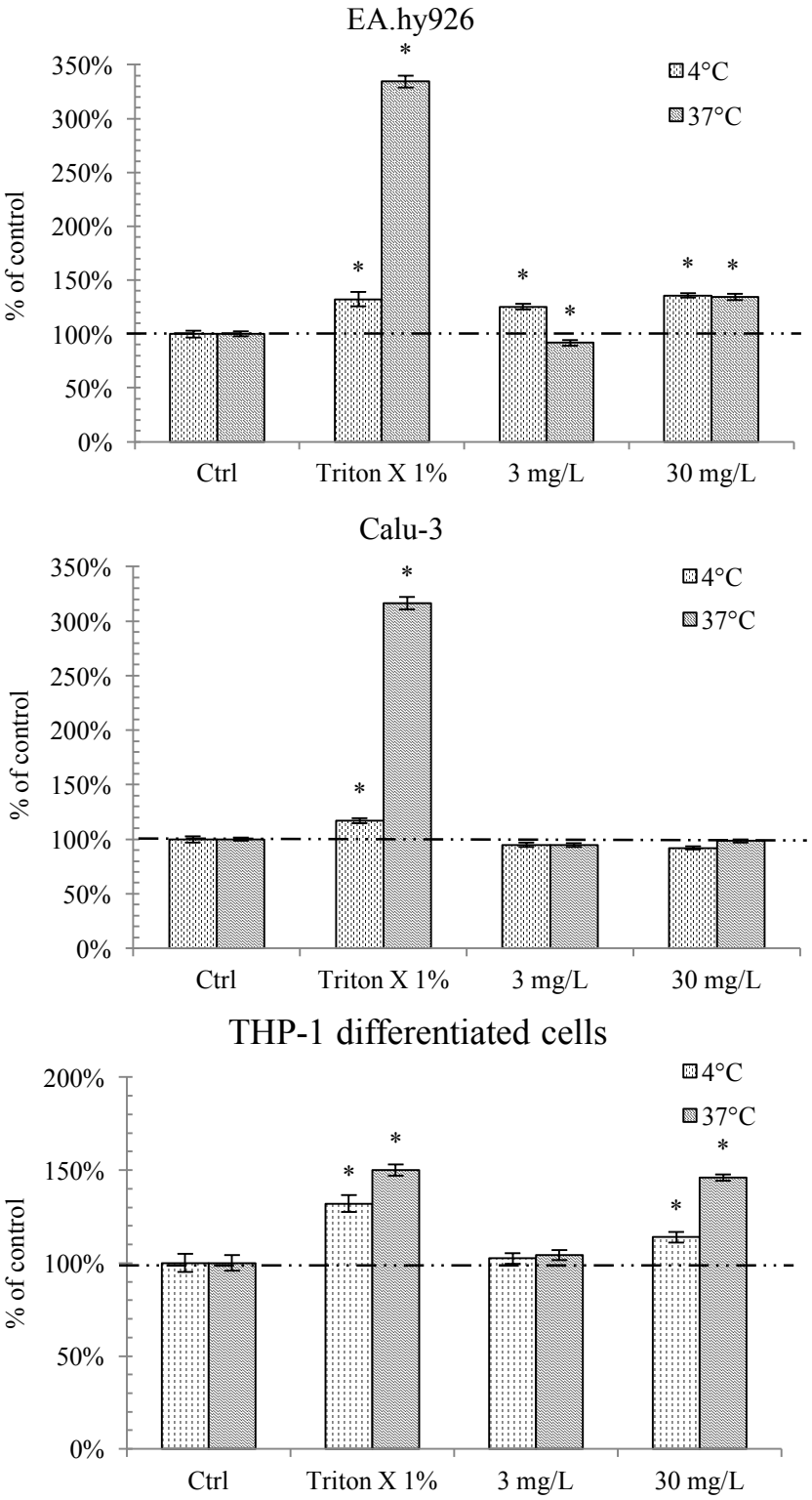

Figure 5.7. Cytotoxicity of AgNPs in three monocultures. Each monoculture was exposed to both 3 mg/L and 30 mg/L AgNPs for 24 hr at either 4ºC or 37°C. Medium was then exacted for LDH content evaluation. Data are presented as mean values ± SEM. *p* values indicate statistical significance to the control, where * $p < .05$.

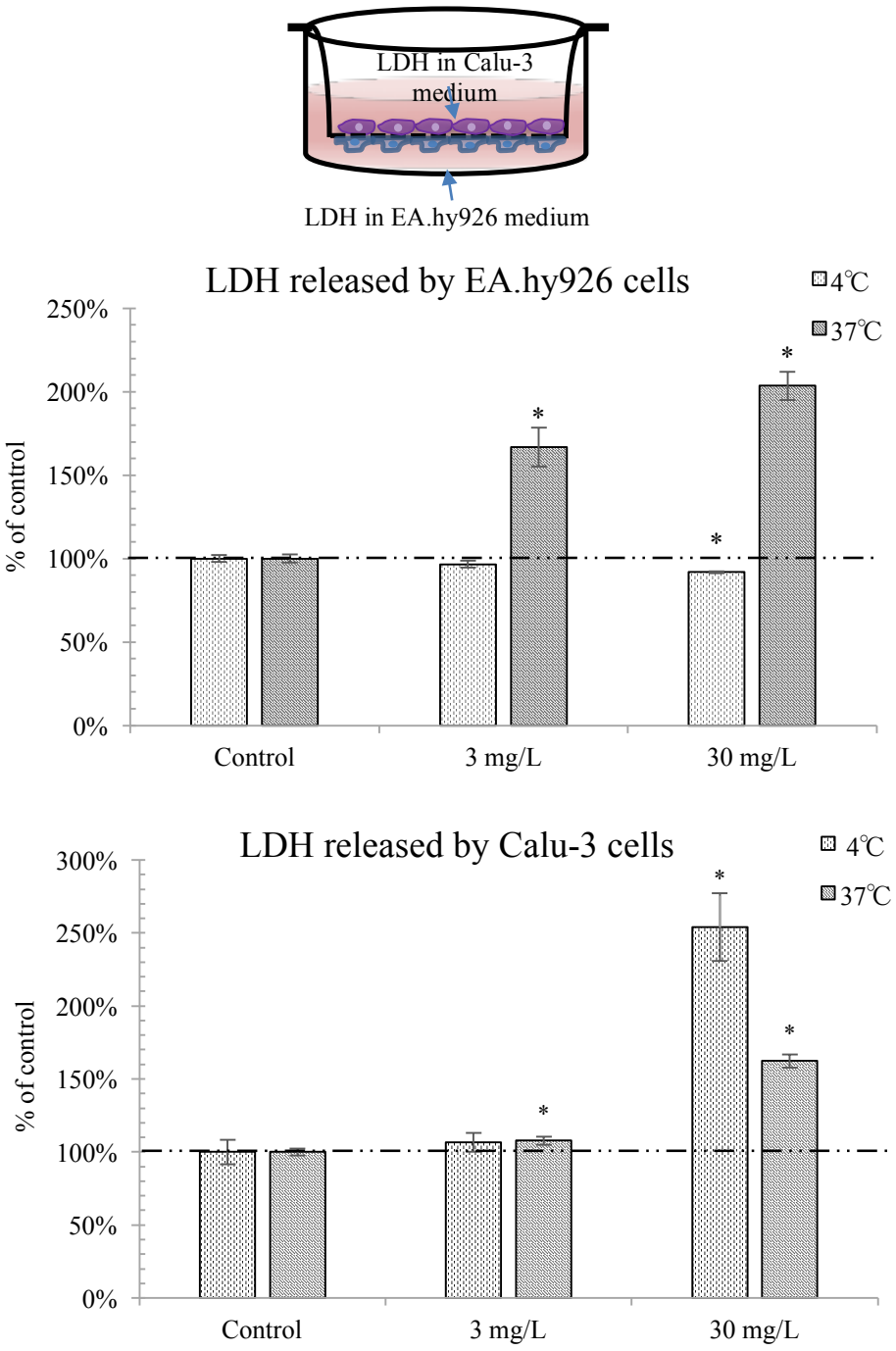

Figure 5.8. Cytotoxicity of AgNPs in terms of LDH release in bi-culture. Bi-culture was incubated with 3 mg/L and 30 mg/L of AgNPs at either 4°C or 37°C for 24 hr. At the end of the exposure, medium from the insert (Calu-3 medium) and receiving well (EA.hy926 medium) was extracted and evaluated separately for cytotoxicity of the individual cell layer. Data are presented as mean values ± SEM. *p* values indicate statistical significance to the control, where * $p < .05$.

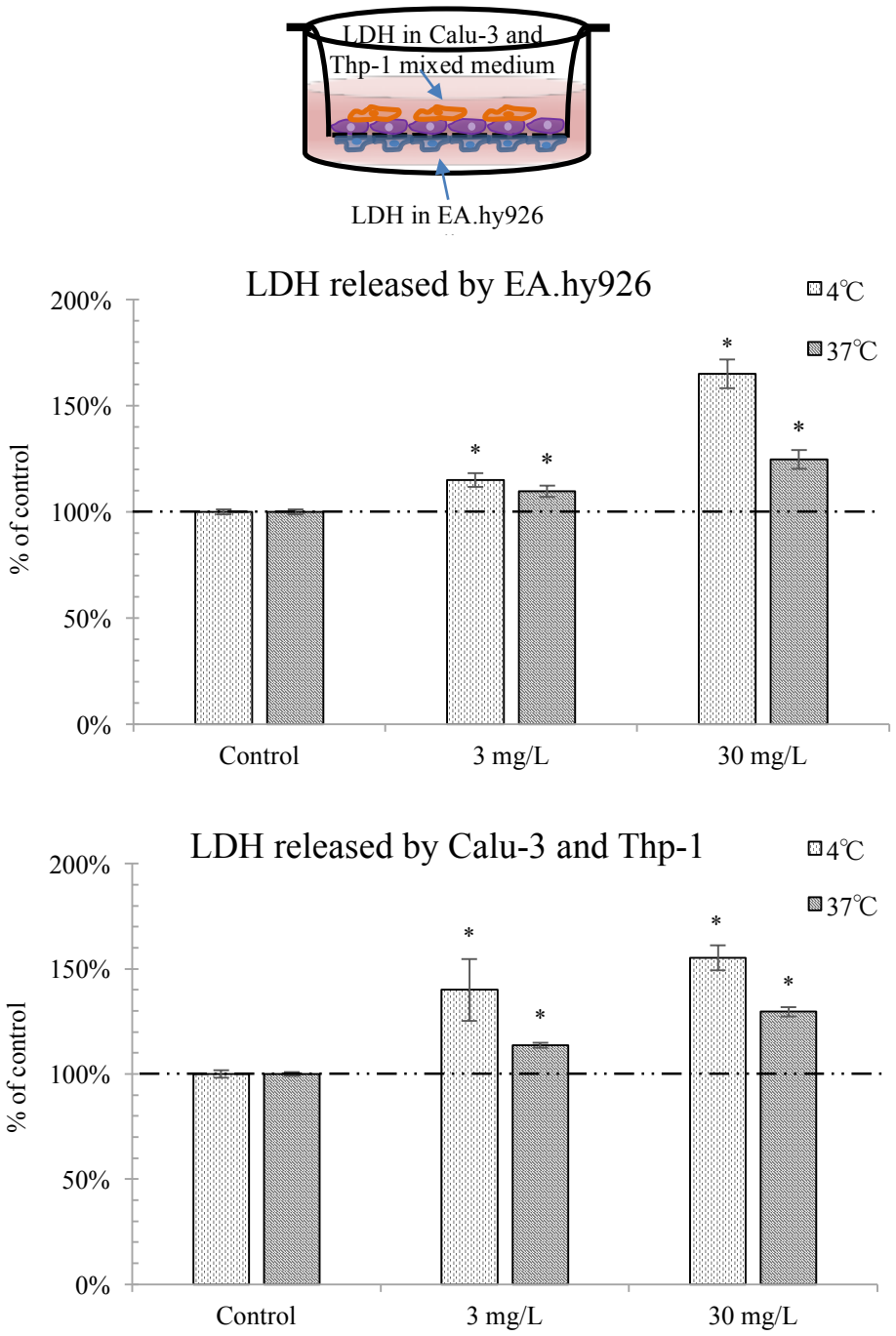

Figure 5.9. Cytotoxicity of AgNPs in terms of LDH release in tri-culture, exposure to 3 mg/L and 30 mg/L of AgNPs at either 4°C or 37°C for 24 hr. As described for bi-culture, media from the insert (Calu-3 and Thp-1 mixed medium) and receiving well (EA.hy926 medium) were extracted and evaluated separately for cytotoxicity in both chambers. Data are presented as mean values ± SEM. *p* values indicate statistical significance to the control, where * $p < .05$.

Uptake and Translocation of AgNPs

Cellular uptake of AgNPs and their migration through epithelial barriers have been frequently reported, yet many of these results were achieved by microscopy imaging and lack adequate quantitative evaluation. To help fill the gap in knowledge in this particular area in literature, the authors quantitatively described the spatial distribution of silver using ICP-MS. Further, each component of the co-culture system was specifically evaluated for their roles in transporting AgNPs through the modeled alveolar-capillary barrier. To explore the mechanism of this process by cells, experiments were conducted at both 4°C and 37°C at two AgNPs concentrations. Overall, the uptake and movement of AgNPs are concentration and energy dependent. When 30 mg/L of AgNPs were administered to bi-cultures at 37°C, Calu-3 cells had one magnitude greater uptake, and the combined transported Ag, including that which was intracellular and that present in lower chamber medium, were approximately 16 times the amount of those in 3 mg/L. Similar observations were noticed in tri-cultures, where the uptake and translocation of Ag was both one magnitude higher at 30 mg/L. It is hypothesized that the cell membrane was significantly compromised at 30 mg/L, and allowed more silver to passively translocate. Although less Ag was translocated at 4°C, the occurrence of this event indicates that Ag was able to passively diffuse into and be released by cells even when ATP synthesis is paused[128]. Generally, 22% to 265% more silver interacted with the co-cultures at 37°C, suggesting active transport by cells that requires energy. The reduced rate of uptake at 4°C is in accordance with recently published work by Betzer et al. (2015) [129] (Betzer et al. 2015) and earlier research completed by Tedja et al. (2012)[129-130] who both noted significantly less cellular uptake of NPs in energy depleted conditions.

Although the exact pathway for cells to internalize particles is still not clear, many researchers support the theory that both passive and active transport contribute to the process[129-131].

Alveolar macrophages are tissue-resident, and they play an important role in the clearance of foreign materials in the alveolar space[127]. The macrophage characteristics of Thp-1 cells is determined by the contact cells, and the co-culture with Calu-3 epithelial cells will enable some phenotypes of alveolar macrophages in Thp-1 macrophages. Cellular uptake and translocation of AgNPs was significantly enhanced at 37°C for tri-culture, implying activated and functioning alveolar like macrophages on site. This phenomenon has been observed by Kim and Choi[132], Mukherjee et al.[133] and Geiser et al.[134]. Furthermore, when incubated in cold (4°C) temperatures, the tri-cultures showed no significant uptake over the bi-cultures. It has been shown that phagocytic uptake by macrophage-like cells requires energy and is therefore not activated at 4°C[135].

Choice of Permeable Membrane Supports

While permeable supports are available in several materials and pore sizes, co-culture experiments typically use polyester (PET) with 0.4 μm, 1 μm and 3 μm pore sizes. PET provides the best optical property, thus enhanced cell visibility and monolayer formation. While 0.4 μm and 1 μm are recommended for studies of drug transport or those requiring fully differentiated monolayers, 3 μm are good for cell invasion and motility studies, as cell migration does not occur with smaller pores[136]. The authors found that 0.4 μm porous membrane have been extensively used in the field, perhaps due to the optimal formation and attachment of monolayers on both apical and basolateral sides[44, 127, 137]. There is increasing discussion; however, about this smaller pore membrane

limiting the passage of particulates from apical to basolateral sides, and thus a good amount of research had been conducted using 3 μm porous supports[138]. Only a few manuscripts have quantified the exact transported or retained particles by the membrane of their choice. In the present study, for the first time in literature, all three sizes of polyester membranes available for co-culture, were quantitatively evaluated for the retention of AgNPs to validate the permeable supports chosen for this study. Further, this allowsfor elucidating the loss of silver observed in Figure 5.4 B and Figure 5.5 B. In fact, in this study all the tested permeable supports hindered the passing of AgNPs at 30 mg/L. Although less than 2% of silver was found in the 1 μm and 3 μm inserts, significant amounts of silver was embedded in all the membranes. AgNPs aggregate when having contact with physiological fluids, and the aggregated size will further mitigate their passage through the pores. Previously, the same tannic acid- coated AgNPs were shown to have a hydrodynamic diameter of 189.6 ± 9.0 nm after 24 hr in media at 3 mg/L, indicating the presence of aggregated silver particles (primary size by TEM 49.8 ± 5.7 nm) in culture[37], and potentially larger aggregates when in higher concentration[139]. Therefore, the loss of silver in the retention experiment (Figure 5.6) and the uptake/translocation experiments (Figures 5.4 and 5.5) is most likely a result of trapped, aggregated silver particles. Our study revealed that the 0.4 μm sized membrane is the least acceptable for NP transport studies as approximately 25% of silver was retained in the inserts, and the pores were significantly clogged by aggregated AgNPs (see Figure 5.7). Since this study experienced repeated problems seeding and maintaining EA.hy926 on basolateral 3 μm membranes due to the relative big pore size, it was conducted on 1 μm permeable membranes for their comparable filtering ability and improved formation

of stable and functional bi-culture barriers. In light of these findings, the authors strongly suggest future transport and permeability studies include membrane retention testing to select the most appropriate membrane supports and limit the interference of particles with the membranes.

Toxicity

Many cytotoxicity assays have been used in literature to evaluate the harmful effects of NPs. LDH leakage was chosen in this study because the procedure is non-invasive to cells. Samples can be collected without having direct contact with the culture, providing a significant advantage over other assays when handling co-cultures especially. In the meantime, media can be extracted and evaluated separately for distinct cytotoxicity from each component in the modeled barrier. Extracellular LDH content indicates failure of membrane integrity or a compromised cell due to disrupted energy production catalyzed by LDH in cells[140]. When comparing cytotoxicity observed in the tri-culture, to bi-culture model or monocultures, it is clear that with the number of cell types growing in the system, the culture becomes more responsive to AgNPs treatment. Physiologically relevant co-cultures are more reactive to AgNPs due to the activated Thp-1 macrophages. Napierska et al. (2012) evaluated cytokine production by co-cultures when exposed to SiO_2-NPs. They found elevated levels of TNF-α, IL-8 and IL-6 only in the Thp-1 containing co-cultures following exposure to 5 μg/cm^2 NPs[124a]. TNF-α, as mentioned earlier, is a pro-inflammation molecule mainly secreted by macrophages, which activates further production of more pro-inflammatory mediators by other cells. Further, it has been reported that TNF-α can increase the permeability of epithelial barriers[141]. There is evidence to support that inflammatory mediators, including TNF-α, IL-6 and IL-8

contribute to the development of pulmonary fibrosis and many other chronic pulmonary diseases[142]. Therefore, activated Thp-1 macrophages in tri-culture, play the central role in providing a physiological relevant response to NPs exposure. Often, the cytotoxicity of AgNPs correlates to the amount of uptake by cells. With less silver in co-culture at 4°C, significant cytotoxicity was constantly observed. This is hypothesized to be due to changes in permeability of cell membranes. Cell membranes tend to have higher permeability at 4°C[128], and with the additional exposure to AgNPs, it is likely that the toxic effects of AgNPs was further augmented in this condition. This was consistently observed as more LDH in extracellular matrix.

Conclusion

Recently, the possibility of nanomaterials translocating through epithelial barriers into the bloodstream has raised concern for the public. Both workers and consumers are susceptible populations to such exposure and are potentially affected. Tracking the movements of nanomaterials from an epithelial barrier, and reaching the endothelial lining, is typically resolved using *in vivo* studies. However, this approach can be lengthy and expensive, with the limitation of insights into the pathobiological pathways at the cellular level. Therefore, a physiologically relevant 3D model, engaging multiple cell types, is a reasonable alternative to mimic *in vivo* conditions, while delivering cost-effective and high throughput results. In this study, the authors present a novel co-culture model that carries similar alveolar-capillary barrier properties to that of *in vivo* conditions by engaging Thp-1 differentiated cells (macrophages), Calu-3 cells (epithelium), and EA.hy926 cells (endothelium) in a two-chamber system. The authors further validated the high sensitivity of this model to track the translocation of AgNPs across the pulmonary

barrier and its resultant toxicity. It has been observed that by engaging Calu-3 and Thp-1 macrophages in the tri-culture, the constructed barrier displays representative characters of the alveolar barrier *in vivo*, and provides a physiologically relevant response to AgNPs. This response differs to that observed in conventional monoculture and further illustrates the improved model system. With its unique three-dimensional setup, the authors not only confirmed the AgNP translocation through the alveolar-capillary barrier, but also quantified the spatial distribution of Ag within each component of the barrier for, to the best of our knowledge, the first time in literature. Cytotoxicity in tri-cultures was more sensitive when compared to bi-culture or monoculture, due to the central role of activated Thp-1 macrophages. Additionally, the authors quantitatively evaluated the retention of AgNPs by commonly used porous membranes, and revealed that all tested membranes retained some aggregated AgNPs. The authors concluded that 1 μm and 3 μm sized porous membranes have better permeability and thus are more suitable for transport studies of macromolecules, however the 3μm pore size membranes may not offer the tight junctions needed to establish satisfactory TEER readings. The significance of this model is that it physiologically resembles the alveolar-capillary barrier, and provides insight into the translocation of AgNPs through the barrier with a more sensitive and reliable response. With these properties, this novel system can be a valuable tool for nano-biotechnologies in the evaluation of the transport, distribution and toxicity of nano-sized therapeutics, and the design of more specific targeting and delivery systems, as well as more biocompatible and safer nano-drug delivery systems. The implications of this model for developing and testing novel nano-delivery systems for use in multiple capacities are significant.

CHAPTER SIX

Conclusion

AgNPs are one of the leading nanomaterial used in industry for the benefit of their enhanced antimicrobial efficacy andthermal and optical properties as compared to the bulk size parent. Consequently, questions were raised about how they interact with environmental and biological matrices after being released from manufacturing sources and consumer products. Many *in vivo* and *in vitro* models have thus been used to simulate exposure scenarios and evaluate the resultant toxicity in biological receptors ranging from microorganisms, to mammalian cells and tissue. The behavior of AgNPs is found to be greatly dependent on the physicochemical properties, such as particle diameter, morphology, and surface net charge. Therefore, three sets of experiments were conducted to expand the understanding of the role of another import physicochemical property of AgNPs, capping agents, in particle-cell interactions using *in vitro* models.

Findings from research conducted for Objective One, revealed that surface functioning group, not only provide different levels of stability to AgNPs, but also affects their biological fate. NPs of different capping agents, exhibited different cell penetration efficacy across human lung and intestinal epithelium. This is hypothesized to be an influence of protein corona, a layer of selective proteins adsorbed to the surface of AgNPs when present in physiological matrices. Research conducted for Objective Two supports the hypothesis by showing irreversible changes on model cell membranes induced by soluble proteins present in concentrations near physiological levels. The

induced rearrangement of membrane bilayers then opened opportunities for entry of other macromolecules (i.e. AgNPs) into the cells. This work highlighted the critical role of the protein corona whose composition is dependent on the specific capping agent, in engaging the NP and cell membrane and the process of subsequent cellular uptake. A novel three dimensional co-culture was developed for Objective Three, and was used to track the movement of AgNPs across the alveolar-capillary barrier. By carefully choosing the cell types to assemble the co-culture system, this study was able to demonstrate exceptional barrier properties similar to that in *in vivo* conditions. AgNPs were found in all spatial units of the system, including the capillary region. The fact that the particles could still translocate into the capillary region without energy support, demonstrates that this process is a combination of both passive and active transport. Monocultures used in Chapter 3 and the 3D-tri-culture system used in Chapter 5, reacted differently when exposed to the same physiologically relevant concentration. Cytotoxicity observed from the sophisticated 3D-tri-culture underlined the critical role of alveolar macrophages in providing reliable and physiologically relevant responses. Furthermore, the tri-culture model introduced in Chapter five is highly applicable as an *in vitro* alternative method and serves the rapidly expanding field of nanomedicine in the evaluation of safety, specificity and biocompatibility of novel nano-therapeutics.

Future experiments will extend the research in Chapter four, examining structural changes in model cell membrane by AgNPs with the protein corona formation. A specification of the exact composition of the protein corona, and investigation of the impact of the major proteins on model cell membranes will be helpful in elucidating the important characteristics of capping agents on particle-cell interactions. Ongoing research

using the 3D- tri-culture lung model is aimed at improvement of the model by adding more physiological relevant components, such as pulmonary surfactant (i.e. chemically defined pulmonary surfactant) and immune cells (i.e. neutrophils), for an enhanced response upon NP exposure. Co-culture models simulating other critical biological barriers, including blood-brain barrier, blood-placenta barrier, can also be created using similar methodology and design approach, which in combination will advance the assessment of nanotoxicology, inform risk management of nanomaterials and guide the growing bio-nanotechnology field in the development of novel, safe therapeutics. Furthermore, the data collected using these types of models can also inform other types of nanodelivery systems such as specific pesticide delivery, water disinfectant regimes, and chemically responsive (i.e. pH sensitive) delivery of compounds.

APPENDICES

APPENDIX A

Supplementary Data of Chapter Three

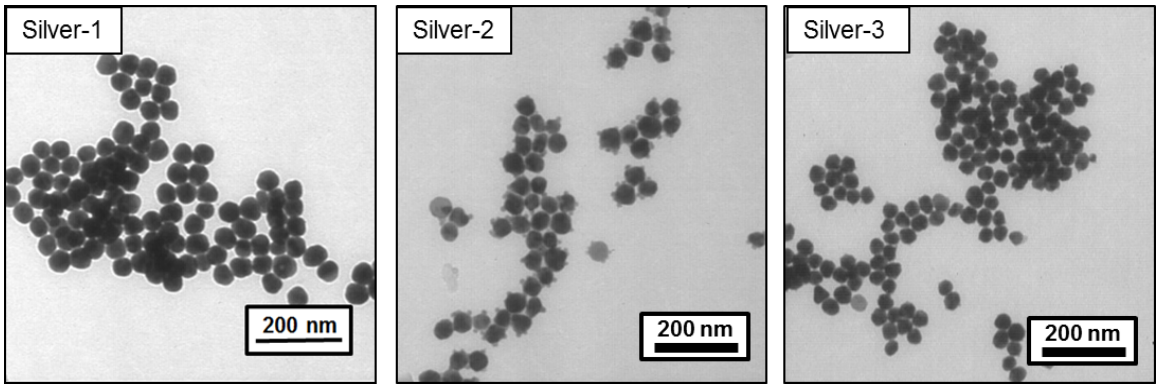

Figure A.1. Representative TEM images (100 keV; Hitachi 7000 Analytical Electron Microscope) of the three tested AgNPs: silver-1, citrate-AgNPs; silver-2, PVP-AgNPs; silver-3, tannic-AgNPs.

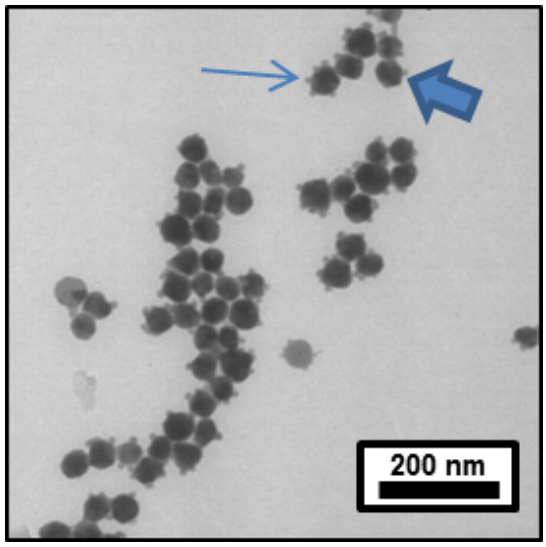

Figure A.2. Zoomed in TEM image of PVP-AgNPs with bi modal distribution. The line arrow points to the smaller particle-type while the block arrow points to the larger particle.

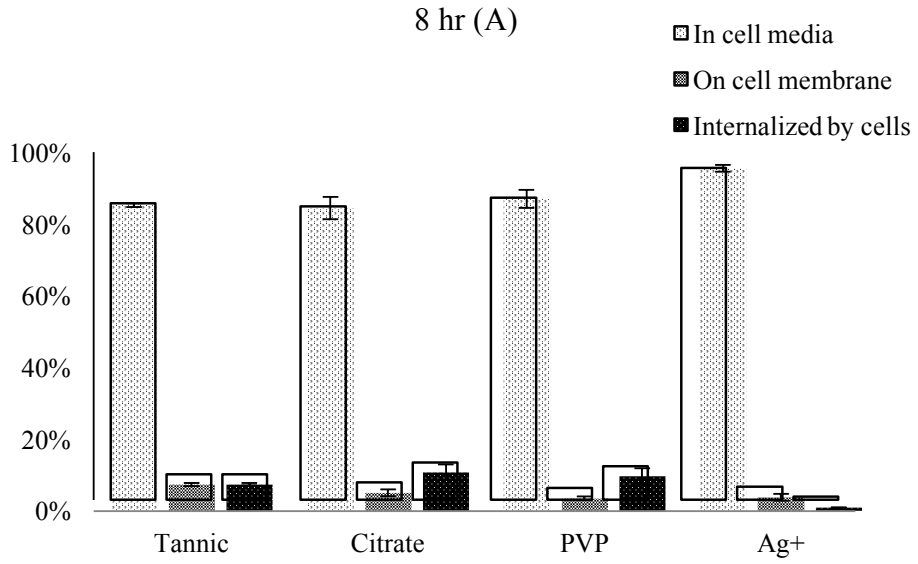
8 hr (A)
In cell media
On cell membrane
Internalized by cells
100%
80%
60%
40%
20%
0%
Tannic
Citrate
PVP
Ag+

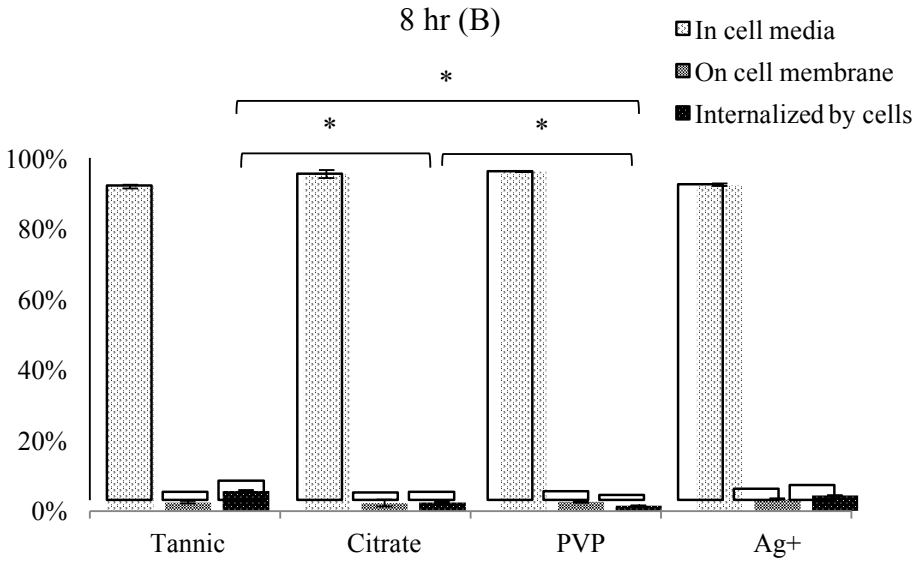
8 hr (B)
In cell media
On cell membrane
Internalized by cells
*
*
*
100%
80%
60%
40%
20%
0%
Tannic
Citrate
PVP
Ag+

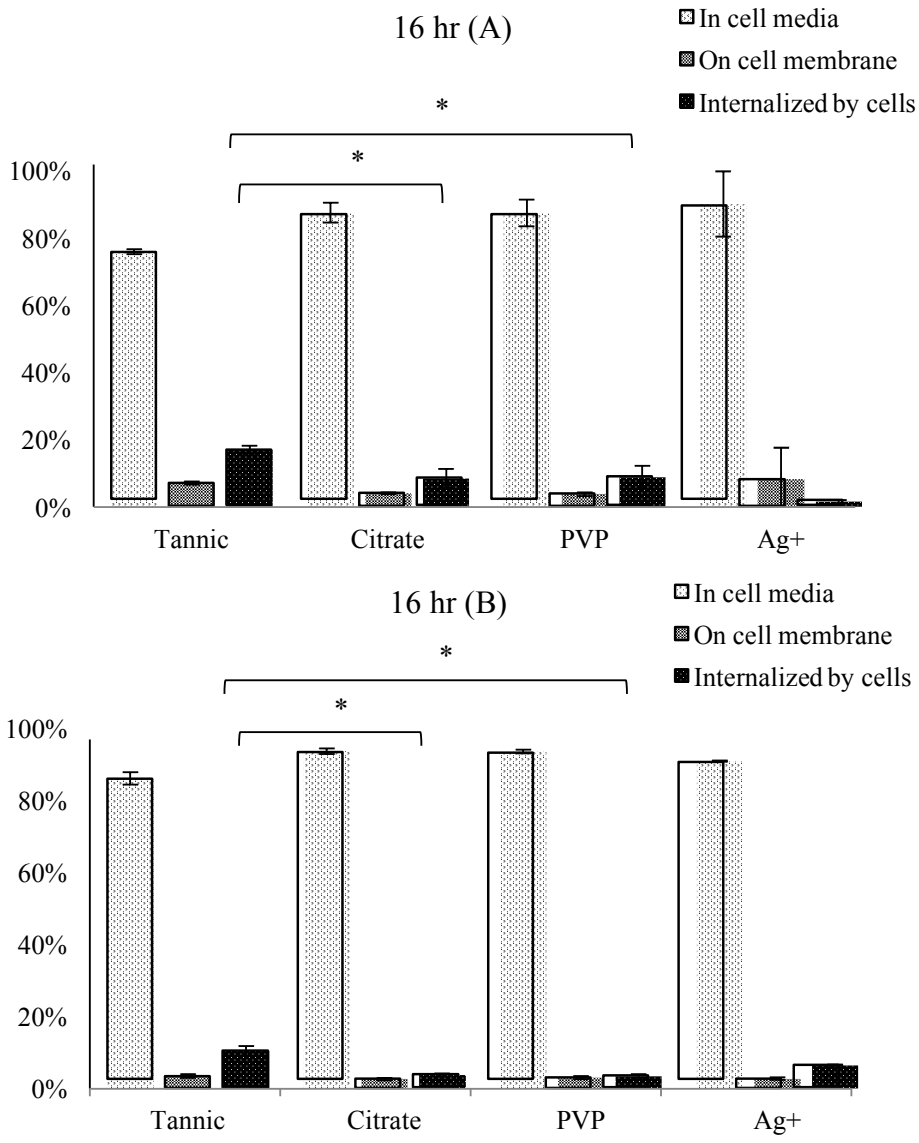

Figure A.3. Spatial distribution of AgNPs in (A) A549 and (B) Caco-2 at 8 hr and 16 hr. Data were presented as mean values ± SD. *p* values indicate statistical significance, which was accepted when $p < 0.05$.

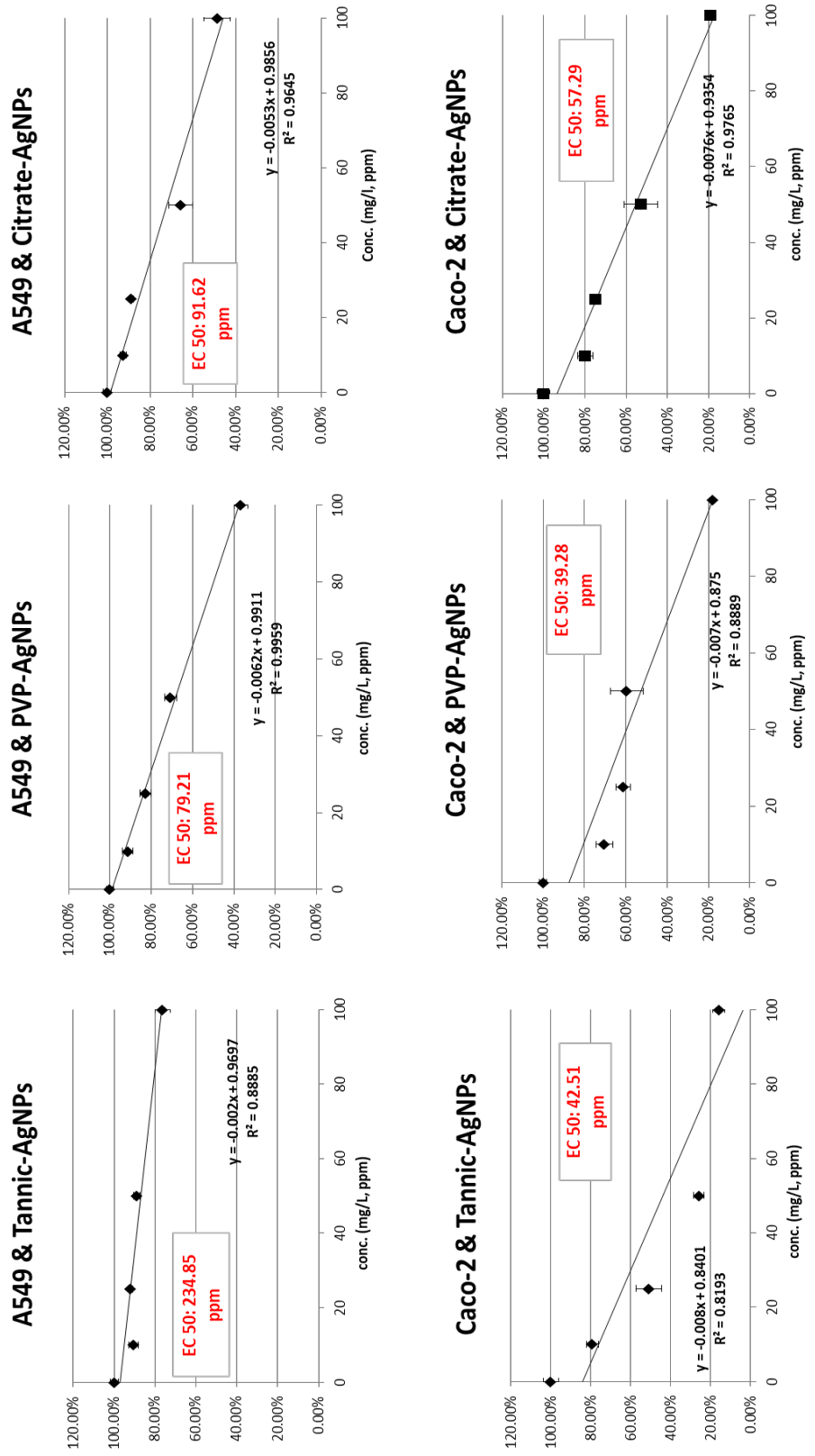

Figure A.4. Dose response toxicity study of AgNPs with A549 and Caco-2.

APPENDIX B

Supporting Information for Chapter Four

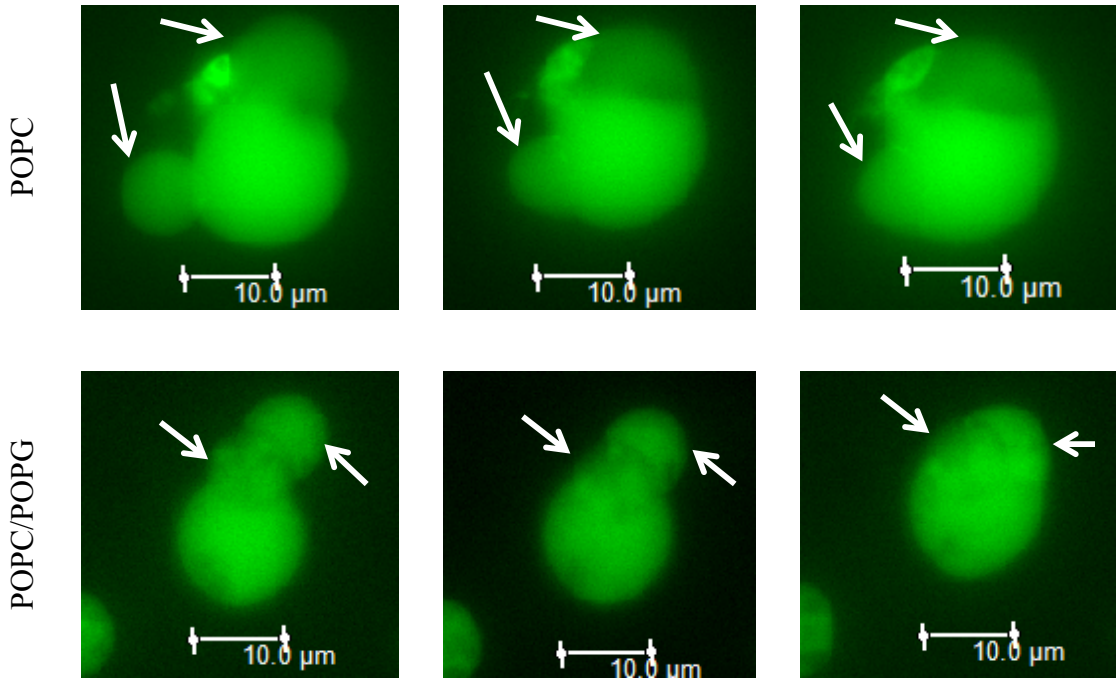

Figure B.1. Progress of vesicles fusion caused by Lysozyme. Arrows indicate vesicles that were in the process of fusing with others.

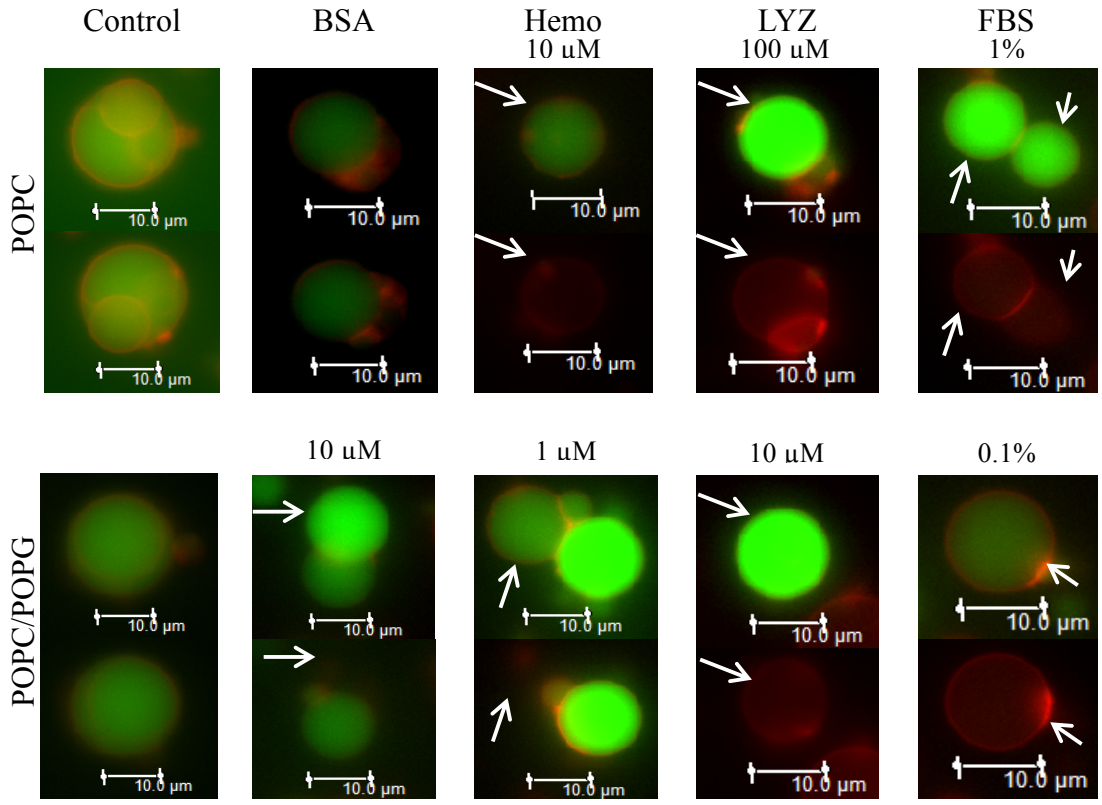

Figure B.2. Microscopy images of GUVs leakage induced by proteins studied BSA, Hemoglobin, Lysozyme and FBS. Arrows indicate the same vesicles before and after dye leakage.

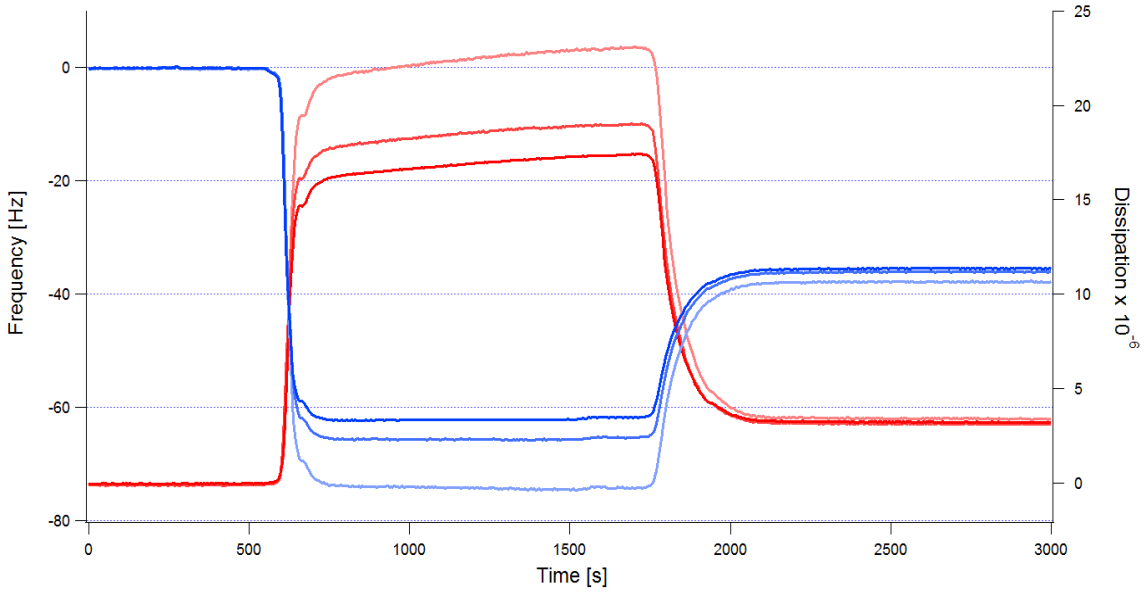

Figure B.3. QCM-D responses for the adsorption of 1 mM BSA (s=600) on silica surfaces and washed with PBS (s=1900).

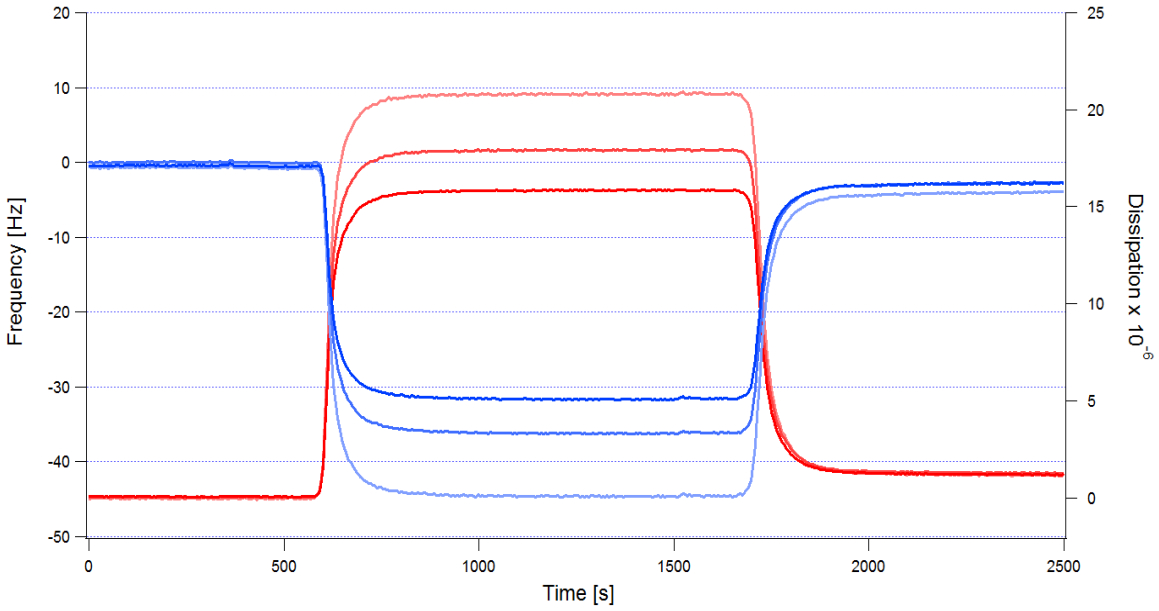

Figure B.4. QCM-D responses for the adsorption of 1 mM BSA (s=600) on POPG surfaces and washed with PBS (s=1900).

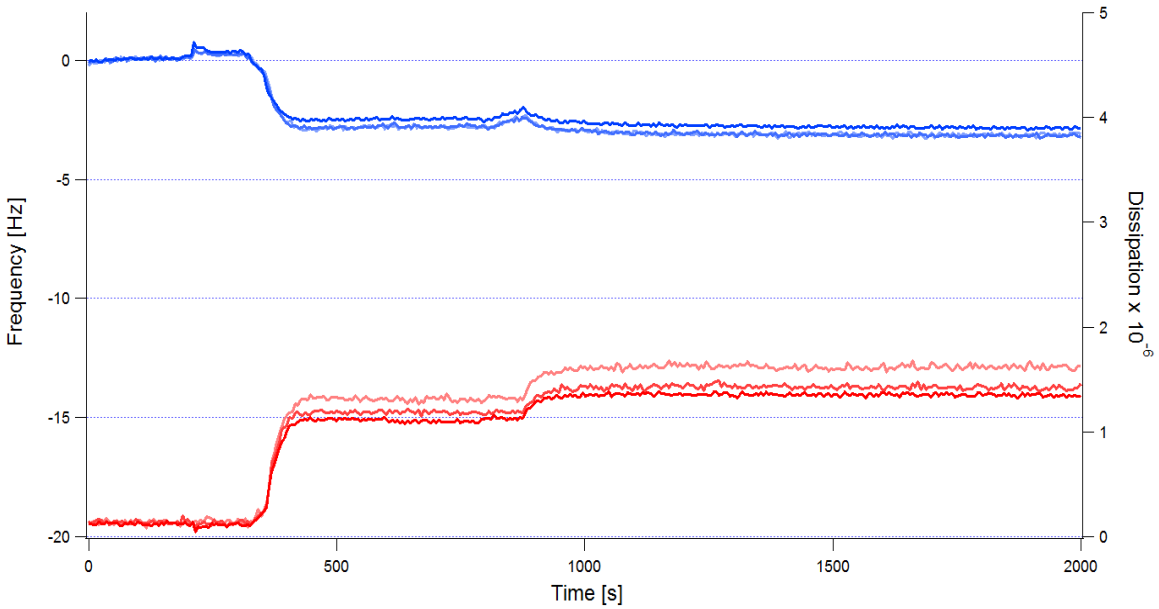

Figure B.5. QCM-D responses for the adsorption of 10 µM BSA (s=400) on POPG surfaces.

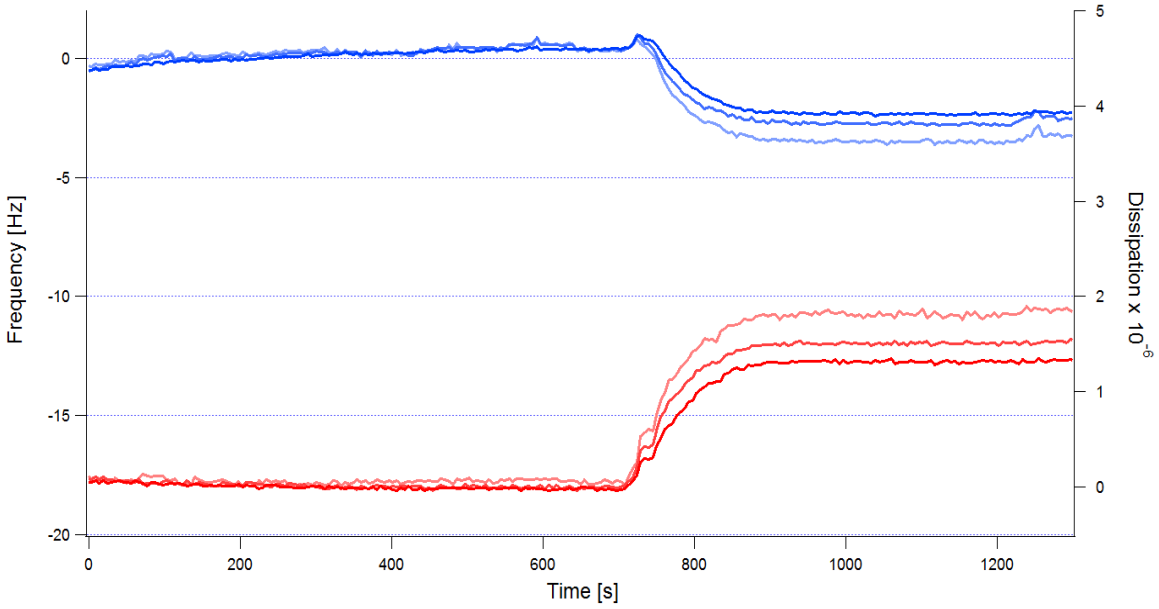

Figure B.6. QCM-D responses for the adsorption of 100 µM BSA (s=400) on POPC surfaces.

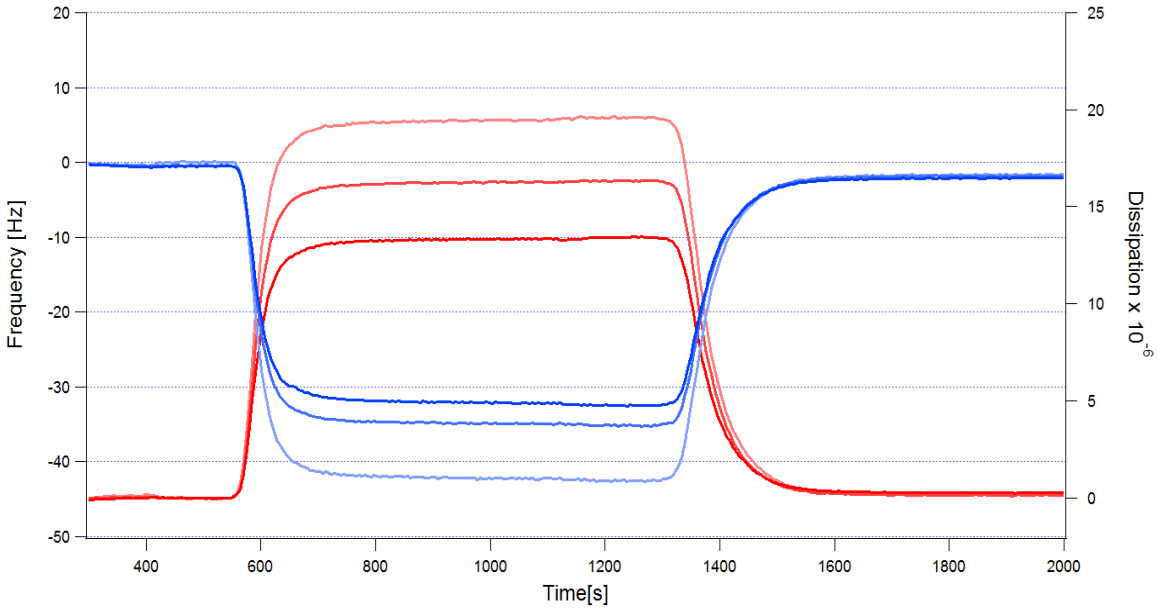

Figure B.7. QCM-D responses for the adsorption of 1mM BSA (s=600) on POPC surfaces and washing with PBS (s=1400).

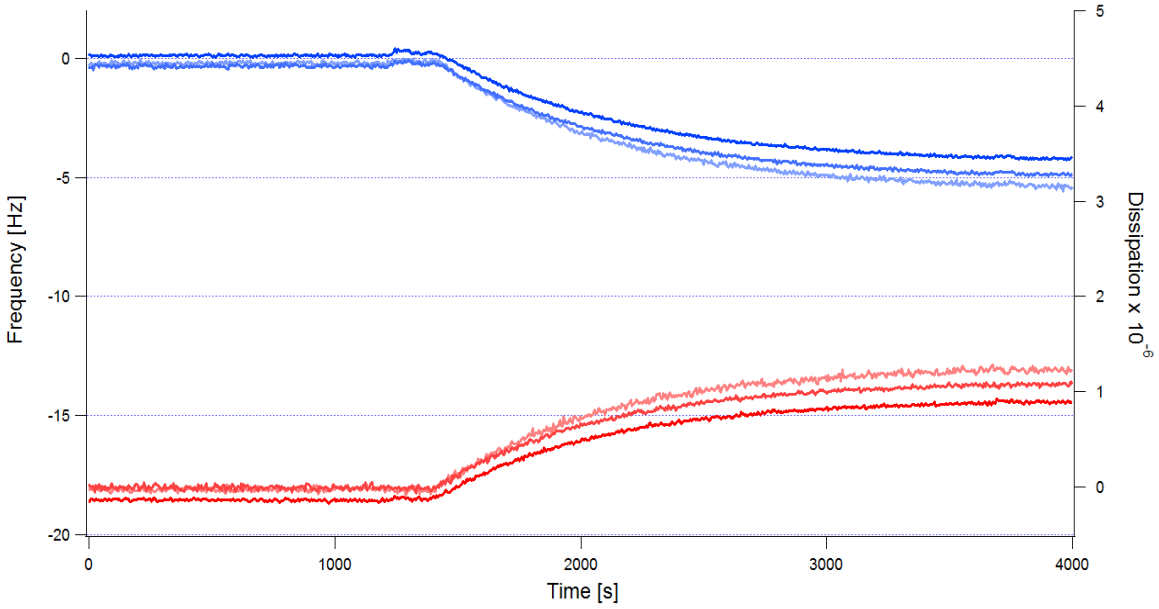

Figure B.8. QCM-D responses for the adsorption of 0.1% FBS (s=1300) on POPG surfaces.

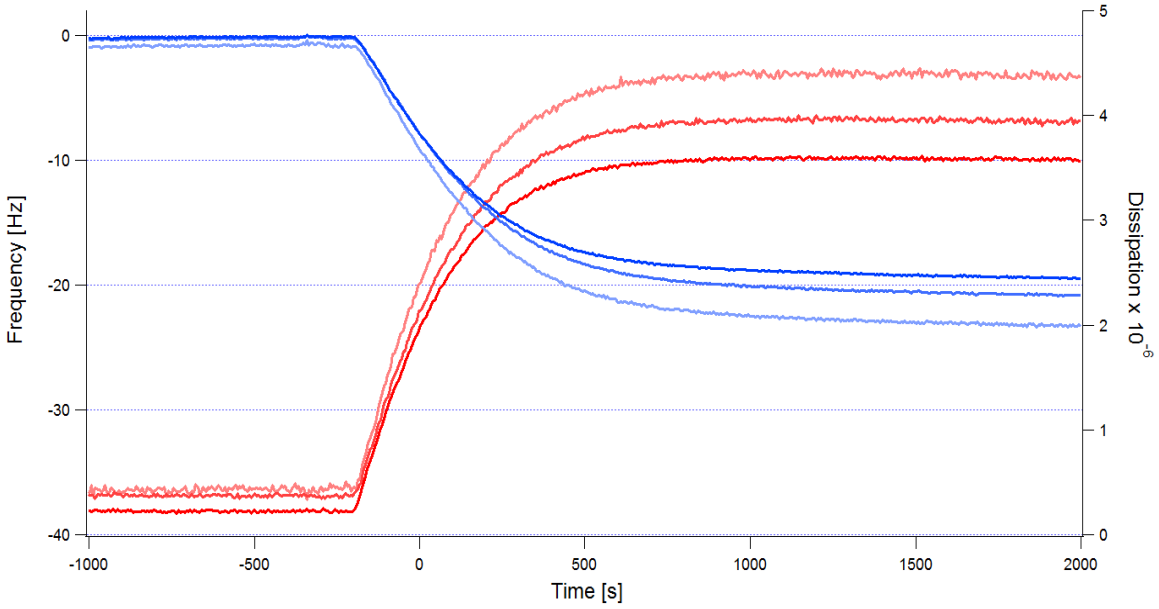

Figure B.9. QCM-D responses for the adsorption of 1% FBS (s=0) on POPC surfaces.

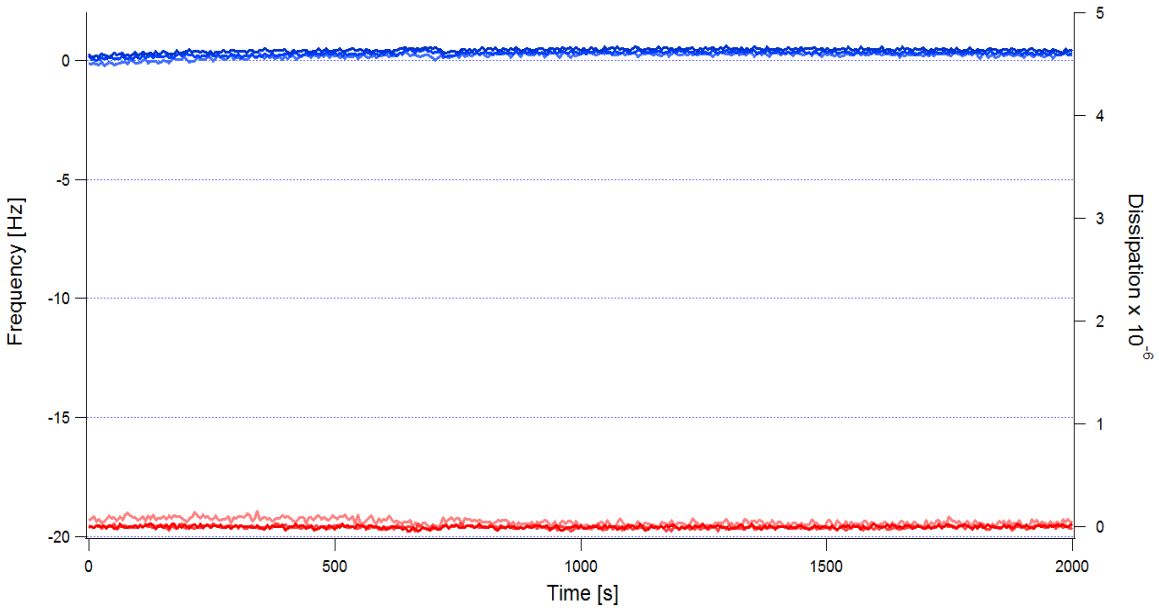

Figure B.10. QCM-D responses for the adsorption of 10 µM Hemoglobin (s=500) on POPG surfaces.

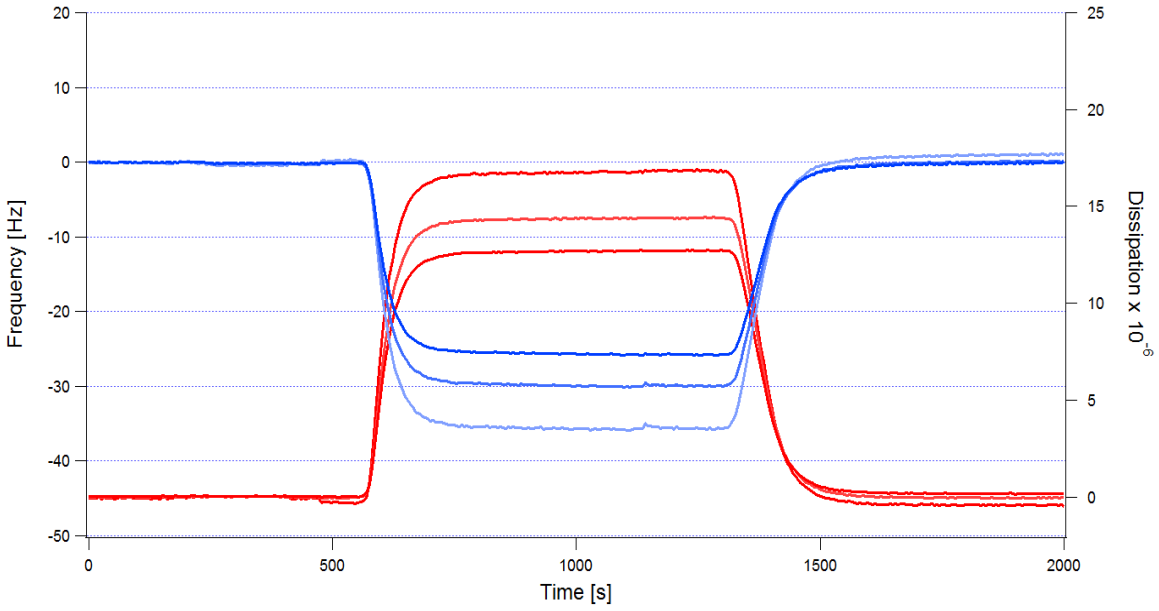

Figure B.11. QCM-D responses for the adsorption of 1mM Hemoglobin (s=600) on POPC surfaces and washing with PBS (s=1400).

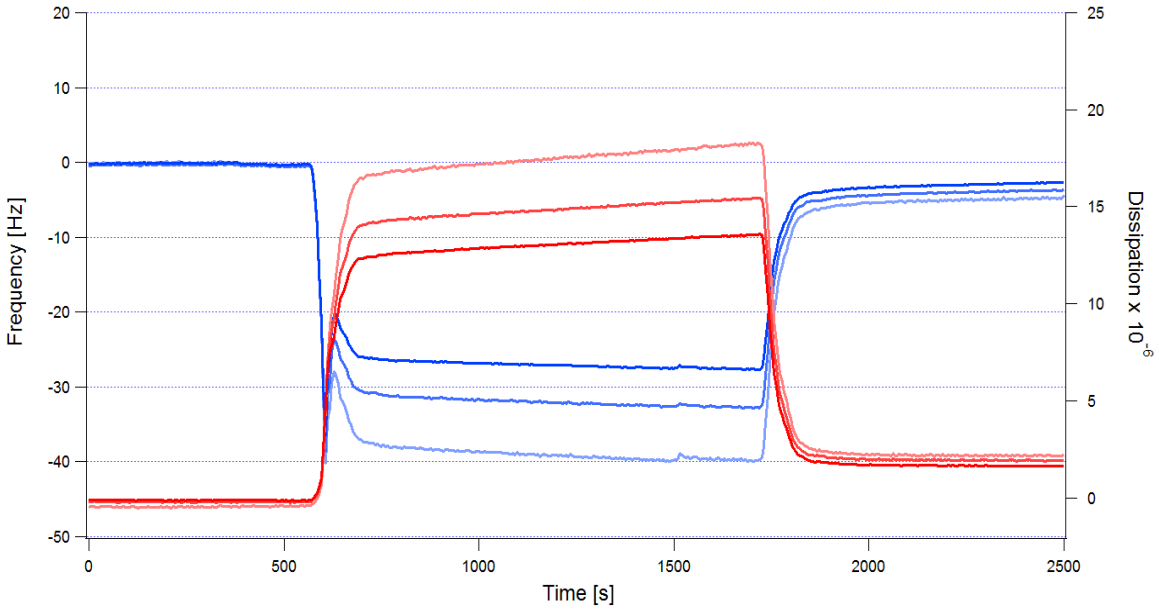

Figure B.12. QCM-D responses for the adsorption of 1mM Hemoglobin (s=600) on POPG surfaces and washing with PBS (s=1400).

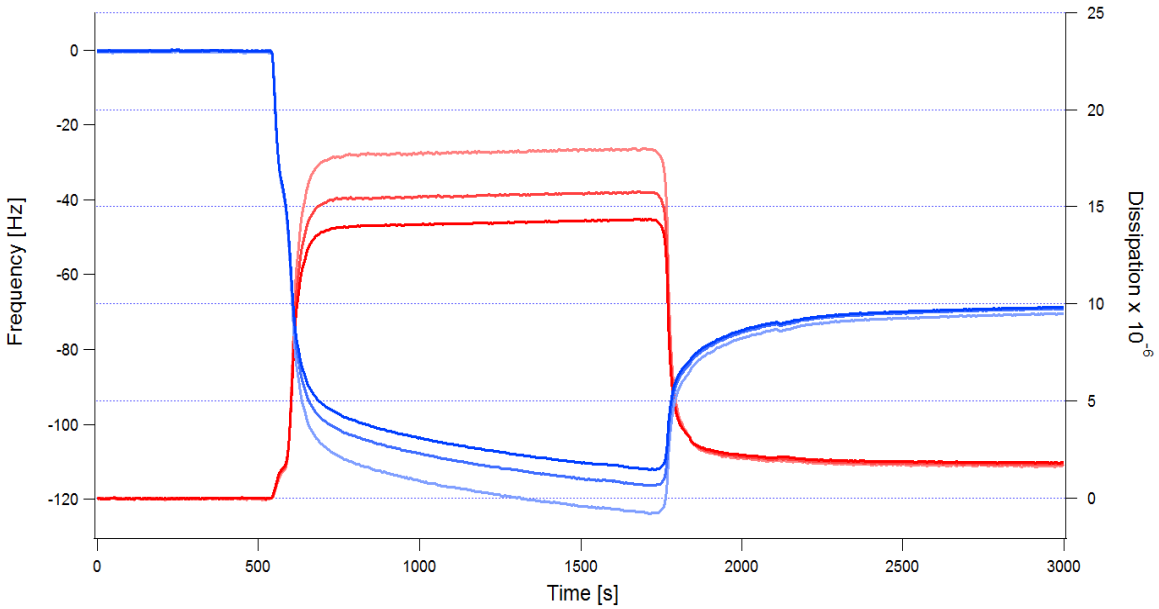

Figure B.13. QCM-D responses for the adsorption of 1mM BSA (s=600) on silica surfaces and washing with PBS (s=1400).

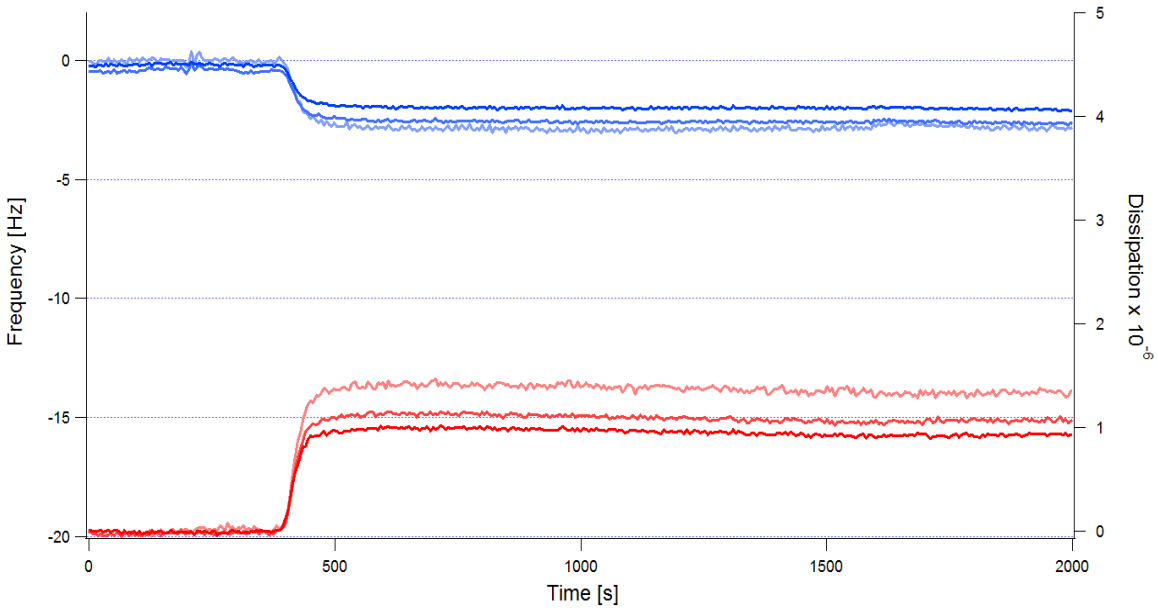

Figure B.14. QCM-D responses for the adsorption of 100 µM of Hemoglobin (s=400) on POPG surfaces.

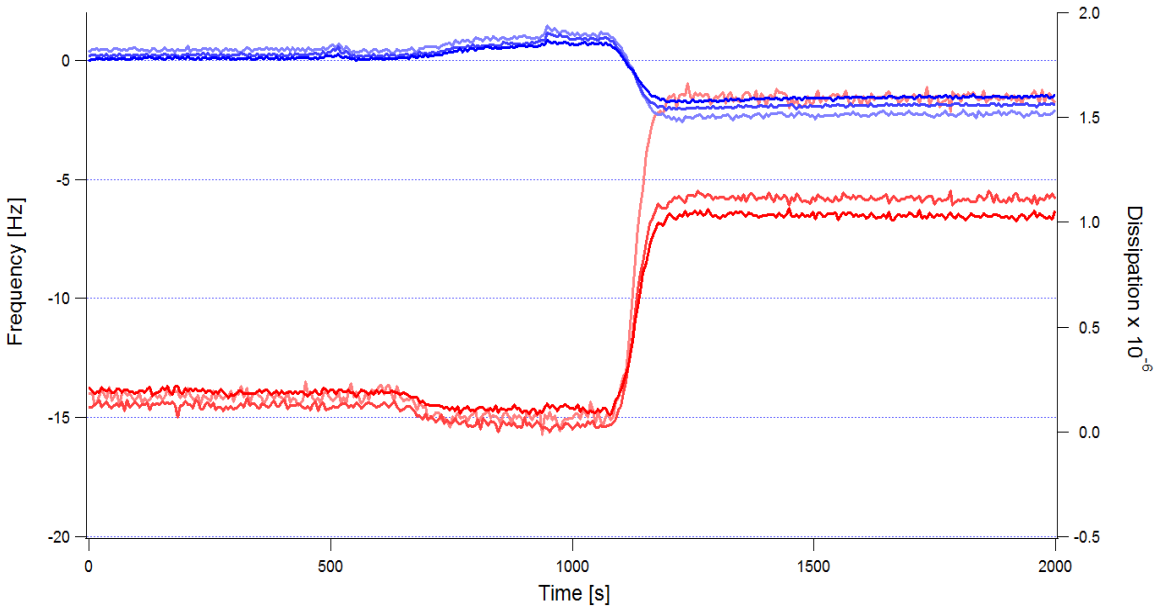

Figure B.15. QCM-D responses for the adsorption of 10 µM of Lysozyme (s=400) on POPG surfaces.

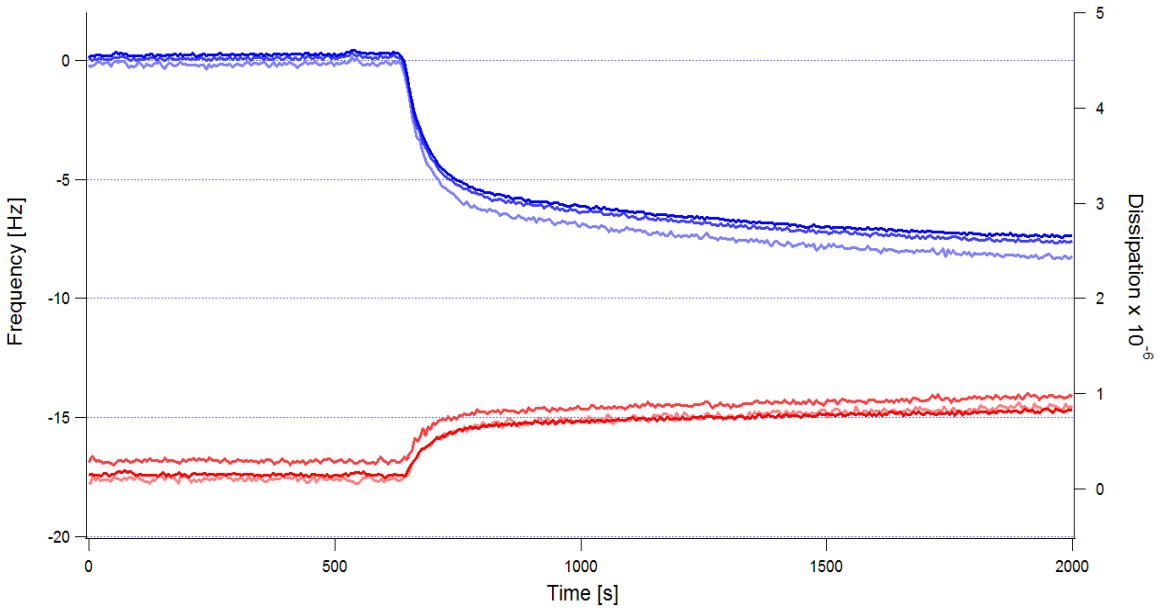

Figure B.16. QCM-D responses for the adsorption of 100 µM of Lysozyme (s=600) on POPC surfaces.

(Frequency in blue, dissipation in red, overtones showed: 5-7-9)

BIBLIOGRAPHY

Abou El-Nour, K. M. M., A. Eftaiha, A. Al-Warthan, and R. A. A. Ammar. "Synthesis and Applications of Silver Nanoparticles." *Arabian Journal of Chemistry* 3, no. 3 (Jul 2010): 135-40. <Go to ISI>://WOS:000290141700001.

Adam, M. and M. Delsanti. "Dynamical Behavior of Semidilute Polymer-Solutions in a Theta-Solvent - Quasi-Elastic Light-Scattering Experiments." *Macromolecules* 18, no. 9 (1985): 1760-70. http://dx.doi.org/10.1021/ma00151a020.

Afshinnia, K., I. Gibson, R. Merrifield, and M. Baalousha. "The Concentration-Dependent Aggregation of Ag Nps Induced by Cystine." *Sci Total Environ* 557-558 (Mar 23 2016): 395-403. http://dx.doi.org/10.1016/j.scitotenv.2016.02.212.

Ahyayauch, H., G. Arana, J. Sot, A. Alonso, and F. M. Goni. "Calcium Inhibits Diacylglycerol Uptake by Serum Albumin." *Biochim Biophys Acta* 1788, no. 3 (Mar 2009): 701-7. http://dx.doi.org/10.1016/j.bbamem.2008.11.016.

Akesson, A., T. Lind, N. Ehrlich, D. Stamou, H. Wacklin, and M. Cardenas. "Composition and Structure of Mixed Phospholipid Supported Bilayers Formed by Popc and Dppc." *Soft Matter* 8, no. 20 (2012): 5658-65. http://dx.doi.org/10.1039/c2sm00013j.

Akesson, A., T. K. Lind, R. Barker, A. Hughes, and M. Cardenas. "Unraveling Dendrimer Translocation across Cell Membrane Mimics." *Langmuir* 28, no. 36 (Sep 2012): 13025-33. http://dx.doi.org/10.1021/la3027144.

Akesson, A., C. V. Lundgaard, N. Ehrlich, T. G. Pomorski, D. Stamou, and M. Cardenas. "Induced Dye Leakage by Pamam G6 Does Not Imply Dendrimer Entry into Vesicle Lumen." *Soft Matter* 8, no. 34 (2012): 8972-80. http://dx.doi.org/10.1039/c2sm25864a.

Alshehri, A. H., M. Jakubowska, A. Mlozniak, M. Horaczek, D. Rudka, C. Free, and J. D. Carey. "Enhanced Electrical Conductivity of Silver Nanoparticles for High Frequency Electronic Applications." *Acs Applied Materials & Interfaces* 4, no. 12 (Dec 2012): 7006-09. <Go to ISI>://WOS:000313149800079.

Amendola, Vincenzo, Stefano Polizzi, and Moreno Meneghetti. "Free Silver Nanoparticles Synthesized by Laser Ablation in Organic Solvents and Their Easy Functionalization." *Langmuir* 23, no. 12 (2007/06/01 2007): 6766-70. http://dx.doi.org/10.1021/la0637061.

Anandhakumar, S., V. Mahalakshmi, and A. M. Raichur. "Silver Nanoparticles Modified Nanocapsules for Ultrasonically Activated Drug Delivery." *Materials Science & Engineering C-Materials for Biological Applications* 32, no. 8 (Dec 1 2012): 2349-55. <Go to ISI>://WOS:000310396900032.

Asati, A., S. Santra, C. Kaittanis, and J. M. Perez. "Surface-Charge-Dependent Cell Localization and Cytotoxicity of Cerium Oxide Nanoparticles." *ACS Nano* 4, no. 9 (Sep 2010): 5321-31. http://dx.doi.org/10.1021/nn100816s.

AshaRani, P. V., M. P. Hande, and S. Valiyaveettil. "Anti-Proliferative Activity of Silver Nanoparticles." *Bmc Cell Biology* 10 (Sep 17 2009). <Go to ISI>://WOS:000271203200001.

AshaRani, P. V., G. L. K. Mun, M. P. Hande, and S. Valiyaveettil. "Cytotoxicity and Genotoxicity of Silver Nanoparticles in Human Cells." *ACS Nano* 3, no. 2 (Feb 2009): 279-90. http://dx.doi.org/Doi 10.1021/Nn800596w.

Asharani, PV, Yi Lian Wu, Zhiyuan Gong, and Suresh Valiyaveettil. "Toxicity of Silver Nanoparticles in Zebrafish Models." *Nanotechnology* 19, no. 25 (2008): 255102.

Badawy, Amro M. El, Todd P. Luxton, Rendahandi G. Silva, Kirk G. Scheckel, Makram T. Suidan, and Thabet M. Tolaymat. "Impact of Environmental Conditions (Ph, Ionic Strength, and Electrolyte Type) on the Surface Charge and Aggregation of Silver Nanoparticles Suspensions." *Environmental Science & Technology* 44, no. 4 (2010/02/15 2010): 1260-66. Accessed 2013/04/01. http://dx.doi.org/10.1021/es902240k.

Banks, Daniel S. and Cécile Fradin. "Anomalous Diffusion of Proteins Due to Molecular Crowding." *Biophysical Journal* 89, no. 5 (11// 2005): 2960-71. http://dx.doi.org/10.1529/biophysj.104.051078.

Bastus, N. G., F. Merkoci, J. Piella, and V. Puntes. "Synthesis of Highly Monodisperse Citrate-Stabilized Silver Nanoparticles of up to 200 Nm: Kinetic Control and Catalytic Properties." *Chemistry of Materials* 26, no. 9 (May 13 2014): 2836-46. <Go to ISI>://WOS:000336020700012.

Beer, C., R. Foldbjerg, Y. Hayashi, D. S. Sutherland, and H. Autrup. "Toxicity of Silver Nanoparticles-Nanoparticle or Silver Ion?" *Toxicology Letters* 208, no. 3 (Feb 2012): 286-92. http://dx.doi.org/10.1016/j.toxlet.2011.11.002.

Berg, J. Michael, Shu Ho, Wonjoong Hwang, Rema Zebda, Kyle Cummins, Manuel P. Soriaga, Robert Taylor, Bing Guo, and Christie M. Sayes. "Internalization of Carbon Black and Maghemite Iron Oxide Nanoparticle Mixtures Leads to Oxidant Production." *Chemical Research in Toxicology* 23, no. 12 (Dec 2010): 1874-82. http://dx.doi.org/10.1021/tx100307h.

Berg, J. Michael, Amelia Romoser, Nivedita Banerjee, Rema Zebda, and Christie M. Sayes. "The Relationship between Ph and Zeta Potential of Similar to 30 Nm Metal Oxide Nanoparticle Suspensions Relevant to in Vitro Toxicological Evaluations." *Nanotoxicology* 3, no. 4 (2009 2009): 276-83. http://dx.doi.org/10.3109/17435390903276941.

Betzer, O., R. Meir, T. Dreifuss, K. Shamalov, M. Motiei, A. Shwartz, K. Baranes, C. J. Cohen, N. Shraga-Heled, R. Ofir, G. Yadid, and R. Popovtzer. "In-Vitro Optimization of Nanoparticle-Cell Labeling Protocols for in-Vivo Cell Tracking Applications." *Scientific Reports* 5 (Oct 28 2015). <Go to ISI>://WOS:000363519900001.

Bolt, G. H. "Determination of the Charge Density of Silica Sols." *The Journal of Physical Chemistry* 61, no. 9 (1957/09/01 1957): 1166-69. Accessed 2012/10/14. http://dx.doi.org/10.1021/j150555a007.

Bopp, K Stephanie K Bopp and Teresa Lettieri. "Comparison of Four Different Colorimetric and Fluorometric Cytotoxicity Assays in a Zebrafish Liver Cell Line " *BMC Pharmacology* 8, no. 8 (2008): 11.

Borm, P. J., D. Robbins, S. Haubold, T. Kuhlbusch, H. Fissan, K. Donaldson, R. Schins, V. Stone, W. Kreyling, J. Lademann, J. Krutmann, D. Warheit, and E. Oberdorster. "The Potential Risks of Nanomaterials: A Review Carried out for Ecetoc." *Part Fibre Toxicol* 3 (2006): 11. http://dx.doi.org/10.1186/1743-8977-3-11.

Bouwmeester, Hans, Jenneke Poortman, Ruud J. Peters, Elly Wijma, Evelien Kramer, Sunday Makama, Kinarsashanti Puspitaninganindita, Hans J. P. Marvin, Ad A. C. M. Peijnenburg, and Peter J. M. Hendriksen. "Characterization of Translocation of Silver Nanoparticles and Effects on Whole-Genome Gene Expression Using an in Vitro Intestinal Epithelium Coculture Model." *ACS Nano* 5, no. 5 (2011/05/24 2011): 4091-103. http://dx.doi.org/10.1021/nn2007145.

Braakhuis, H. M., S. K. Kloet, S. Kezic, F. Kuper, M. V. D. Z. Park, S. Bellmann, M. van der Zande, S. Le Gac, P. Krystek, R. J. B. Peters, I. M. C. M. Rietjens, and H. Bouwmeester. "Progress and Future of in Vitro Models to Study Translocation of Nanoparticles." *Archives of Toxicology* 89, no. 9 (Sep 2015): 1469-95. <Go to ISI>://WOS:000360412500004.

Braun, G. B., T. Friman, H. B. Pang, A. Pallaoro, T. Hurtado de Mendoza, A. M. Willmore, V. R. Kotamraju, A. P. Mann, Z. G. She, K. N. Sugahara, N. O. Reich, T. Teesalu, and E. Ruoslahti. "Etchable Plasmonic Nanoparticle Probes to Image and Quantify Cellular Internalization." *Nat Mater* 13, no. 9 (Sep 2014): 904-11. http://dx.doi.org/10.1038/nmat3982.

Broberg, Craig S., Ananda R. Jayaweera, Gerhard P. Diller, Sanjay K. Prasad, Swee Lay Thein, Bridget E. Bax, John Burman, and Michael A. Gatzoulis. "Seeking Optimal Relation between Oxygen Saturation and Hemoglobin Concentration in Adults with Cyanosis from Congenital Heart Disease." *The American Journal of Cardiology* 107, no. 4 (2/15/ 2011): 595-99. http://dx.doi.org/10.1016/j.amjcard.2010.10.019.

Brun, E., F. Barreau, G. Veronesi, B. Fayard, S. Sorieul, C. Chaneac, C. Carapito, T. Rabilloud, A. Mabondzo, N. Herlin-Boime, and M. Carriere. "Titanium Dioxide Nanoparticle Impact and Translocation through Ex Vivo, in Vivo and in Vitro Gut Epithelia." *Particle and Fibre Toxicology* 11 (Mar 25 2014). <Go to ISI>://WOS:000335534800001.

Cegielska-Radziejewska, Renata, Grzegorz Lesnierowski, and Jacek Kijowski. "Antibacterial Activity of Hen Egg White Lysozyme Modified by Thermochemical Technique." *European Food Research and Technology* 228, no. 5 (2009): 841-45. http://dx.doi.org/10.1007/s00217-008-0997-5.

Chandak, P. G., B. Radovic, E. Aflaki, D. Kolb, M. Buchebner, E. Frohlich, C. Magnes, F. Sinner, G. Haemmerle, R. Zechner, I. Tabas, S. Levak-Frank, and D. Kratky. "Efficient Phagocytosis Requires Triacylglycerol Hydrolysis by Adipose Triglyceride Lipase." *Journal of Biological Chemistry* 285, no. 26 (Jun 25 2010): 20192-201. <Go to ISI>://WOS:000279012000054.

Chithrani, B. D. and W. C. W. Chan. "Elucidating the Mechanism of Cellular Uptake and Removal of Protein-Coated Gold Nanoparticles of Different Sizes and Shapes." *Nano Letters* 7, no. 6 (Jun 2007): 1542-50. http://dx.doi.org/10.1021/nl070363y.

Chithrani, B. D., A. A. Ghazani, and W. C. W. Chan. "Determining the Size and Shape Dependence of Gold Nanoparticle Uptake into Mammalian Cells." *Nano Letters* 6, no. 4 (Apr 2006): 662-68. http://dx.doi.org/10.1021/nl052396o.

Choi, J., J. H. Chung, G. Y. Kwon, K. W. Kim, S. Kim, and H. Chang. "Effectiveness of Autologous Serum as an Alternative to Fetal Bovine Serum in Adipose-Derived Stem Cell Engineering." *Cell Tissue Bank* (Sep 13 2012). http://dx.doi.org/10.1007/s10561-012-9341-1.

Cohen, J. M., R. Derk, L. Y. Wang, J. Godleski, L. Kobzik, J. Brain, and P. Demokritou. "Tracking Translocation of Industrially Relevant Engineered Nanomaterials (Enms) across Alveolar Epithelial Monolayers in Vitro." *Nanotoxicology* 8 (Aug 2014): 216-25. <Go to ISI>://WOS:000340524300022
http://www.ncbi.nlm.nih.gov/pmc/articles/PMC4387897/pdf/nihms-676717.pdf.

Conner, S. D. and S. L. Schmid. "Regulated Portals of Entry into the Cell." *Nature* 422, no. 6927 (Mar 2003): 37-44. http://dx.doi.org/10.1038/nature01451.

Corbett, Jason C. W., Malcolm T. Connah, and Kevin Mattison. "Advances in the Measurement of Protein Mobility Using Laser Doppler Electrophoresis - the Diffusion Barrier Technique." *Electrophoresis* 32, no. 14 (Jul 2011): 1787-94. http://dx.doi.org/10.1002/elps.201100108.

Corning. "Permeable Supports Selection Guide Including Transwell® and Falcon® Cell Culture Inserts." Corning Incorporated. Last modified 2014. Accessed. http://csmedia2.corning.com/LifeSciences/Media/pdf/transwell_guide.pdf.

Das, Vidhya Lakshmi, Roshmi Thomas, Rintu T. Varghese, E. V. Soniya, Jyothis Mathew, and E. K. Radhakrishnan. "Extracellular Synthesis of Silver Nanoparticles by the Bacillus Strain Cs 11 Isolated from Industrialized Area." *3 Biotech* 4, no. 2 (2014): 121-26. http://dx.doi.org/10.1007/s13205-013-0130-8.

Dekali, Samir, Christelle Gamez, Thierry Kortulewski, Kelly Blazy, Patrice Rat, and Ghislaine Lacroix. "Assessment of an in Vitro Model of Pulmonary Barrier to Study the Translocation of Nanoparticles." *Toxicology Reports* 1 (// 2014): 157-71. http://dx.doi.org/http://dx.doi.org/10.1016/j.toxrep.2014.03.003.

Detivaud, L., E. Nemeth, K. Boudjema, B. Turlin, M. B. Troadec, P. Leroyer, M. Ropert, S. Jacquelinet, B. Courselaud, T. Ganz, P. Brissot, and O. Loreal. "Hepcidin Levels in Humans Are Correlated with Hepatic Iron Stores, Hemoglobin Levels, and Hepatic Function." *Blood* 106, no. 2 (Jul 2005): 746-48. http://dx.doi.org/10.1182/blood-2004-12-4855.

Dickey, A. and R. Faller. "Examining the Contributions of Lipid Shape and Headgroup Charge on Bilayer Behavior." *Biophys J* 95, no. 6 (Sep 15 2008): 2636-46. http://dx.doi.org/10.1529/biophysj.107.128074.

Divertie, M. B. and A. L. Brown, Jr. "The Pulmonary Alveolar Macrophage." *Med Clin North Am* 48 (Jul 1964): 1049-54. http://www.ncbi.nlm.nih.gov/pubmed/14148148.

dos Santos, T., J. Varela, I. Lynch, A. Salvati, and K. A. Dawson. "Effects of Transport Inhibitors on the Cellular Uptake of Carboxylated Polystyrene Nanoparticles in Different Cell Lines." *Plos One* 6, no. 9 (Sep 19 2011). <Go to ISI>://WOS:000295257900015.

Drent, M., N. A. M. Cobben, R. F. Henderson, E. F. M. Wouters, and M. vanDieijenVisser. "Usefulness of Lactate Dehydrogenase and Its Isoenzymes as Indicators of Lung Damage or Inflammation." *European Respiratory Journal* 9, no. 8 (Aug 1996): 1736-42. <Go to ISI>://WOS:A1996VD95300028.

Duncan, Timothy V. "Applications of Nanotechnology in Food Packaging and Food Safety: Barrier Materials, Antimicrobials and Sensors." *J Colloid Interface Sci* 363, no. 1 (11/1/ 2011): 1-24. http://dx.doi.org/http://dx.doi.org/10.1016/j.jcis.2011.07.017.

Duran, N., C. P. Silveira, M. Duran, and D. S. Martinez. "Silver Nanoparticle Protein Corona and Toxicity: A Mini-Review." *J Nanobiotechnology* 13 (2015): 55. http://dx.doi.org/10.1186/s12951-015-0114-4.

El Badawy, A. M., R. G. Silva, B. Morris, K. G. Scheckel, M. T. Suidan, and T. M. Tolaymat. "Surface Charge-Dependent Toxicity of Silver Nanoparticles." *Environmental Science & Technology* 45, no. 1 (Jan 1 2011): 283-87. <Go to ISI>://WOS:000285679300043.

Elcock, A. H. "Models of Macromolecular Crowding Effects and the Need for Quantitative Comparisons with Experiment." *Curr Opin Struct Biol* 20, no. 2 (Apr 2010): 196-206. http://dx.doi.org/10.1016/j.sbi.2010.01.008.

Farkas, J., P. Christian, J. A. Gallego-Urrea, N. Roos, M. Hassellov, K. E. Tollefsen, and K. V. Thomas. "Uptake and Effects of Manufactured Silver Nanoparticles in Rainbow Trout (Oncorhynchus Mykiss) Gill Cells." *Aquatic Toxicology* 101, no. 1 (Jan 17 2011): 117-25. http://dx.doi.org/DOI 10.1016/j.aquatox.2010.09.010.

Foldbjerg, R., D. A. Dang, and H. Autrup. "Cytotoxicity and Genotoxicity of Silver Nanoparticles in the Human Lung Cancer Cell Line, A549." *Archives of Toxicology* 85, no. 7 (Jul 2011): 743-50. http://dx.doi.org/10.1007/s00204-010-0545-5.

Frohlich, E. and S. Salar-Behzadi. "Toxicological Assessment of Inhaled Nanoparticles: Role of in Vivo, Ex Vivo, in Vitro, and in Silico Studies." *Int J Mol Sci* 15, no. 3 (2014): 4795-822. http://dx.doi.org/10.3390/ijms15034795.

Fuertes, G., D. Gimenez, S. Esteban-Martin, A. Garcia-Saez, O. Sanchez, and J. Salgado. "Role of Membrane Lipids for the Activity of Pore Forming Peptides and Proteins." *Adv Exp Med Biol* 677 (2010): 31-55.

Garcia, Tania, Daisy Lafuente, Jordi Blanco, Domènec J. Sánchez, Juan J. Sirvent, José L. Domingo, and Mercedes Gómez. "Oral Subchronic Exposure to Silver Nanoparticles in Rats." *Food and Chemical Toxicology* 92 (6// 2016): 177-87. http://dx.doi.org/http://dx.doi.org/10.1016/j.fct.2016.04.010.

Geiser, M., M. Casaulta, B. Kupferschmid, H. Schulz, M. Semirriler-Behinke, and W. Kreyling. "The Role of Macrophages in the Clearance of Inhaled Ultrafine Titanium Dioxide Particles." *American Journal of Respiratory Cell and Molecular Biology* 38, no. 3 (Mar 2008): 371-76. <Go to ISI>://WOS:000253435500017.

Genter, M. B., N. C. Newman, H. G. Shertzer, S. F. Ali, and B. Bolon. "Distribution and Systemic Effects of Intranasally Administered 25 Nm Silver Nanoparticles in Adult Mice." *Toxicologic Pathology* 40, no. 7 (Oct 2012): 1004-13. <Go to ISI>://WOS:000317078200003.

Geys, J., L. Coenegrachts, J. Vercammen, Y. Engelborghs, A. Nemmar, B. Nemery, and P. H. Hoet. "In Vitro Study of the Pulmonary Translocation of Nanoparticles: A Preliminary Study." *Toxicol Lett* 160, no. 3 (Jan 25 2006): 218-26. http://dx.doi.org/10.1016/j.toxlet.2005.07.005.

Gliga, A. R., S. Skoglund, I. O. Wallinder, B. Fadeel, and H. L. Karlsson. "Size-Dependent Cytotoxicity of Silver Nanoparticles in Human Lung Cells: The Role of Cellular Uptake, Agglomeration and Ag Release." *Part Fibre Toxicol* 11 (2014): 11. http://dx.doi.org/10.1186/1743-8977-11-11.

Glover, R. D., J. M. Miller, and J. E. Hutchison. "Generation of Metal Nanoparticles from Silver and Copper Objects: Nanoparticle Dynamics on Surfaces and Potential Sources of Nanoparticles in the Environment." *ACS Nano* 5, no. 11 (Nov 2011): 8950-57. http://dx.doi.org/10.1021/nn2031319.

González Flecha, F. Luis and Valeria Levi. "Determination of the Molecular Size of Bsa by Fluorescence Anisotropy." *Biochemistry and Molecular Biology Education* 31, no. 5 (2003): 319-22. http://dx.doi.org/10.1002/bmb.2003.494031050261.

Greulich, C., J. Diendorf, T. Simon, G. Eggeler, M. Epple, and M. Koller. "Uptake and Intracellular Distribution of Silver Nanoparticles in Human Mesenchymal Stem Cells." *Acta Biomaterialia* 7, no. 1 (Jan 2011): 347-54. http://dx.doi.org/10.1016/j.actbio.2010.08.003.

Halperin, S. J. and K. L. Koster. "Sugar Effects on Membrane Damage During Desiccation of Pea Embryo Protoplasts." *J Exp Bot* 57, no. 10 (2006): 2303-11. http://dx.doi.org/10.1093/jxb/erj208.

Han, Jae Woong, Sangiliyandi Gurunathan, Jae-Kyo Jeong, Yun-Jung Choi, Deug-Nam Kwon, Jin-Ki Park, and Jin-Hoi Kim. "Oxidative Stress Mediated Cytotoxicity of Biologically Synthesized Silver Nanoparticles in Human Lung Epithelial Adenocarcinoma Cell Line." *Nanoscale Research Letters* 9, no. 1 (2014): 1-14. http://dx.doi.org/10.1186/1556-276x-9-459.

Harland, C. W., Z. Botyanszki, D. Rabuka, C. R. Bertozzi, and R. Parthasarathy. "Synthetic Trehalose Glycolipids Confer Desiccation Resistance to Supported Lipid Monolayers." *Langmuir* 25, no. 9 (May 5 2009): 5193-8. http://dx.doi.org/10.1021/la804007a.

Hawkins, A. D., C. Thornton, A. J. Kennedy, K. X. Bu, J. Cizdziel, B. W. Jones, J. A. Steevens, and K. L. Willett. "Gill Histopathologies Following Exposure to Nanosilver or Silver Nitrate." *Journal of Toxicology and Environmental Health-Part a-Current Issues* 78, no. 5 (Mar 4 2015): 301-15. <Go to ISI>://WOS:000350298500002.

Hendren, C. O., X. Mesnard, J. Droge, and M. R. Wiesner. "Estimating Production Data for Five Engineered Nanomaterials as a Basis for Exposure Assessment." *Environmental Science & Technology* 45, no. 7 (Apr 2011): 2562-69. http://dx.doi.org/10.1021/es103300g.

Hern, #xe1, Norma Y. ndez-Pedro, Rangel-L, #xf3, Edgar pez, Maga, #xf1, Roxana a-Maldonado, Ver de la Cruz, #xf3, nica P, #xe9, rez, Santamar, #xed, Abel a del Angel, Benjam Pineda, #xed, and Julio Sotelo. "Application of Nanoparticles on Diagnosis and Therapy in Gliomas." *BioMed Research International* 2013 (2013): 20. http://dx.doi.org/10.1155/2013/351031.

Holder, Amara L. and Linsey C. Marr. "Toxicity of Silver Nanoparticles at the Air-Liquid Interface." *BioMed Research International* 2013 (2013): 11. http://dx.doi.org/10.1155/2013/328934.

Hunt, Lisa, David L. Hacker, Frédéric Grosjean, Maria De Jesus, Lorenz Uebersax, Martin Jordan, and Florian M. Wurm. "Low-Temperature Pausing of Cultivated Mammalian Cells." *Biotechnology and Bioengineering* 89, no. 2 (2005): 157-63. http://dx.doi.org/10.1002/bit.20320.

Hussain, S. M., K. L. Hess, J. M. Gearhart, K. T. Geiss, and J. J. Schlager. "In Vitro Toxicity of Nanoparticles in Brl 3a Rat Liver Cells." *Toxicology in Vitro* 19, no. 7 (Oct 2005): 975-83. http://dx.doi.org/DOI 10.1016/j.tiv.2005.06.034.

Huynh, K. A. and K. L. Chen. "Aggregation Kinetics of Citrate and Polyvinylpyrrolidone Coated Silver Nanoparticles in Monovalent and Divalent Electrolyte Solutions." *Environmental Science & Technology* 45, no. 13 (Jul 2011): 5564-71. http://dx.doi.org/10.1021/es200157h.

Iacono, V. J., B. J. MacKay, S. DiRienzo, and J. J. Pollock. "Selective Antibacterial Properties of Lysozyme for Oral Microorganisms." *Infect Immun* 29, no. 2 (Aug 1980): 623-32.

Incorporated, Corning. "Effective Blocking Procedures, Elisa Technical Bulletin No. 3".

Initiative, United States National Nanotechnology. "Nanotechnology 101." www.nano.gov. Last modified 2000. Accessed. http://www.nano.gov/timeline.

Iwata, M. and S. S. Carlson. "A Large Chondroitin Sulfate Proteoglycan Has the Characteristics of a General Extracellular-Matrix Component of Adult Brain." *Journal of Neuroscience* 13, no. 1 (Jan 1993): 195-207. <Go to ISI>://WOS:A1993KG65900015.

Jachimska, B. and A. Pajor. "Physico-Chemical Characterization of Bovine Serum Albumin in Solution and as Deposited on Surfaces." *Bioelectrochemistry* 87 (Oct 2012): 138-46. http://dx.doi.org/10.1016/j.bioelechem.2011.09.004.

Ji, J. H., J. H. Jung, S. S. Kim, J. U. Yoon, J. D. Park, B. S. Choi, Y. H. Chung, I. H. Kwon, J. Jeong, B. S. Han, J. H. Shin, J. H. Sung, K. S. Song, and I. J. Yu. "Twenty-Eight-Day Inhalation Toxicity Study of Silver Nanoparticles in Sprague-Dawley Rats." *Inhalation Toxicology* 19, no. 10 (2007): 857-71. http://dx.doi.org/10.1080/08958370701432108.

Jiang, R. D., H. Shen, and Y. J. Piao. "The Morphometrical Analysis on the Ultrastructure of A549 Cells." *Romanian Journal of Morphology and Embryology* 51, no. 4 (2010): 663-67. <Go to ISI>://WOS:000285641200009.

JOGIKALMATH, Gangadhar. "Method for Blocking Non-Specific Protein Binding on a Functionalized Surface." *United States Patent Application Pubblication* US 2008/0213910 (2008).

Jung, Jae Hee, Hyun Cheol Oh, Hyung Soo Noh, Jun Ho Ji, and Sang Soo Kim. "Metal Nanoparticle Generation Using a Small Ceramic Heater with a Local Heating Area." *Journal of Aerosol Science* 37, no. 12 (12// 2006): 1662-70. http://dx.doi.org/http://dx.doi.org/10.1016/j.jaerosci.2006.09.002.

Kawata, K., M. Osawa, and S. Okabe. "In Vitro Toxicity of Silver Nanoparticles at Noncytotoxic Doses to Hepg2 Human Hepatoma Cells." *Environmental Science & Technology* 43, no. 15 (Aug 1 2009): 6046-51. http://dx.doi.org/Doi 10.1021/Es900754q.

Kayitmazer, A. Basak, Daniel Seeman, Burcu Baykal Minsky, Paul L. Dubin, and Yisheng Xu. "Protein-Polyelectrolyte Interactions." *Soft Matter* (2013). http://dx.doi.org/10.1039/C2SM27002A.

Kennedy, D. C., G. Orts-Gil, C. H. Lai, L. Mller, A. Haase, A. Luch, and P. H. Seeberger. "Carbohydrate Functionalization of Silver Nanoparticles Modulates Cytotoxicity and Cellular Uptake." *Journal of Nanobiotechnology* 12 (Dec 19 2014). <Go to ISI>://WOS:000348548100001.

Khayati, G. R. and K. Janghorban. "The Nanostructure Evolution of Ag Powder Synthesized by High Energy Ball Milling." *Advanced Powder Technology* 23, no. 3 (5// 2012): 393-97. http://dx.doi.org/http://dx.doi.org/10.1016/j.apt.2011.05.005.

Kim, Jin Sik, Jae Hyuck Sung, Jun Ho Ji, Kyung Seuk Song, Ji Hyun Lee, Chang Soo Kang, and Il Je Yu. "In Vivo Genotoxicity of Silver Nanoparticles after 90-Day Silver Nanoparticle Inhalation Exposure." *Safety and Health at Work* 2, no. 1 (3// 2011): 34-38. http://dx.doi.org/http://dx.doi.org/10.5491/SHAW.2011.2.1.34.

Kim, S. and I. H. Choi. "Phagocytosis and Endocytosis of Silver Nanoparticles Induce Interleukin-8 Production in Human Macrophages." *Yonsei Medical Journal* 53, no. 3 (May 1 2012): 654-57. <Go to ISI>://WOS:000302674100027.

Kim, Y. S., J. S. Kim, H. S. Cho, D. S. Rha, J. M. Kim, J. D. Park, B. S. Choi, R. Lim, H. K. Chang, Y. H. Chung, I. H. Kwon, J. Jeong, B. S. Han, and I. J. Yu. "Twenty-Eight-Day Oral Toxicity, Genotoxicity, and Gender-Related Tissue Distribution of Silver Nanoparticles in Sprague-Dawley Rats." *Inhalation Toxicology* 20, no. 6 (2008): 575-83. http://dx.doi.org/10.1080/08958370701874663.

Kim, Y. S., M. Y. Song, J. D. Park, K. S. Song, H. R. Ryu, Y. H. Chung, H. K. Chang, J. H. Lee, K. H. Oh, B. J. Kelman, I. K. Hwang, and I. J. Yu. "Subchronic Oral Toxicity of Silver Nanoparticles." *Particle and Fibre Toxicology* 7 (Aug 2010). http://dx.doi.org/2010.1186/1743-8977-7-20.

Kiselev, A. V. "Non-Specific and Specific Interactions of Molecules of Different Electronic Structures with Solid Surfaces." *Discussions of the Faraday Society*, no. 40 (1965): 205-&. <Go to ISI>://WOS:A19657877900022.

Klein, S. G., J. Hennen, T. Serchi, B. Blomeke, and A. C. Gutleb. "Potential of Coculture in Vitro Models to Study Inflammatory and Sensitizing Effects of Particles on the Lung." *Toxicology in Vitro* 25, no. 8 (Dec 2011): 1516-34. http://dx.doi.org/10.1016/j.tiv.2011.09.006.

Klein, S. G., T. Serchi, L. Hoffmann, B. Blomeke, and A. C. Gutleb. "An Improved 3d Tetraculture System Mimicking the Cellular Organisation at the Alveolar Barrier to Study the Potential Toxic Effects of Particles on the Lung." *Particle and Fibre Toxicology* 10 (Jul 26 2013). <Go to ISI>://WOS:000323550600001.

Kuhn, D. A., R. Hartmann, K. Fytianos, A. Petri-Fink, B. Rothen-Rutishauser, and W. J. Parak. "Cellular Uptake and Cell-to-Cell Transfer of Polyelectrolyte Microcapsules within a Triple Co-Culture System Representing Parts of the Respiratory Tract." *Science and Technology of Advanced Materials* 16, no. 3 (Jun 2015). <Go to ISI>://WOS:000357424000015.

Kuttner, Y. Y., N. Kozer, E. Segal, G. Schreiber, and G. Haran. "Separating the Contribution of Translational and Rotational Diffusion to Protein Association." *J Am Chem Soc* 127, no. 43 (Nov 2 2005): 15138-44. http://dx.doi.org/10.1021/ja053681c.

Kwan, K. H. L., X. L. Liu, M. K. T. To, K. W. K. Yeung, C. M. Ho, and K. K. Y. Wong. "Modulation of Collagen Alignment by Silver Nanoparticles Results in Better Mechanical Properties in Wound Healing." *Nanomedicine-Nanotechnology Biology and Medicine* 7, no. 4 (Aug 2011): 497-504. <Go to ISI>://WOS:000293218800015.

Kwok, K. W. H., M. Auffan, A. R. Badireddy, C. M. Nelson, M. R. Wiesner, A. Chilkoti, J. Liu, S. M. Marinakos, and D. E. Hinton. "Uptake of Silver Nanoparticles and Toxicity to Early Life Stages of Japanese Medaka (Oryzias Latipes): Effect of Coating Materials." *Aquatic Toxicology* 120 (Sep 2012): 59-66. http://dx.doi.org/10.1016/j.aquatox.2012.04.012.

Larsson, C., M. Rodahl, and F. Hook. "Characterization of DNA Immobilization and Subsequent Hybridization on a 2d Arrangement of Streptavidin on a Biotin-Modified Lipid Bilayer Supported on Sio2." *Anal Chem* 75, no. 19 (Oct 1 2003): 5080-7. http://www.ncbi.nlm.nih.gov/pubmed/14708781.

Le, T. T., H. Karmouty-Quintana, E. Melicoff, T. T. Le, T. Weng, N. Y. Chen, M. Pedroza, Y. Zhou, J. Davies, K. Philip, J. Molina, F. Luo, A. T. George, L. J. Garcia-Morales, R. R. Bunge, B. A. Bruckner, M. Loebe, H. Seethamraju, S. K. Agarwal, and M. R. Blackburn. "Blockade of Il-6 Trans Signaling Attenuates Pulmonary Fibrosis." *J Immunol* 193, no. 7 (Oct 1 2014): 3755-68. http://dx.doi.org/10.4049/jimmunol.1302470.

Lehmann, A. D., N. Daum, M. Bur, C. M. Lehr, P. Gehr, and B. M. Rothen-Rutishauser. "An in Vitro Triple Cell Co-Culture Model with Primary Cells Mimicking the Human Alveolar Epithelial Barrier." *European Journal of Pharmaceutics and Biopharmaceutics* 77, no. 3 (Apr 2011): 398-406. <Go to ISI>://WOS:000289380300010.

Leslie, S. B., E. Israeli, B. Lighthart, J. H. Crowe, and L. M. Crowe. "Trehalose and Sucrose Protect Both Membranes and Proteins in Intact Bacteria During Drying." *Appl Environ Microbiol* 61, no. 10 (Oct 1995): 3592-7.

Lieber, M., B. Smith, A. Szakal, W. Nelsonrees, and G. Todaro. "Continuous Tumor-Cell Line from a Human Lung Carcinoma with Properties of Type-Ii Alveolar Epithelial Cells." *International Journal of Cancer* 17, no. 1 (1976): 62-70. http://dx.doi.org/10.1002/ijc.2910170110.

Limbach, L. K., P. Wick, P. Manser, R. N. Grass, A. Bruinink, and W. J. Stark. "Exposure of Engineered Nanoparticles to Human Lung Epithelial Cells: Influence of Chemical Composition and Catalytic Activity on Oxidative Stress." *Environmental Science & Technology* 41, no. 11 (Jun 2007): 4158-63. http://dx.doi.org/10.1021/es062629t.

Logeswari, Peter, Sivagnanam Silambarasan, and Jayanthi Abraham. "Synthesis of Silver Nanoparticles Using Plants Extract and Analysis of Their Antimicrobial Property." *Journal of Saudi Chemical Society* 19, no. 3 (5// 2015): 311-17. http://dx.doi.org/http://dx.doi.org/10.1016/j.jscs.2012.04.007.

Lundblad, Roger L. "Consideration for the Use of Blood Plasma and Serum for Proteomic Analysis." *The Internet Journal of Genomics and Proteomics* 1, no. 2 (2005).

Luyts, K., D. Napierska, D. Dinsdale, S. G. Klein, T. Serchi, and P. H. M. Hoet. "A Coculture Model of the Lung-Blood Barrier: The Role of Activated Phagocytic Cells." *Toxicology in Vitro* 29, no. 1 (Feb 2015): 234-41. <Go to ISI>://WOS:000347746600031.

Marambio-Jones, C. and E. M. V. Hoek. "A Review of the Antibacterial Effects of Silver Nanomaterials and Potential Implications for Human Health and the Environment." *Journal of Nanoparticle Research* 12, no. 5 (Jun 2010): 1531-51. <Go to ISI>://WOS:000277956800002.

Matzke, M., K. Jurkschat, and T. Backhaus. "Toxicity of Differently Sized and Coated Silver Nanoparticles to the Bacterium Pseudomonas Putida: Risks for the Aquatic Environment?" *Ecotoxicology* 23, no. 5 (Jul 2014): 818-29. http://dx.doi.org/10.1007/s10646-014-1222-x.

McShan, Danielle, Paresh C. Ray, and Hongtao Yu. "Molecular Toxicity Mechanism of Nanosilver." *Journal of Food and Drug Analysis* 22, no. 1 (3// 2014): 116-27. http://dx.doi.org/http://dx.doi.org/10.1016/j.jfda.2014.01.010.

Mechler, A., S. Praporski, K. Atmuri, M. Boland, F. Separovic, and L. L. Martin. "Specific and Selective Peptide-Membrane Interactions Revealed Using Quartz Crystal Microbalance." *Biophysical Journal* 93, no. 11 (Dec 2007): 3907-16. http://dx.doi.org/10.1529/biophysj.107.116525.

Milani, S., F. B. Bombelli, A. S. Pitek, K. A. Dawson, and J. Radler. "Reversible Versus Irreversible Binding of Transferrin to Polystyrene Nanoparticles: Soft and Hard Corona." *ACS Nano* 6, no. 3 (Mar 27 2012): 2532-41. http://dx.doi.org/10.1021/nn204951s.

Morones, J. R., J. L. Elechiguerra, A. Camacho, K. Holt, J. B. Kouri, J. T. Ramirez, and M. J. Yacaman. "The Bactericidal Effect of Silver Nanoparticles." *Nanotechnology* 16, no. 10 (Oct 2005): 2346-53. http://dx.doi.org/10.1088/0957-4484/16/10/059.

Mukherjee, D., S. G. Royce, S. Sarkar, A. Thorley, S. Schwander, M. P. Ryan, A. E. Porter, K. F. Chung, T. D. Tetley, J. Zhang, and P. G. Georgopoulos. "Modeling in Vitro Cellular Responses to Silver Nanoparticles." *J Toxicol* 2014 (2014): 852890. http://dx.doi.org/10.1155/2014/852890.

Mukherjee, Priyabrata, Absar Ahmad, Deendayal Mandal, Satyajyoti Senapati, Sudhakar R. Sainkar, Mohammad I. Khan, Renu Parishcha, P. V. Ajaykumar, Mansoor Alam, Rajiv Kumar, and Murali Sastry. "Fungus-Mediated Synthesis of Silver Nanoparticles and Their Immobilization in the Mycelial Matrix: A Novel Biological Approach to Nanoparticle Synthesis." *Nano Letters* 1, no. 10 (2001/10/01 2001): 515-19. http://dx.doi.org/10.1021/nl0155274.

Mukherjee, S., M. M. Waegele, P. Chowdhury, L. Guo, and F. Gai. "Effect of Macromolecular Crowding on Protein Folding Dynamics at the Secondary Structure Level." *J Mol Biol* 393, no. 1 (Oct 16 2009): 227-36. http://dx.doi.org/10.1016/j.jmb.2009.08.016.

Napierska, D., L. C. J. Thomassen, B. Vanaudenaerde, K. Luyts, D. Lison, J. A. Martens, B. Nemery, and P. H. M. Hoet. "Cytokine Production by Co-Cultures Exposed to Monodisperse Amorphous Silica Nanoparticles: The Role of Size and Surface Area." *Toxicology Letters* 211, no. 2 (Jun 1 2012): 98-104. <Go to ISI>://WOS:000304744700002.

Narita, M., H. Tanaka, S. Yamada, S. Abe, T. Ariga, and Y. Sakiyama. "Significant Role of Interleukin-8 in Pathogenesis of Pulmonary Disease Due to Mycoplasma Pneumoniae Infection." *Clin Diagn Lab Immunol* 8, no. 5 (Sep 2001): 1028-30. http://dx.doi.org/10.1128/CDLI.8.5.1028-1030.2001.

Nielsen, S. B., K. Wilhelm, B. Vad, J. Schleucher, L. A. Morozova-Roche, and D. Otzen. "The Interaction of Equine Lysozyme:Oleic Acid Complexes with Lipid Membranes Suggests a Cargo Off-Loading Mechanism." *J Mol Biol* 398, no. 2 (Apr 30 2010): 351-61. http://dx.doi.org/10.1016/j.jmb.2010.03.012.

Ojcius, D. M. and J. D. Young. "Characterization of the Inhibitory Effect of Lysolipids on Perforin-Mediated Hemolysis." *Mol Immunol* 27, no. 3 (Mar 1990): 257-61.

Olanya, G., E. Thormann, I. Varga, R. Makuska, and P. M. Claesson. "Protein Interactions with Bottle-Brush Polymer Layers: Effect of Side Chain and Charge Density Ratio Probed by Qcm-D and Afm." *J Colloid Interface Sci* 349, no. 1 (Sep 1 2010): 265-74. http://dx.doi.org/10.1016/j.jcis.2010.05.061.

Pantelidis, P., D. S. McGrath, A. M. Southcott, C. M. Black, and R. M. du Bois. "Tumour Necrosis Factor-Alpha Production in Fibrosing Alveolitis Is Macrophage Subset Specific." *Respiratory Research* 2, no. 6 (2001): 365-72. <Go to ISI>://WOS:000172159800009.

Papadopoulos, S., K. D. Jurgens, and G. Gros. "Protein Diffusion in Living Skeletal Muscle Fibers: Dependence on Protein Size, Fiber Type, and Contraction." *Biophys J* 79, no. 4 (Oct 2000): 2084-94. http://dx.doi.org/10.1016/s0006-3495(00)76456-3.

Park, E. J., J. Yi, Y. Kim, K. Choi, and K. Park. "Silver Nanoparticles Induce Cytotoxicity by a Trojan-Horse Type Mechanism." *Toxicology in Vitro* 24, no. 3 (Apr 2010): 872-78. http://dx.doi.org/10.1016/j.tiv.2009.12.001.

Phalen, R. F., M. J. Oldham, and A. E. Nel. "Tracheobronchial Particle Dose Considerations for in Vitro Toxicology Studies." *Toxicological Sciences* 92, no. 1 (Jul 2006): 126-32. http://dx.doi.org/10.1093/toxsci/kfj182.

Pietrzak, W. S. and I. F. Miller. "Oxidative Interactions between Hemoglobin and Egg Lecithin Liposomes." *Biomater Artif Cells Artif Organs* 17, no. 5 (1989): 563-81.

Powers, C. M., A. R. Badireddy, I. T. Ryde, F. J. Seidler, and T. A. Slotkin. "Silver Nanoparticles Compromise Neurodevelopment in Pc12 Cells: Critical Contributions of Silver Ion, Particle Size, Coating, and Composition." *Environmental Health Perspectives* 119, no. 1 (Jan 2011): 37-44. http://dx.doi.org/10.1289/ehp.1002337.

Pozio, Edoardo, Ljiljana Sofronic-Milosavljevic, Maria Angeles Gomez Morales, Pascal Boireau, and Karsten Nöckler. "Evaluation of Elisa and Western Blot Analysis Using Three Antigens to Detect Anti-Trichinella Igg in Horses." *Veterinary Parasitology* 108, no. 2 (9/10/ 2002): 163-78. http://dx.doi.org/10.1016/S0304-4017(02)00185-1.

Quadros, M. E. and L. C. Marr. "Environmental and Human Health Risks of Aerosolized Silver Nanoparticles." *Journal of the Air & Waste Management Association* 60, no. 7 (Jul 2010): 770-81. http://dx.doi.org/10.3155/1047-3289.60.7.770.

Ratte, H. T. "Bioaccumulation and Toxicity of Silver Compounds: A Review." *Environmental Toxicology and Chemistry* 18, no. 1 (Jan 1999): 89-108. <Go to ISI>://000077722400012.

Robinson, P. C., D. R. Voelker, and R. J. Mason. "Isolation and Culture of Human Alveolar Type-Ii Epithelial-Cells - Characterization of Their Phospholipid Secretion." *American Review of Respiratory Disease* 130, no. 6 (1984): 1156-60. <Go to ISI>://WOS:A1984TW55400038.

Romoser, Amelia A., Michael F. Criscitiello, and Christie M. Sayes. "Engineered Nanoparticles Induce DNA Damage in Primary Human Skin Cells, Even at Low Doses." *Nano LIFE* 4, no. 1 (2014): 1-13.

Rothen-Rutishauser, Barbara M., Stephen G. Kiama, and Peter Gehr. "A Three-Dimensional Cellular Model of the Human Respiratory Tract to Study the Interaction with Particles." *American Journal of Respiratory Cell and Molecular Biology* 32, no. 4 (2005/04/01 2005): 281-89. Accessed 2016/04/26. http://dx.doi.org/10.1165/rcmb.2004-0187OC.

Ruge, Christian A., Julian Kirch, Olga Canadas, Marc Schneider, Jesus Perez-Gil, Ulrich F. Schaefer, Cristina Casals, and Claus-Michael Lehr. "Uptake of Nanoparticles by Alveolar Macrophages Is Triggered by Surfactant Protein A." *Nanomedicine-Nanotechnology Biology and Medicine* 7, no. 6 (Dec 2011): 690-93. http://dx.doi.org/10.1016/j.nano.2011.07.009.

Saito, S., M. Tsugeno, D. Koto, Y. Mori, Y. Yoshioka, S. Nohara, and K. Murase. "Impact of Surface Coating and Particle Size on the Uptake of Small and Ultrasmall Superparamagnetic Iron Oxide Nanoparticles by Macrophages." *International Journal of Nanomedicine* 7 (2012): 5415-21. http://dx.doi.org/10.2147/ijn.s33709.

Sambuy, Y., I. Angelis, G. Ranaldi, M. L. Scarino, A. Stammati, and F. Zucco. "The Caco-2 Cell Line as a Model of the Intestinal Barrier: Influence of Cell and Culture-Related Factors on Caco-2 Cell Functional Characteristics." *Cell Biology and Toxicology* 21, no. 1 (Jan 2005): 1-26. http://dx.doi.org/10.1007/s10565-005-0085-6.

Sayes, Christie M., P. Alex Smith, and Ivan V. Ivanov. "A Framework for Grouping Nanoparticles Based on Their Measurable Characteristics." *International Journal of Nanomedicine* 8 (2013 2013): 45-56. http://dx.doi.org/10.2147/ijn.s40521.

Schleh, C., C. Muhlfeld, K. Pulskamp, A. Schmiedl, M. Nassimi, H. D. Lauenstein, A. Braun, N. Krug, V. J. Erpenbeck, and J. M. Hohlfeld. "The Effect of Titanium Dioxide Nanoparticles on Pulmonary Surfactant Function and Ultrastructure." *Respiratory Research* 10 (Sep 2009). http://dx.doi.org/9010.1186/1465-9921-10-90.

Schmid, Günter. *Nanoparticles: From Theory to Application*. Vol. 3, 7 vols. Weinheim: WILEY-VCH Verlag GmbH & Co. KGaA, 2004.

Schneeberger-Keeley, E. E. and M. J. Karnovsky. "The Ultrastructural Basis of Alveolar-Capillary Membrane Permeability to Peroxidase Used as a Tracer." *J Cell Biol* 37, no. 3 (Jun 1968): 781-93. http://www.ncbi.nlm.nih.gov/pubmed/11905208.

Scown, T. M., E. M. Santos, B. D. Johnston, B. Gaiser, M. Baalousha, S. Mitov, J. R. Lead, V. Stone, T. F. Fernandes, M. Jepson, R. van Aerle, and C. R. Tyler. "Effects of Aqueous Exposure to Silver Nanoparticles of Different Sizes in Rainbow Trout." *Toxicological Sciences* 115, no. 2 (Jun 2010): 521-34. <Go to ISI>://WOS:000277997100022.

Seiffert, J., F. Hussain, C. Wiegman, F. Li, L. Bey, W. Baker, A. Porter, M. P. Ryan, Y. Chang, A. Gow, J. F. Zhang, J. Zhu, T. D. Tetley, and K. F. Chung. "Pulmonary Toxicity of Instilled Silver Nanoparticles: Influence of Size, Coating and Rat Strain." *Plos One* 10, no. 3 (Mar 6 2015). <Go to ISI>://WOS:000350689400086.

Selzer, T., S. Albeck, and G. Schreiber. "Rational Design of Faster Associating and Tighter Binding Protein Complexes." *Nature Structural Biology* 7, no. 7 (Jul 2000): 537-41. <Go to ISI>://WOS:000087966300007.

Shannahan, J. H., R. Podila, A. A. Aldossari, H. Emerson, B. A. Powell, P. C. Ke, A. M. Rao, and J. M. Brown. "Formation of a Protein Corona on Silver Nanoparticles Mediates Cellular Toxicity Via Scavenger Receptors." *Toxicological Sciences* 143, no. 1 (Jan 2015): 136-46. <Go to ISI>://WOS:000350101700015.

Sharma, V. K., R. A. Yngard, and Y. Lin. "Silver Nanoparticles: Green Synthesis and Their Antimicrobial Activities." *Advances in Colloid and Interface Science* 145, no. 1-2 (Jan 30 2009): 83-96. <Go to ISI>://WOS:000262219500004.

Shi, Q., Y. Zhou, and Y. Sun. "Influence of Ph and Ionic Strength on the Steric Mass-Action Model Parameters around the Isoelectric Point of Protein." *Biotechnol Prog* 21, no. 2 (Mar-Apr 2005): 516-23. http://dx.doi.org/10.1021/bp049735o.

Smith, D. G. "Inhibition of Swarming in Proteus Spp by Tannic-Acid." *Journal of Applied Bacteriology* 38, no. 1 (1975): 29-+. http://dx.doi.org/10.1111/j.1365-2672.1975.tb00496.x.

Sperling, R. A. and W. J. Parak. "Surface Modification, Functionalization and Bioconjugation of Colloidal Inorganic Nanoparticles." *Philos Trans A Math Phys Eng Sci* 368, no. 1915 (Mar 28 2010): 1333-83. http://dx.doi.org/10.1098/rsta.2009.0273.

Stoehr, L. C., E. Gonzalez, A. Stampfl, E. Casals, A. Duschl, V. Puntes, and G. J. Oostingh. "Shape Matters: Effects of Silver Nanospheres and Wires on Human Alveolar Epithelial Cells." *Part Fibre Toxicol* 8 (2011): 36. http://dx.doi.org/10.1186/1743-8977-8-36.

Sun, D. P., D. I. Liao, and S. J. Remington. "Electrostatic Fields in the Active Sites of Lysozymes." *Proc Natl Acad Sci U S A* 86, no. 14 (Jul 1989): 5361-5.

Sung, J. H., J. H. Ji, J. D. Park, J. U. Yoon, D. S. Kim, K. S. Jeon, M. Y. Song, J. Jeong, B. S. Han, J. H. Han, Y. H. Chung, H. K. Chang, J. H. Lee, M. H. Cho, B. J. Kelman, and I. J. Yu. "Subchronic Inhalation Toxicity of Silver Nanoparticles." *Toxicological Sciences* 108, no. 2 (Apr 2009): 452-61. <Go to ISI>://WOS:000264891300022.

Szebeni, J., H. Hauser, C. D. Eskelson, R. R. Watson, and K. H. Winterhalter. "Interaction of Hemoglobin Derivatives with Liposomes. Membrane Cholesterol Protects against the Changes of Hemoglobin." *Biochemistry* 27, no. 17 (Aug 23 1988): 6425-34.

Szebeni, J., C. C. Winterbourn, and R. W. Carrell. "Oxidative Interactions between Haemoglobin and Membrane Lipid. A Liposome Model." *Biochem J* 220, no. 3 (Jun 15 1984): 685-92.

Tamer Al Kayal , Silvia Nappini , Edda Russo , Debora Berti , Monica Bucciantini , Massimo Stefani and Piero Baglioni "Lysozyme Interaction with Negatively Charged Lipid Bilayers: Protein Aggregation and Membrane Fusion " *Soft Matter* 8 (2012): 4524-34.

Tan, Siliu, Melek Erol, Athula Attygalle, Henry Du, and Svetlana Sukhishvili. "Synthesis of Positively Charged Silver Nanoparticles Via Photoreduction of Agno3 in Branched Polyethyleneimine/Hepes Solutions." *Langmuir* 23, no. 19 (2007/09/01 2007): 9836-43. http://dx.doi.org/10.1021/la701236v.

Tedja, Roslyn, May Lim, Rose Amal, and Christopher Marquis. "Effects of Serum Adsorption on Cellular Uptake Profile and Consequent Impact of Titanium Dioxide Nanoparticles on Human Lung Cell Lines." *ACS Nano* 6, no. 5 (2012/05/22 2012): 4083-93. http://dx.doi.org/10.1021/nn3004845.

Thakur Prasad Yadav, Ram Manohar Yadav, Dinesh Pratap Singh. "Mechanical Milling: A Top Down Approach for the Synthesis of Nanomaterials and Nanocomposites." *Nanoscience and Nanotechnology* 2, no. 3 (2012): 22-48. http://dx.doi.org/10.5923/j.nn.20120203.01.

Tian, J., K. K. Wong, C. M. Ho, C. N. Lok, W. Y. Yu, C. M. Che, J. F. Chiu, and P. K. Tam. "Topical Delivery of Silver Nanoparticles Promotes Wound Healing." *ChemMedChem* 2, no. 1 (Jan 2007): 129-36. http://dx.doi.org/10.1002/cmdc.200600171.

Tolaymat, T. M., A. M. El Badawy, A. Genaidy, K. G. Scheckel, T. P. Luxton, and M. Suidan. "An Evidence-Based Environmental Perspective of Manufactured Silver Nanoparticle in Syntheses and Applications: A Systematic Review and Critical Appraisal of Peer-Reviewed Scientific Papers." *Science of the Total Environment* 408, no. 5 (Feb 1 2010): 999-1006. <Go to ISI>://WOS:000274365000001.

Toumey, Christopher P. "Reading Feynman into Nanotechnology." *Techné: Research in Philosophy and Technology* 12, no. 3 (2008): 133-68.

Valverde-Alva, M. A., T. García-Fernández, M. Villagrán-Muniz, C. Sánchez-Aké, R. Castañeda-Guzmán, E. Esparza-Alegría, C. F. Sánchez-Valdés, J. L. Sánchez Llamazares, and C. E. Márquez Herrera. "Synthesis of Silver Nanoparticles by Laser Ablation in Ethanol: A Pulsed Photoacoustic Study." *Applied Surface Science* 355 (11/15/ 2015): 341-49. http://dx.doi.org/http://dx.doi.org/10.1016/j.apsusc.2015.07.133.

Vance, M. E., T. Kuiken, E. P. Vejerano, S. P. McGinnis, M. F. Hochella, D. Rejeski, and M. S. Hull. "Nanotechnology in the Real World: Redeveloping the Nanomaterial Consumer Products Inventory." *Beilstein Journal of Nanotechnology* 6 (Aug 21 2015): 1769-80. <Go to ISI>://WOS:000359834400001.

Varani, I., A. Terzaghi, L. Donati, M. Marazzi, M. Masserini, and G. Tettamanti. "Protective Effect of Some Exogenous Glycolipids on Human Cultured Keratinocytes against Lipid Peroxidation." *Archives of Dermatological Research* 286, no. 8 (1994): 481-83. http://dx.doi.org/10.1007/BF00371576.

Varki, A. "Biological Roles of Oligosaccharides - All of the Theories Are Correct." *Glycobiology* 3, no. 2 (Apr 1993): 97-130. http://dx.doi.org/10.1093/glycob/3.2.97.

Walczak, A. P., E. Kramer, P. J. Hendriksen, R. Helsdingen, M. van der Zande, I. M. Rietjens, and H. Bouwmeester. "In Vitro Gastrointestinal Digestion Increases the Translocation of Polystyrene Nanoparticles in an in Vitro Intestinal Co-Culture Model." *Nanotoxicology* 9, no. 7 (2015): 886-94. http://dx.doi.org/10.3109/17435390.2014.988664.

Wang, L., D. K. Nagesha, S. Selvarasah, M. R. Dokmeci, and R. L. Carrier. "Toxicity of Cdse Nanoparticles in Caco-2 Cell Cultures." In *J Nanobiotechnology*, vol 6, 11. England, 2008.

Wang, S. X., K. C. Pandey, J. R. Somoza, P. S. Sijwali, T. Kortemme, L. S. Brinen, R. J. Fletterick, P. J. Rosenthal, and J. H. McKerrow. "Structural Basis for Unique Mechanisms of Folding and Hemoglobin Binding by a Malarial Protease." *Proc Natl Acad Sci U S A* 103, no. 31 (Aug 1 2006): 11503-8. http://dx.doi.org/10.1073/pnas.0600489103.

Wang, W., S. Lv, Y. Zhou, J. Fu, C. Li, and P. Liu. "Tumor Necrosis Factor-Alpha Affects Blood-Brain Barrier Permeability in Acetaminophen-Induced Acute Liver Failure." *Eur J Gastroenterol Hepatol* 23, no. 7 (Jul 2011): 552-8. http://dx.doi.org/10.1097/MEG.0b013e3283470212.

Weiss, Matthias, Markus Elsner, Fredrik Kartberg, and Tommy Nilsson. "Anomalous Subdiffusion Is a Measure for Cytoplasmic Crowding in Living Cells." *Biophysical Journal* 87, no. 5 (11// 2004): 3518-24. http://dx.doi.org/10.1529/biophysj.104.044263.

Win, K. Y. and S. S. Feng. "Effects of Particle Size and Surface Coating on Cellular Uptake of Polymeric Nanoparticles for Oral Delivery of Anticancer Drugs." *Biomaterials* 26, no. 15 (May 2005): 2713-22. http://dx.doi.org/10.1016/j.biomaterials.2004.07.050.

Wolny, P. M., J. P. Spatz, and R. P. Richter. "On the Adsorption Behavior of Biotin-Binding Proteins on Gold and Silica." *Langmuir* 26, no. 2 (Jan 2010): 1029-34. http://dx.doi.org/10.1021/la902226b.

Wottrich, R., S. Diabate, and H. F. Krug. "Biological Effects of Ultrafine Model Particles in Human Macrophages and Epithelial Cells in Mono- and Co-Culture." *International Journal of Hygiene and Environmental Health* 207, no. 4 (Sep 2004): 353-61. <Go to ISI>://WOS:000224097200006.

Yacobi, N. R., L. Demaio, J. Xie, S. F. Hamm-Alvarez, Z. Borok, K. J. Kim, and E. D. Crandall. "Polystyrene Nanoparticle Trafficking across Alveolar Epithelium." *Nanomedicine* 4, no. 2 (Jun 2008): 139-45. http://dx.doi.org/10.1016/j.nano.2008.02.002.

Yacobi, Nazanin Rebecca. "Nanoparticle Interactions with Alveolar Epithelium: Barrier and Trafficking Properties." Dissertation, Univerisity of Southern California, 2008.

Ybert, C. and J.M. di Meglio. "Study of Protein Adsorption by Dynamic Surface Tension Measurements: Diffusive Regime." *Langmuir* 14 (1998): 471-75.

Ye, D., I. Ma, and T. Y. Ma. "Molecular Mechanism of Tumor Necrosis Factor-Alpha Modulation of Intestinal Epithelial Tight Junction Barrier." *Am J Physiol Gastrointest Liver Physiol* 290, no. 3 (Mar 2006): G496-504. http://dx.doi.org/10.1152/ajpgi.00318.2005.

Yousefzadi, Morteza, Zohreh Rahimi, and Vahid Ghafori. "The Green Synthesis, Characterization and Antimicrobial Activities of Silver Nanoparticles Synthesized from Green Alga Enteromorpha Flexuosa (Wulfen) J. Agardh." *Materials Letters* 137 (12/15/ 2014): 1-4. http://dx.doi.org/http://dx.doi.org/10.1016/j.matlet.2014.08.110.

Zhang, Fan, Phillip Durham, Christie M. Sayes, Boris L. T. Lau, and Erica D. Bruce. "Particle Uptake Efficiency Is Significantly Affected by Type of Capping Agent and Cell Line." *Journal of Applied Toxicology* 35, no. 10 (2015): 1114-21. http://dx.doi.org/10.1002/jat.3138.

Zhang, T., L. Wang, Q. Chen, and C. Chen. "Cytotoxic Potential of Silver Nanoparticles." *Yonsei Med J* 55, no. 2 (Mar 2014): 283-91. http://dx.doi.org/10.3349/ymj.2014.55.2.283.

Zuckermann, M. J. and T. Heimburg. "Insertion and Pore Formation Driven by Adsorption of Proteins onto Lipid Bilayer Membrane-Water Interfaces." *Biophys J* 81, no. 5 (Nov 2001): 2458-72. http://dx.doi.org/10.1016/s0006-3495(01)75892-4.